SKB

TECHNICAL REPORT 91-13

Discrete fracture modelling of the Finnsjön rock mass Phase 1: Feasibility study

J E Geier, C-L Axelsson
Golder Geosystem AB, Uppsala

March 1991

SVENSK KÄRNBRÄNSLEHANTERING AB
SWEDISH NUCLEAR FUEL AND WASTE MANAGEMENT CO
BOX 5864 S-102 48 STOCKHOLM
TEL 08-665 28 00 TELEX 13108 SKB S
TELEFAX 08-661 57 19

DISCRETE FRACTURE MODELLING OF THE FINNSJÖN ROCK MASS PHASE 1 FEASIBILITY STUDY

J E Geier, C-L Axelsson

Golder Geosystem AB, Uppsala

March 1991

DISCRETE FRACTURE MODELLING OF THE FINNSJÖN ROCK MASS PHASE 1 FEASIBILITY STUDY

Prepared by:

J.E. Geier and C.-L. Axelsson
Golder Geosystem AB
Uppsala

For

Svensk Kärnbränslehantering AB
Swedish Nuclear Fuel and Waste Management Company
Stockholm

March 1991

91-470

ABSTRACT

The geometry and properties of discrete fractures are expected to control local heterogeneity in flow and solute transport within crystalline rock in the Finnsjön area. Safety assessment of a generic repository located in this rock must take this local heterogeneity into account. The present report describes the first phase of a discrete-fracture modelling study, the goal of which is to develop stochastic-continuum and channel-network descriptions of the Finnsjön rock based upon observed fracture geometric and hydrologic properties. In the first phase of this study, the FracMan discrete fracture modelling package was used to analyse discrete fracture geometrical and hydrological data. Constant-pressure packer tests were analysed using fractional dimensional methods to estimate effective transmissivities and flow dimension for the packer test intervals. Discrete fracture data on orientation, size, shape, and location were combined with hydrologic data to develop a preliminary conceptual model for the conductive fractures at the site. The variability of fracture properties was expressed in the model by probability distributions. The preliminary conceptual model was used to simulate three-dimensional populations of conductive fractures in 25 m and 50 m cubes of rock. Transient packer tests were simulated in these fracture populations, and the simulated results were used to validate the preliminary conceptual model. The calibrated model was used to estimate the components of effective conductivity tensors for the rock by simulating steady-state groundwater flow through the cubes in three orthogonal directions. Monte Carlo stochastic simulations were performed for alternative realizations of the conceptual model. The number of simulations was insufficient to give a quantitative prediction of the effective conductivity heterogeneity and anisotropy on the scales of the cubes. However, the results give preliminary, rough estimates of these properties, and provide a demonstration of how the discrete-fracture network concept can be applied to derive data that is necessary for stochastic continuum and channel network modelling.

Key words: Finnsjön, safety assesment, site characterization, discrete fracture flow modelling, joint statistics.

TABLE OF CONTENTS

TABLE OF CONTENTS (Continued)

LIST OF APPENDICES

TABLE OF CONTENTS (Continued)

LIST OF FIGURES

1. INTRODUCTION

The Swedish Nuclear Fuel and Waste Management Company (SKB) is currently performing a safety assessment study, SKB 91, for a generic, high-level waste repository situated in the Finnsjön block (Figure 1-1). A major objective of the study is to predict the probability of migration of radionuclides to the biosphere within a time span of thousands of years.

The rock in the Finnsjön block is mainly granitic. Unfractured blocks of granitic rock typically have very low hydraulic conductivities. However, large volumes of granitic rock generally contain numerous fractures induced during emplacement or during geological deformations. Such fractures, if they connect to form networks, can be expected to form the principal pathways for fluid flow and radionuclide transport through the rock mass at Finnsjön.

The hydraulic conductivity of individual fractures in granitic rock can vary over several orders of magnitude, and the geometry of interconnection of the fractures is generally irregular. For these reasons, the properties of the fractured rock mass with respect to groundwater flow are, on a local scale, extremely heterogeneous.

Hydrological testing methods that are commonly used to characterize less heterogeneous rock are of questionable value for characterizing rock masses similar to that at the Finnsjön site. Traditional methods for interpretation of hydrological test results are based on assumptions of flow through an approximately homogeneous porous medium, with simple flow geometries (*e.g.* radial or spherical flow). In fractured rock the test results are, in general, controlled by fracture properties on a very localized scale, and the flow geometry can be very irregular.

Extension of hydrologic data from localized test results to the larger rock mass requires adoption of a realistic, validated conceptual model for rock mass heterogeneity. Such a model provides a basis for extrapolation of localized hydrological measurements to predict the large-scale, hydrological behaviour of the rock mass.

This report describes the first phase of an ongoing project to model fluid flow through networks of discrete fractures that are statistically similar to the fracture population observed at the Finnsjön site. The purpose of this modelling is to contribute to the development of a valid conceptual model, based on the observable, geometric and hydrologic characteristics of the fracture population, that can be used to predict groundwater flow and radionuclide transport through the fractured rock mass in the Finnsjön area. The specific goals of this modelling are:

- To characterize the large-scale heterogeneity and anisotropy of the flow properties of the rock mass.
- To characterize the relationship between hydrological test results and large-scale flow properties of the rock mass.
- To demonstrate the practical application of discrete fracture approaches within the integrated safety assessment strategy of SKB 91.

The present study seeks to accomplish these goals by use of a detailed-scale conceptual model that is consistent with the directly observable properties of the fracture population at the Finnsjön site. The modelling approach is based upon a statistical interpretation of the data, which provides a framework for considering the manifold uncertainties inherent to the collection and interpretation of fracture data.

In the present study, generic blocks of the Finnsjön rock mass are simulated using a discrete fracture network (DFN) model. The geometry of the fractures in the model is specified by statistics derived from site characterization data. The fracture model is calibrated by comparison of simulated hydrological test results with observed hydrological test results. The resulting detailed-scale model is used in combination with the Monte Carlo technique to produce statistics that can be used for modelling on a larger scale, which is to be performed using a combination of stochastic continuum and channel-network modelling approaches.

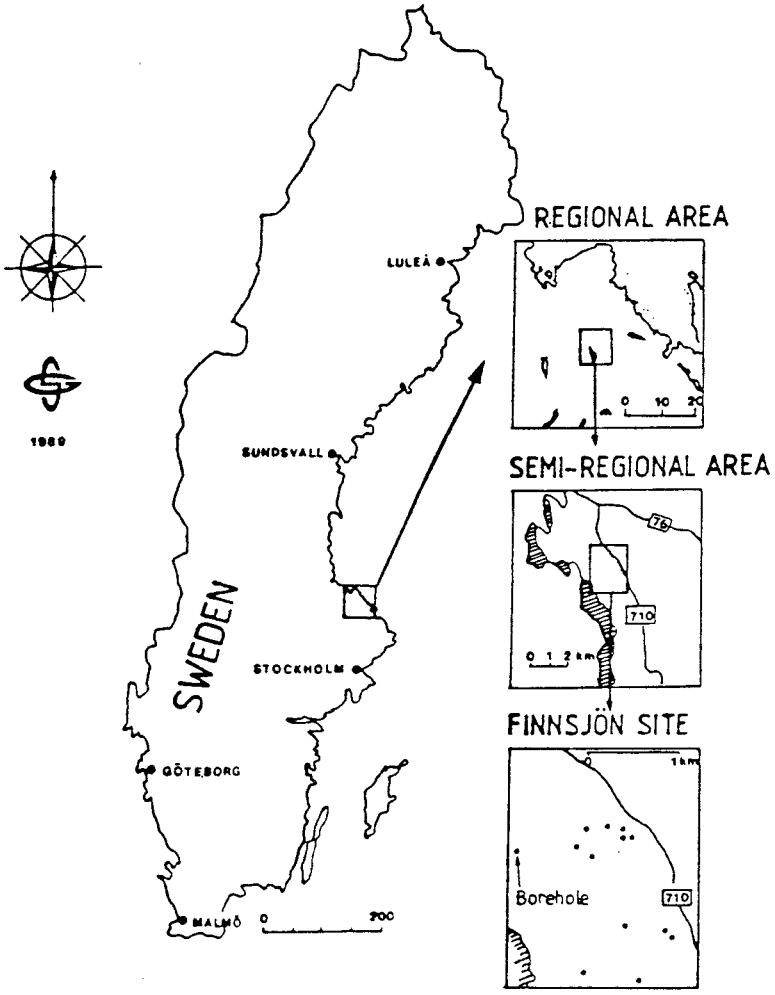

Location of regional area (northeastern Uppland), semi-regional area (Gåvastbo area), and the Finnsjön site (local area).

(Andersson et. al, 1989)

FIGURE 1-1
LOCATION OF FINNSJÖN SITE

2. BACKGROUND

Detailed investigations have been conducted to describe the geologic and hydrogeologic conditions in the Finnsjön area. These investigations have been summarized by Andersson et al. (1989), who proposed conceptual models of the Finnsjön area for hydrological modelling on three different scales:

- Semiregional
- Local
- Detailed

The semiregional-scale model is used to obtain appropriate boundary conditions for the local- and detailed-scale models. The local-scale model will be used to predict transport of radionuclides from the hypothetical repository. Detailed-scale models will consider flow and transport in the immediate vicinity of the repository. The regions considered in the semiregional- and local-scale models (Figure 1-1) are delimited by sets of fracture zones that are expected to dominate the groundwater flow field within the respective regions.

The present study is concerned with characterizing the rock within the region of the local-scale model. In particular, this study considers the properties of the rock in this region within and below a subhorizontal fracture zone referred to as Zone 2. The interpreted conductivities from hydrological tests within Zone 2 were generally much higher than for the rock below Zone 2. Andersson *et al.* (1989) suggested that Zone 2 should be treated as a distinct hydrological unit within the local-scale model.

Phase 1 of the present study, as described in this report, considered only the rock below Zone 2, *exclusive of other interpreted fracture zones* in the lower part of the Finnsjön block. The rock mass within Zone 2 and the other interpreted fracture zones will be considered in Phase 2 of the study.

Geological and hydrological data that are available for the local-scale model are described briefly in Sections 2.1 and 2.2, respectively.

2.1 Fracture Geology

Geological information for the local-scale model is available from a variety of sources. Fourteen deep core boreholes, BFI 01-02 and KFI 01-12, have been drilled and investigated with respect to rock type distribution, fracture frequency and fracture filling (Figure 2-1). Table 2.1 shows the amount of unoriented core data that are available from below Zone 2. No oriented core was available for the rock below Zone 2.

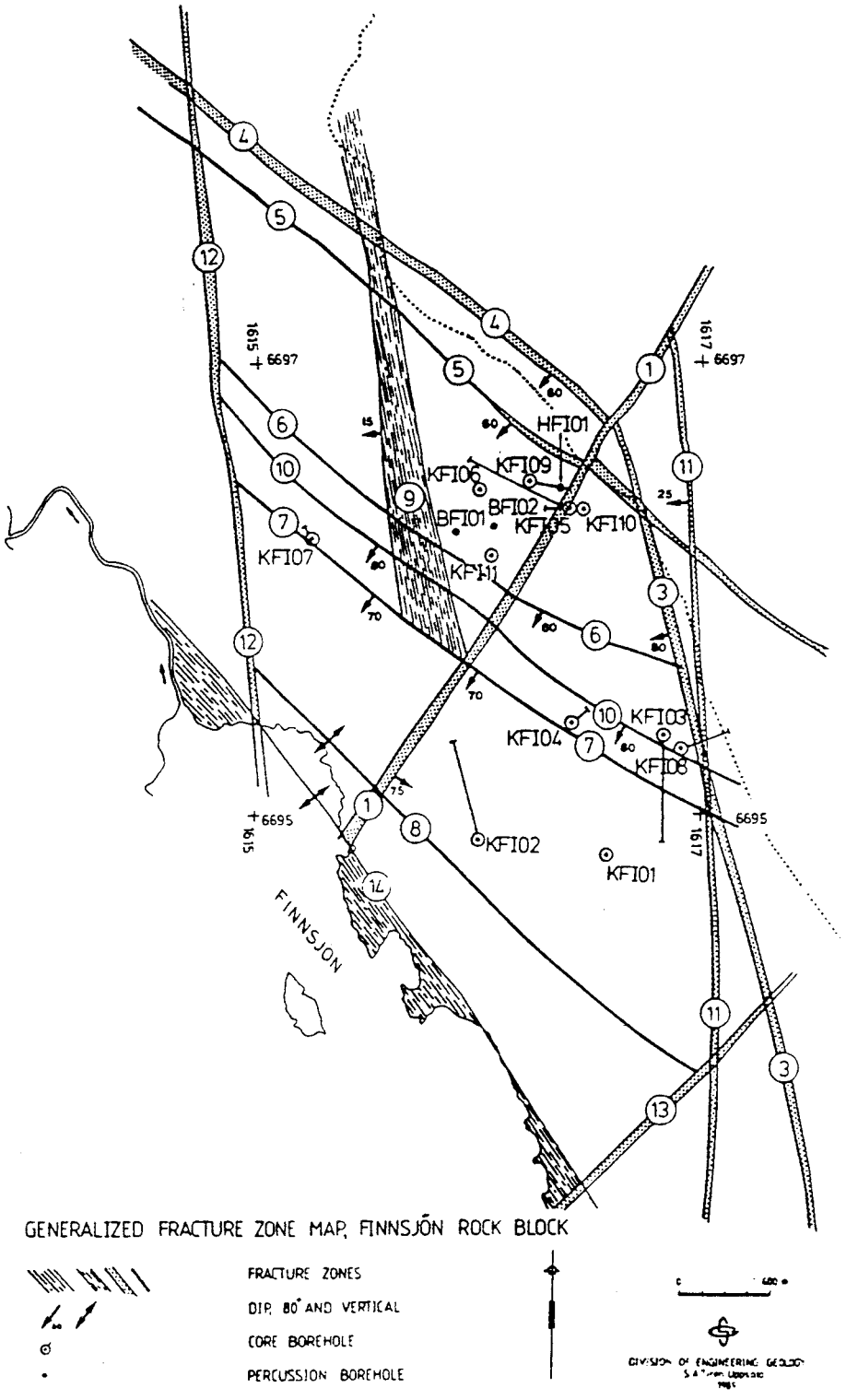

(Andersson et. al, 1989)

FIGURE **2-1**

LOCATION OF BOREHOLES AND SCANLINES

Table 2.1 Core data available for the Finnsjön block below Zone 2 (Andersson *et al.*, 1990).

Borehole	Inclination	Interpreted Limits of Zone 2 (m)	Borehole Length (m)	Length Below Zone 2 (m)
BFI 01	90°	242-356*	460	104
BFI 02	90°	200-280*	289	9
HFI 01	90°	105-125+	129	4
KFI 01	90°	-	500	-
KFI 02	50°	-	698	-
KFI 03	50°	-	730	-
KFI 04	80°	-	602	-
KFI 05	50°	166-305	750	445
KFI 06	90°	201-305	691	386
KFI 07	85°	295-380	552	172
KFI 08	60°	-	464	-
KFI 09	60°	130-212	375	163
KFI 10	50°	152-255+	255	-
KFI 11	90°	221-338*	389	61
TOTAL			6884	1344

* Personal communication J-E Andersson, October 1990.

Mapping of fractures and lineaments at the surface was carried out on 4 different areal mapping scales (Andersson et al., 1989):

- 50×50 km^2 Regional area
- 10×10 km^2 Semi-regional area
- 2×2.5 km^2 Local area
- 1×48 m^2 Cell maps

This mapping produced data for fracture tracelengths, fracture orientations, and relative fracture locations on a wide range of scales. Additional data for fracture orientations are available from scanline surveys (PRAV study, 1978). All of these data are for fractures located

at the surface, and thus above Zone 2. No tracelength or fracture location data are available for the rock below Zone 2, because it does not outcrop within the Finnsjön block.

2.1.1 Lineament and Outcrop Mapping

Figures 2-2 shows lineament maps for regional, semiregional, and local-scale lineaments. Coordinates for the endpoints of these lineaments are given by Andersson *et al.* (1989). The local-scale mapping gives information about the size distribution of the largest fractures or fracture zones that may occur within the local-scale model. The regional-scale and semiregional-scale lineaments are beyond the scale of the fractures and lineaments considered in the local-scale model. However, these data are useful because they describe fracturing patterns that may possibly be repeated over a range of scales.

The lineament maps give tracelength data on a very large scale, but little information on the scale of discrete fracture models of blocks within the local-scale model. Measurements of fracture tracelength on a finer scale have been obtained from cell maps near the borehole KFI 11 (Figure 2-3). The fracturing in the rock mass away from fracture zones has been mapped on a 90 m long and 5 m wide trench close to borehole KFI11.

Data on the orientations, lengths, apertures and fracture fillings of fracture traces were mapped in a 1×48 m^2 section of a cleaned trench, and have been presented by Tirén (1990). Fracture traces longer than about 0.1 m were mapped in this trench. A stereonet plot of the fracture orientations (Figure 2-4) shows that most of the fractures can be assigned to either of two groups: N20-75E/70-90 and N30-80W/60-90. The trace length distributions for the two groups of fractures (Figure 2-5) are strongly skewed toward the lower end of the scale.

For each scale of mapping, the lineament length distribution is skewed in the direction of smaller lengths (Figure 2-6). These data are influenced by truncation of the lineaments by the survey boundaries, as evidenced by the large numbers of lineaments with one or both ends outside of the survey areas.

Scanline data are available from two sets of scanline surveys at the site. These surveys provide information on fracture orientation, but not fracture size. In the earlier surveys (PRAV study, 1978), only fracture strike was recorded, not fracture dip. In the later surveys (Tirén, 1990), both fracture strike and dip were measured and recorded.

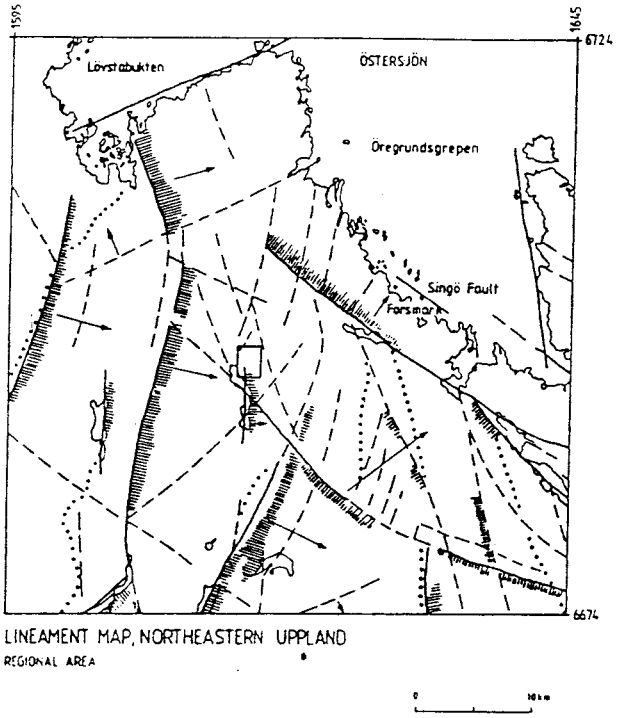

a) Regional Scale

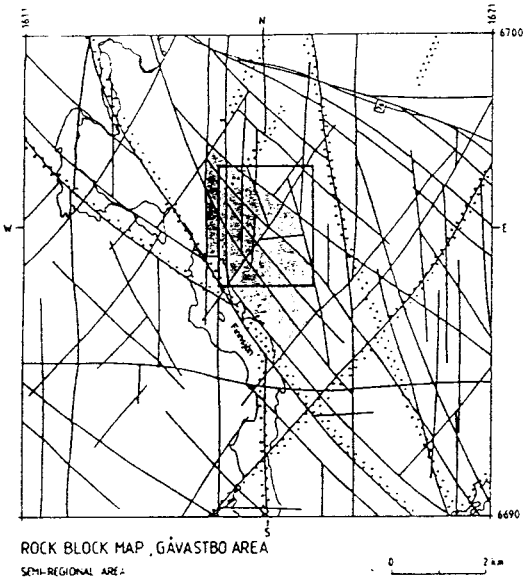

b) Semiregional Scale

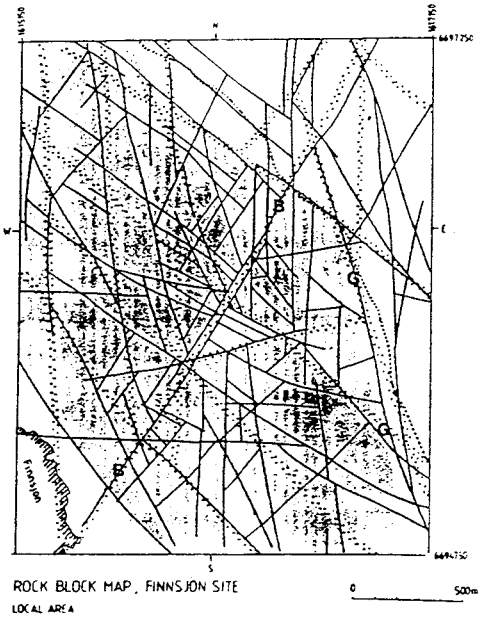

c) Local Scale

(from Andersson et. al, 1989)

FIGURE 2-2
LINEAMENT MAPS

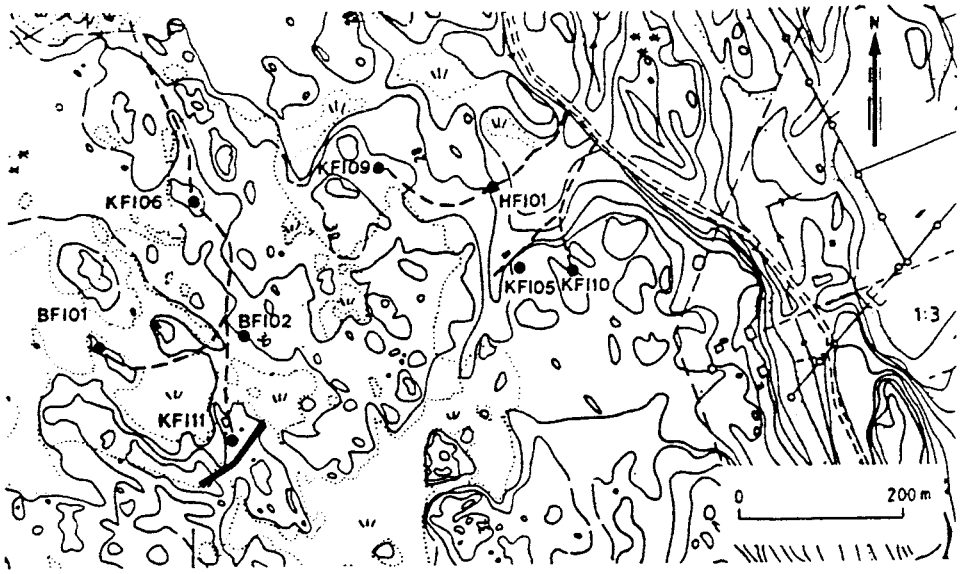

a) Location of Excavated Trench Just SE of Borehole KFI 11

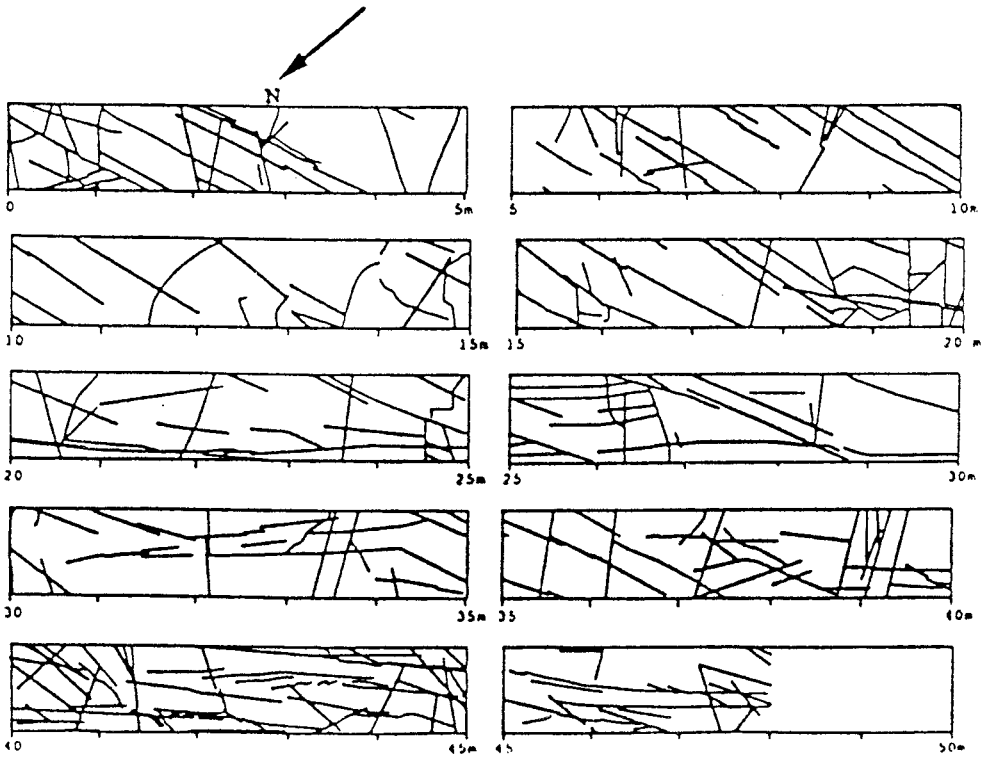

b) Fracture Maps in Eastern Portion of Trench

(Andersson et. al, 1989)

FIGURE 2-3
DETAILED SCALE MAPPING NEAR BOREHOLE KFI 11

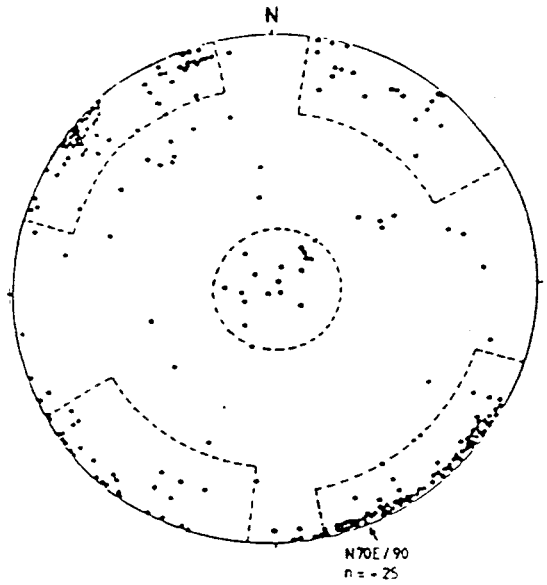

a) Inside Cell Map

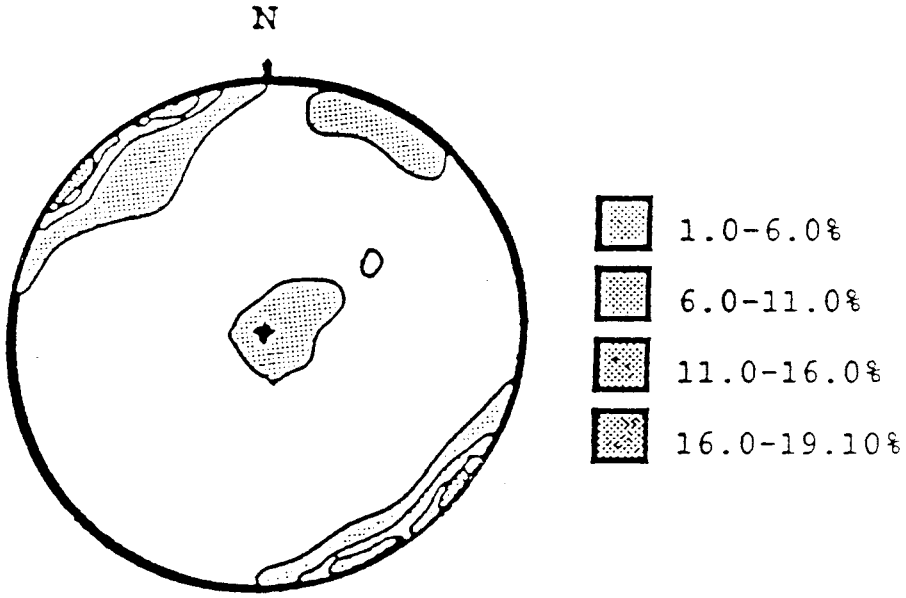

b) Inside Cell Map and Along Scanline in Trench

Equal-Area Projection

(From Andersson et. al, 1989)

FIGURE 2-4
STEREONET PLOT OF CELL MAP ORIENTATIONS

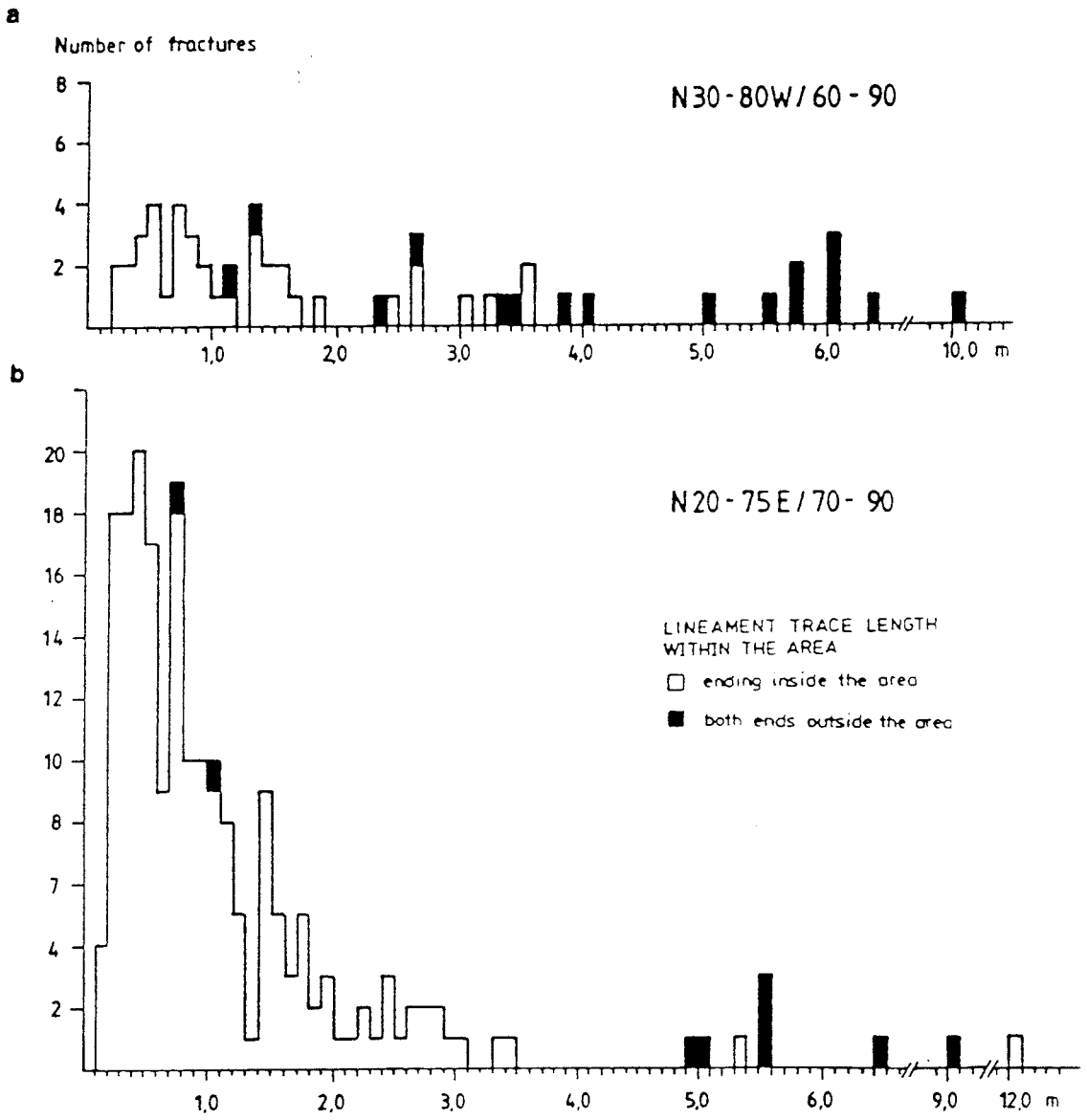

(from Andersson et. al, 1989)

FIGURE 2-5
LENGTH DISTRIBUTIONS FROM TWO SETS OF CELL MAP FRACTURES

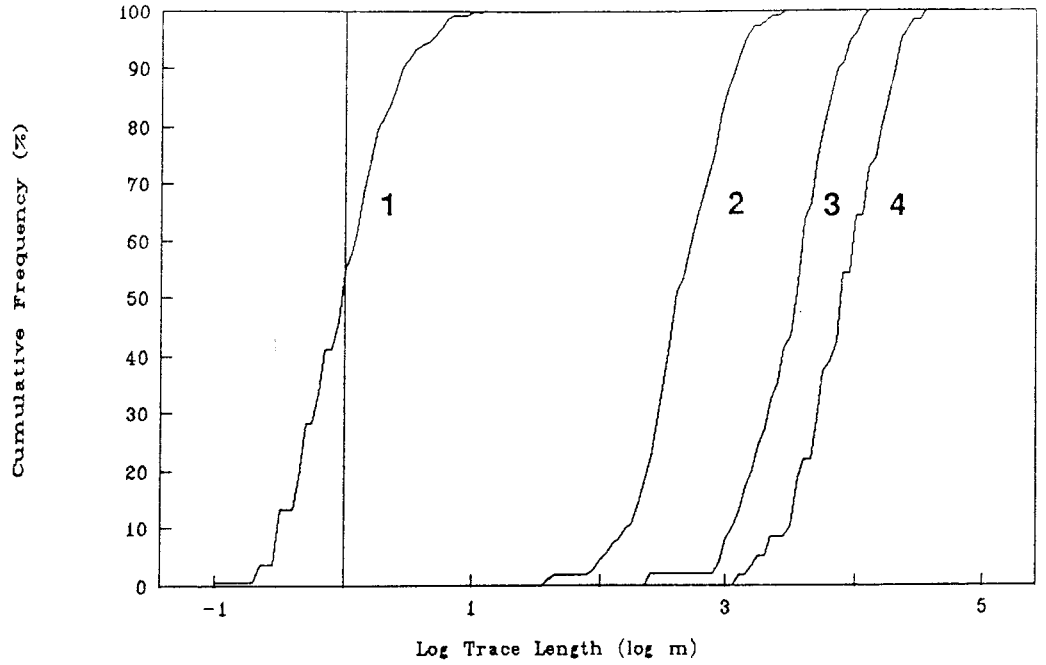

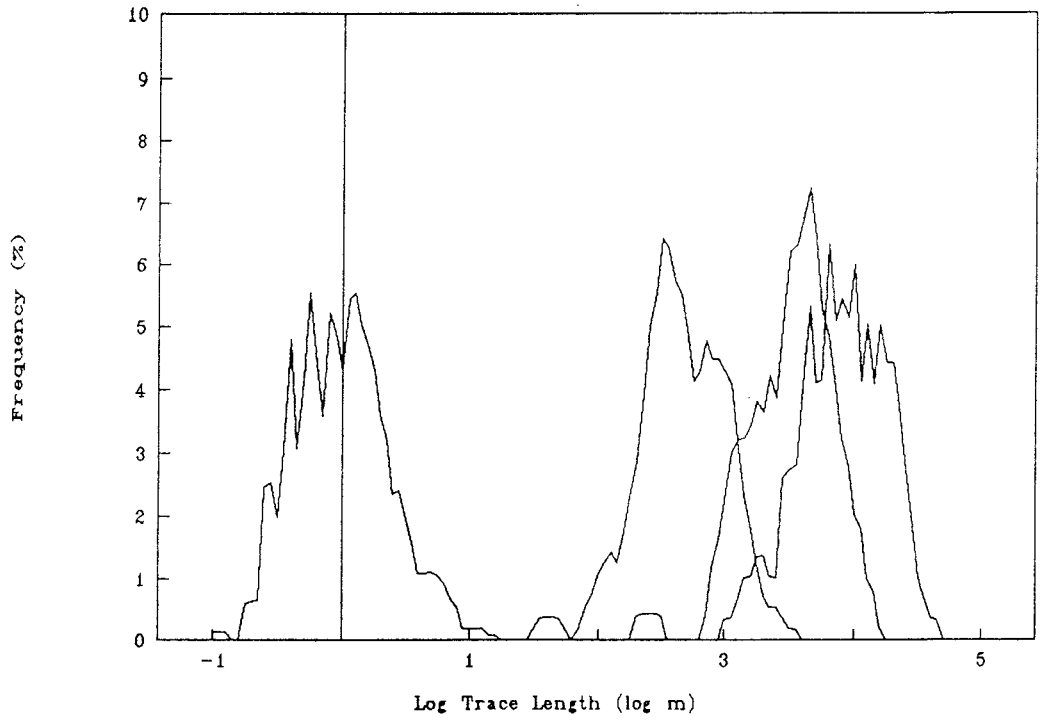

1 - Cell Map Fracture
2 - Local-Scale Lineaments
3 - Semiregional Lineaments
4 - Regional Lineaments

FIGURE 2-6
LINEAMENT AND FRACTURE TRACE LENGTH DISTRIBUTIONS

The data from the scanline surveys contain two types of bias:

- **Directional sampling bias**: The survey is biased toward fractures that are steeply dipping and perpendicular to the scanline direction.
- **Morphological bias**: "Morphological" fractures, *i.e.*, the fractures that form the surfaces of the outcrops, are included in the scanline data; although the inclusion of morphological fractures helps to improve the sampling of subhorizontal fractures, a biasing effect arises from the fact that outcrops occur only in the planes of these morphological fractures.

Theoretical corrections are available to account for directional sampling bias (*e.g.*, Terzaghi, 1965). Morphological bias can be eliminated by excluding morphological fractures from the data set, but this is undesirable because in so doing, much data for subhorizontal fractures are discarded. A further problem with the scanline data is that, for many fractures, dip angles are not recorded, so that only fracture strike directions are available.

The scanline surveys give only orientation data, not size data. Thus the cell maps represent the only detailed-scale fracture size data for the Finnsjön site. The scanline data constitute a much larger sample of the fracture population, but do not provide all of the data needed for discrete fracture network modelling. One question that must be answered is whether the cell map fractures are representative of the small-scale fractures throughout the site. One basis for comparison is the distribution of fracture strike directions. If the cell map fractures are a representative population, the strike angle distribution for the cell map sample should be similar to that for the much larger scanline sample.

Figure 2-7 shows a Terzaghi-corrected rose diagram which compares the strike angle distributions for these two samples. The plot shows that the populations are similar in the SE and SW quadrants, but that in the NE and NW quadrants the cell map fractures are skewed strongly toward the east with respect to the scanline fractures. Most noticeable is an anomalously large number of cell map fractures that have strike directions of approximately N70E. Thus the cell map fractures may not be fully representative of the fracture population throughout the site, possibly due to local heterogeneity in the fracture population. More cell maps at different locations within the site would be desirable. However, the resemblance between the two populations of strike angles is sufficient to warrant use of the cell map data for a demonstration of the discrete fracture network approach during the present study.

One weakness of the dataset for the Finnsjön block is that all of the data from scanlines and area maps at the surface are taken from exposures of the rock above Zone 2. These surface data are the only data related to fracture size, and, due to the lack of oriented core, the only data giving complete fracture orientations. To model the rock below Zone 2, it is necessary to decide whether the surface data are applicable to the rock below Zone 2. This decision must be made based on a comparison with core data from below Zone 2. This is discussed in the following section.

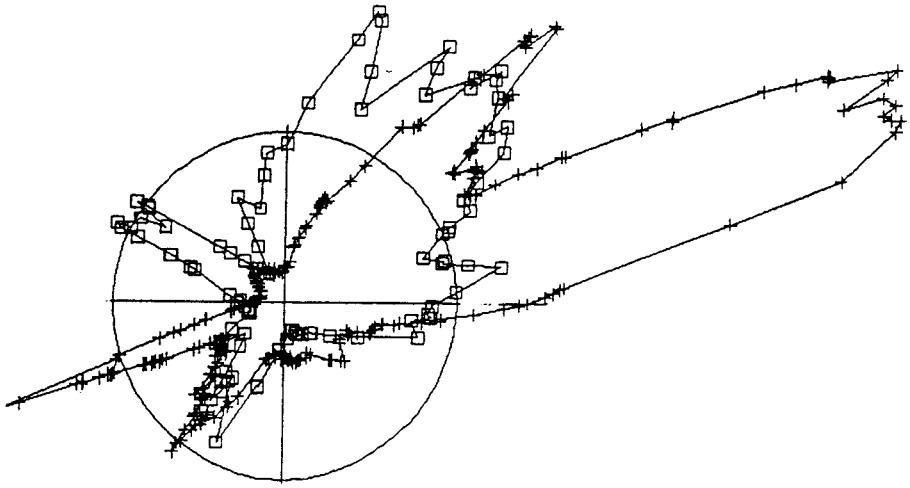

□ Scanlines + Cell Maps

Terzaghi-Corrected Data

FIGURE 2-7
STRIKE ANGLE DISTRIBUTION FROM SCANLINES AND CELL MAPS

2.1.2 Core Data

Core data give information that is complementary to data from surface mapping. Although core data give no information about fracture size, they give information on the orientations of subhorizontal fractures that are rarely seen on outcrops. Both core and surface data were used in the analysis for discrete-fracture modelling.

The lack of oriented core means that there are no complete orientation data available from below Zone 2. Unoriented core from holes of several distinct orientations can be interpreted using maximum-likelihood methods to estimate the most likely clustering of orientation distributions, but this analysis is complex and involves making a number of assumptions that cannot easily be verified. On the other hand, unoriented core from vertical boreholes gives direct information on the distribution of dip angles, which can be used to compare the fractures at depth with fractures mapped at the surface.

Core data are strongly biased toward fractures perpendicular to the core, and therefore the distribution of fracture dip angles from core cannot be compared directly with the distribution of dip angles measured at the surface. A theoretical correction for this bias is given by Terzaghi (1965). A similar correction can be applied to the surface data, which are biased toward steeply-dipping fractures. Figure 2-8 compares fracture dip angles determined from unoriented core (from two of the vertical boreholes KFI 06 and KFI 11) with dip angles from surface mapping, after applying Terzaghi corrections to compensate for directional sampling bias. Morphological fractures from the scanline data were heuristically assigned a weight of one half that for ordinary fracture traces, in preparing this plot.

This plot shows that, after correcting for orientation bias, the distributions of dip angle for surface and borehole data show a rough resemblance to each other. For dip angles of less than 60°, the sampled frequency is more or less uniform with respect to dip angle. For steeper dip angles the sampled frequency increases with increasing dip angle for all data sets, but there is considerable discrepancy among the data sets. Very steep dips of over 80° or so are not sampled at all by the boreholes, so comparisons are not possible for dip angles above 80°. Thus on the basis of dip angle distribution there is no indication that the populations of fractures from the surface mapping and from core are distinct. This suggests that fracture size and orientation data from surface mapping may be representative of the rock below Zone 2.

2.2 Hydrologic Properties

Local measurements of the hydraulic properties of the rock mass have been obtained from single-hole water injection tests in boreholes. Single-hole water injection tests have been carried out for several different section lengths in the boreholes at the Finnsjön site. Table 2.2 shows the number of test sections for different interval lengths that are available from within and below Zone 2. The earliest tests, with a packer interval of 3m, gave data in terms of a "steady state" flowrate at the end of water injection. For the later 2m and 20m packer interval tests, the transient response was measured for both injection and recovery stages of the tests. These tests have been described by Andersson *et al.* (1989).

Table 2.2 Number of test sections for single-hole water injection tests with different packer intervals in the Brändan area.

Borehole	WITHIN ZONE 2			BELOW ZONE 2		
	Section Length			Section Length		
	2 m	3 m	20 m	2 m	3 m	20 m
KFI 05	69	46	-	7	146	-
KFI 06	30	20	-	10	136	-
KFI 07	22	15	-	13	69	-
KFI 09	41	-	5	25	-	7
KFI 10	35	-	4	7	-	1
KFI 11	57	-	6	12	-	3
BFI 01	56	-	6	47	-	5
BFI 02	39	-	-	3	-	-
HFI 01	9	-	-	-	-	-
All	358	81	21	124	351	16

Profiles of interpreted hydraulic conductivities versus test section depth are given for boreholes BFI 01-02, HFI 01, and KFI 01-12 in Appendix 1. Examination of the data from below Zone 2 (in the plots for Boreholes KFI 05-07, KFI 09 and BFI 01) shows that, within any given hole, there is no clear trend with depth for the interpreted hydraulic conductivity values. Based on this observation, within the scope of the present study it is assumed that hydraulic conductivity is independent of depth. No attempt was made to quantify this observation in the Phase 1 feasibility study.

Considerable variation in conductivity magnitudes is seen ***between*** holes, for rock within and outside of the identified fracture zones. In some cases the magnitude of the difference between holes for a single fracture zone is close to that between the fracture zones and the rock mass. This suggests the possibility of treating the fracture zones as expressions of the ordinary variability of the rock mass. This possibility was not investigated in Phase 1, but should be considered in the continuation of the study.

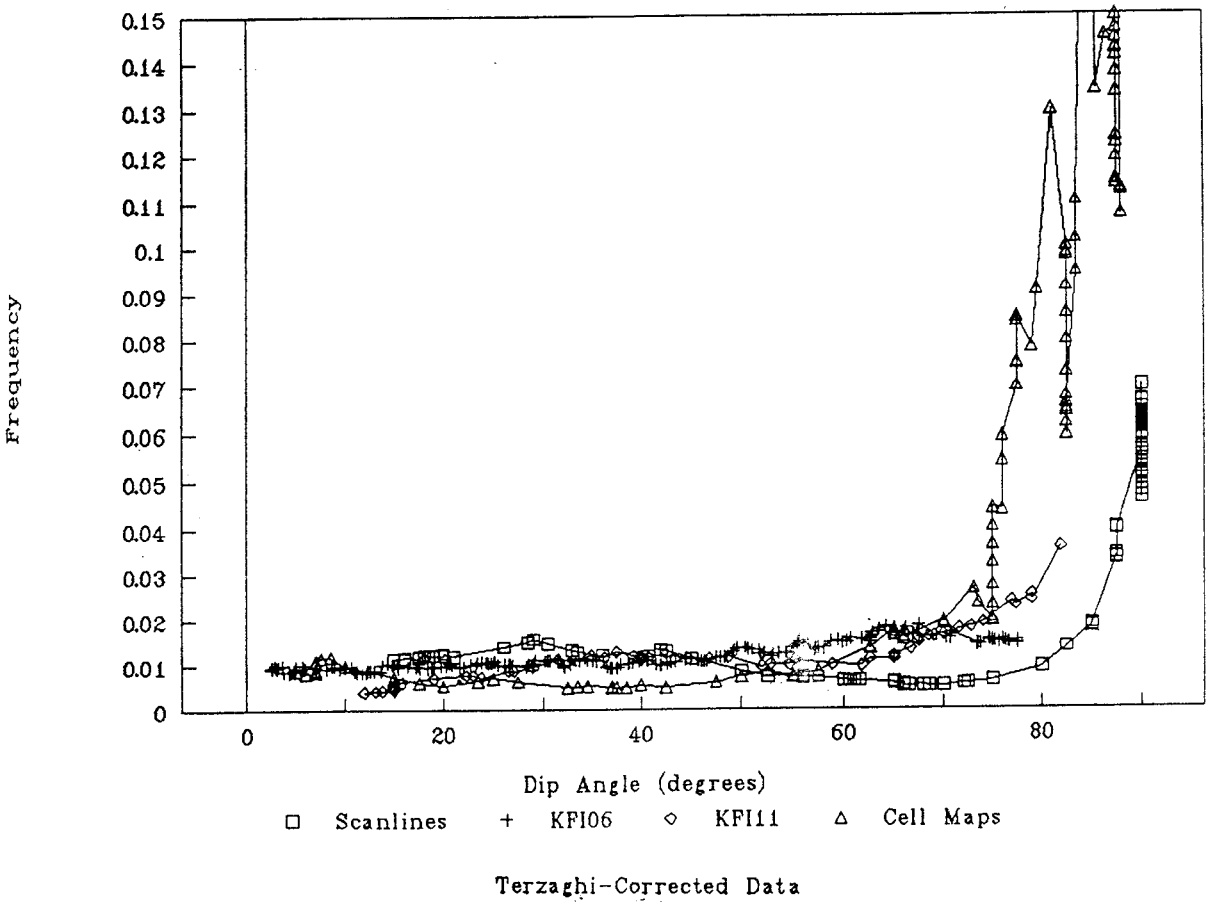

FIGURE 2-8
COMPARISON OF CORRECTED DIP ANGLE DISTRIBUTIONS FROM CORE AND SURFACE DATA

3. TECHNICAL APPROACH

Groundwater flow and radionuclide transport at Finnsjön are expected to occur mainly through networks of interconnected fractures, due to the extremely low conductivity of unfractured volumes of the granite. The process of radionuclide transport through fracture networks is believed to be markedly different from transport in a homogeneous, porous continuum. Transport occurs along discrete pathways rather than as smooth, continuous front throughout the rock. Accurate prediction of radionuclide transport through granitic rock similar to that at Finnsjön must be based upon a model that accurately represents the discontinuous nature of the flow paths through the granite.

Discrete-fracture network (DFN) models provide a means of explicitly representing flow path geometries in such cases. In DFN models, processes of flow and transport are assumed to take place primarily or entirely through networks of discrete fractures. The geometry of interconnection among fractures determines the locations and directions of the pathways. The statistical geometry of fractures can be deduced directly from observations of fractures in boreholes, on tunnel walls, and at outcrops at the surface (Dershowitz and Einstein, 1988). Thus the flow paths in DFN models arise as a direct consequence of observed fracture geometry, rather than as the result of conditioning on cross-hole hydrological data. This is advantageous because, in general, only a limited amount of cross-hole data are available, and, as each cross-hole test typically measures only one dominant flow path, the sample of pathways on which the conditioning can be based is extremely limited.

At the time of this study, the applicability of DFN models is limited in terms of the volume of the flow regions and the complexity of the chemical transport processes that can be modelled. The maximum volume that can be modelled depends upon the intensity of fracturing and the resolution (in terms of minimum fracture conductivity) that is desired, but in general the largest region that can be modelled is considerably less than the region scale considered in repository safety assessment studies. Chemical transport modelling in three-dimensional DFN models is limited at present to the processes of advection and dispersion in single-phase, saturated fluid flow models; other processes such as adsorption, reaction, decay and matrix diffusion could in principle be added to the models, at the cost of additional computational complexity.

Due to these limitations, DFN models must be used in conjunction with other modelling approaches to predict large-scale radionuclide transport for the SKB 91 safety assessment study. In this study, DFN models are used in conjunction with stochastic continuum (SC) and channel-network (CN) models. A SC model is used to model fluid flow within the Finnsjön block, to predict the groundwater flow field. Dual-porosity streamtube modelling is used to predict radionuclide transport. Channel network models are used as an alternative model for transport within the dominant flow pathways. The DFN model is used to provide information required for the other two modelling approaches.

Figure 3-1 shows a highly simplified comparison of DFN, stochastic continuum, and channel-network modelling approaches. Stochastic continuum (SC) models use blocks of an "equivalent porous medium" (EPM) to represent blocks of fractured rock. The hydrological properties of

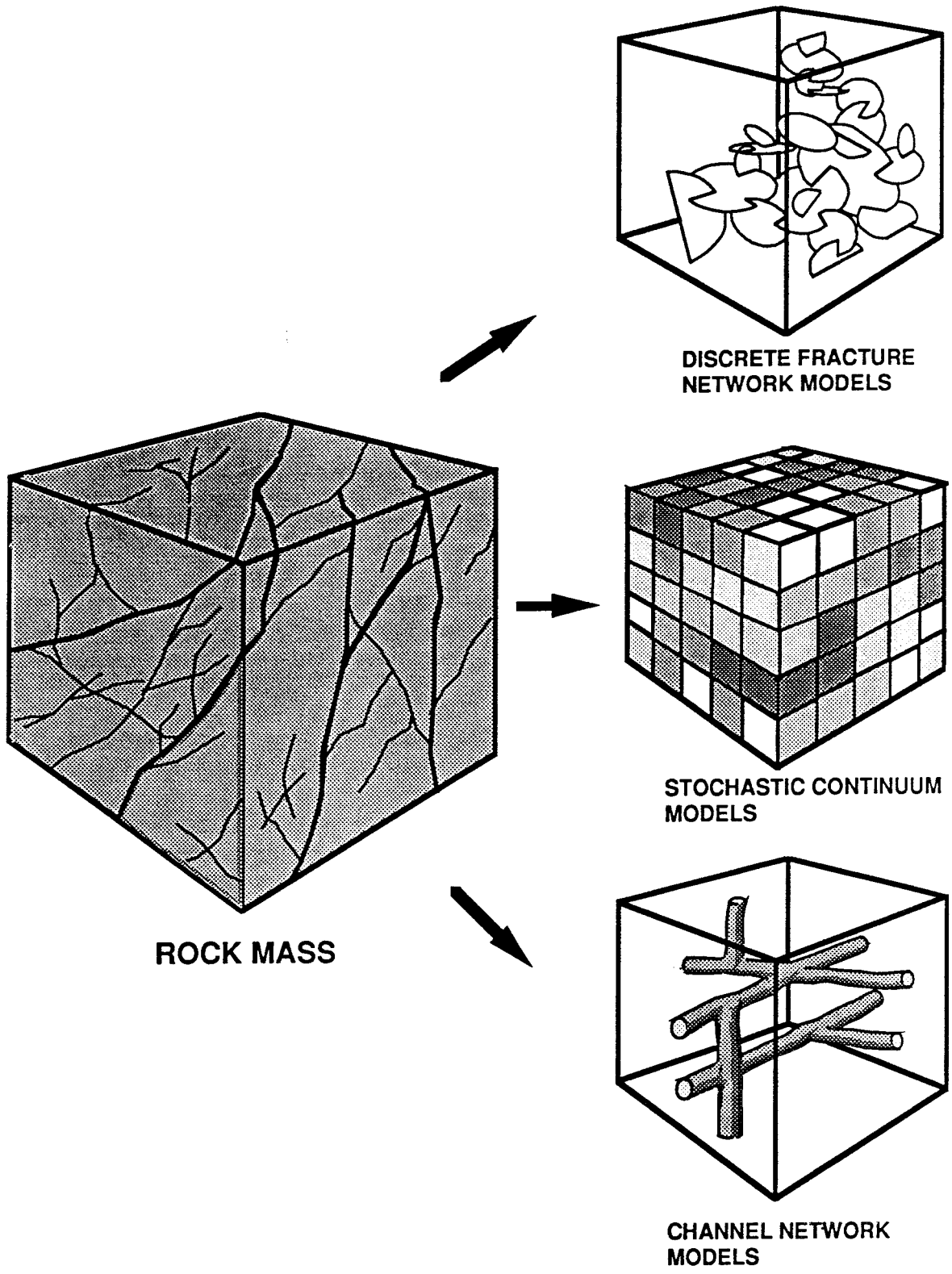

FIGURE 3-1
COMPARISON OF DFN, SC AND CN MODELLING APPROACHES

the EPM blocks may be anisotropic, and may vary from one block to another. Using this approach, large volumes of rock can be modelled at a relatively low computational cost.

At large scales, the details of fracture geometry and fracture properties may be unimportant with respect to fluid flow, making it possible to carry out flow modelling with SC approaches, provided the approach selected properly reflects the anisotropy and heterogeneity of the fractured rock masses, and the inherent uncertainty of local properties. However, the SC approach is inaccurate if the rock does not behave as a porous medium on the scale of the blocks. In very sparsely fractured rock, fractured rock may not act as a porous medium on any scale (Long and Witherspoon, 1985). In particular, if the rock mass is close to the percolation threshold, the rock will show increasingly bimodal behaviour with increasing scale, with separate populations of conductive and non-conductive blocks (Figure 3-2).

In more intensely fractured rock, the smallest scale at which the rock behaves as a porous medium is generally large relative to the scale on which hydrologic test data are available. Hydrologic tests in fractured rock usually do not test large blocks of rock; rather they test the properties of those individual fractures and networks of fractures intercepted by the boreholes in which testing is conducted. Thus the results of borehole hydrologic testing are not directly applicable to SC modelling.

Derivation of a SC model from borehole data requires definition of the relationship between test results and SC parameters. SC modellers have developed a number of possible solutions to this problem, among which are:

- Derivation of a scaling law from the basic definitions of a stochastic continuum in terms of covariance functions. This approach implicitly assumes the applicability of the covariance functions on the scale of a packer interval.
- Derivation of block-scale properties from a set of test results based explicitly only upon the assumption of a linear system. This requires an implicit assumption that the rock behaves as a porous continuum on the scale of a SC block.

In the SKB 91 safety analysis, an alternative approach is considered in which the DFN model is used to determine the scale (if any) at which the rock may be approximated by an equivalent porous medium, and to derive the scaling relationship between borehole test results and the properties of the equivalent porous medium on that scale.

Channel-network (CN) models are similar to DFN models in that flow is restricted to discrete conduits. In CN models the flow through the conduits is assumed to be essentially one-dimensional. This approach amounts to a simplification of the DFN approach, accomplished by ignoring the less conductive pathways (these may be taken into account by dual-porosity formulations) and reducing the assumed geometry of flow within conduits to one dimension, as compared with two-dimensional conduits in DFN models. Field investigations (Abelin *et al.*, 1990) have given indication that flow through fractures is often restricted to narrow channels within fracture planes. Hence these simplifications may be realistic.

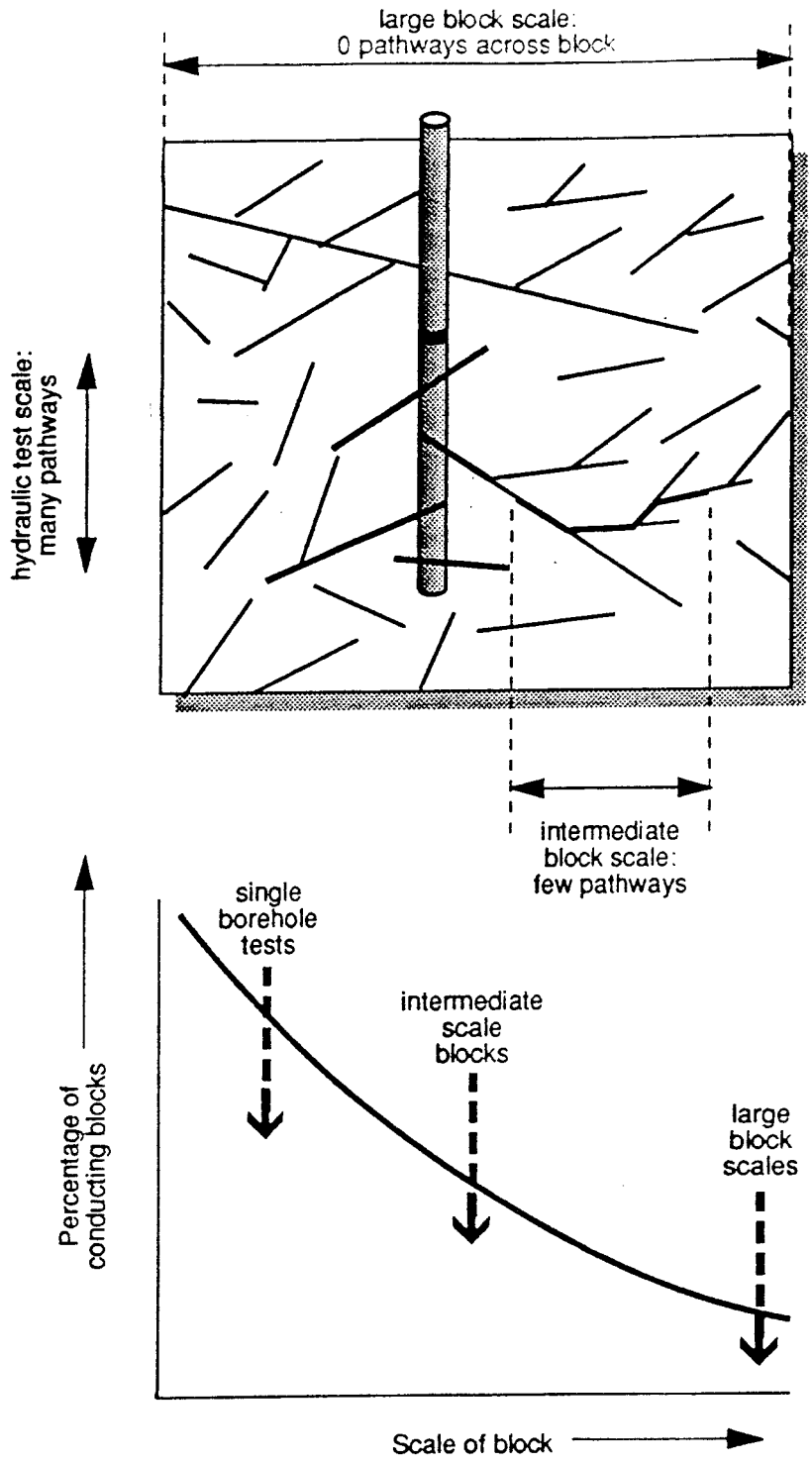

Note: For conductive fracture intensities near percolation threshold see Dershowitz (1984).

FIGURE 3-2
SCALE EFFECTS AND PERCOLATION PROBABILITY

A problem with the CN approach is to ascertain the geometry of the channel networks from field data. Although the number of channels in a given volume of space, and the variability of conductivity of the channels can be estimated at least approximately from observations of inflow into tunnels and boreholes (personal communication, I.Neretnieks and L. Moreno, 1990), the way in which the channels are interconnected in three-dimensional space is not so easily determined.

One way to produce realistic interconnection among channels is given by Tsang and Tsang (1987), who proposed generating channels within fracture planes defined by a DFN model. The geometry of the channels within the planes may be specified in terms of an autocovariance structure for aperture variation within the fracture plane (Tsang and Tsang, 1987), and/or by specifying linear conductors of increased conductivity along intersections between fracture planes (personal communications, I. Neretnieks, 1990 and W.S. Dershowitz, 1990). These approaches are functionally equivalent to the use of DFN models with variable transmissivity within the fracture planes. This last approach is considered in the present study.

3.1 Modelling Objectives

The objectives of the present project are to augment stochastic continuum and channel network modelling approaches by application of DFN modelling. The DFN modelling is intended to serve two functions in this regard:

- To convert field data into a form suitable for definition of the SC and CN models.
- To allow limited cross-verification of certain aspects of the modelling approaches used on a larger scale.

The following sections describe specific objectives in regard to SC and CN modelling, and organization of the modelling effort in two separate phases of work.

3.1.1 Objectives Related to Stochastic Continuum Modelling

The following types of information are needed for SC modelling of fractured rock, and are to be provided by DFN modelling:

- The minimal scale (the "representative elementary volume," or REV), if any, on which the rock mass can be said to behave as an equivalent porous medium.
- The variability of (average) rock mass effective hydraulic conductivity (K).
- The variability of anisotropy, expressed in terms of the ratios of the principal components of the (presumed) hydraulic conductivity tensor (K_1, K_2, K_3) to the average hydraulic conductivity K.

- The form of spatial correlation of rock mass conductivity that results from fracture network effects.

- The relationship between apparent hydraulic conductivities measured by borehole testing and the effective hydraulic conductivities of the rock mass on the scale of blocks used in SC modelling.

The present project seeks to quantify these types of information in terms of probability distributions and covariance functions, using DFN models.

3.1.2 Objectives Related to Channel-Network Modelling

The following types of information that are needed for CN modelling can perhaps be furnished by DFN modelling:

- The spatial intensity of channels (number per unit volume) as a function of channel length and channel conductivity, based upon the observable geometric characteristics of the fracture population.

- The interconnectivity of flow channels (number of intersections with other channels per unit length of channel) in three-dimensions.

The spatial intensity of channels can be estimated directly from packer test data, but DFN models may provide independent ways for deducing the same data.

One method for deriving this information that was considered in the present study is the DFN methodology of pathways analysis (Figure 3-3), which has been described by Dershowitz and Black (1990). The method is used to predict the occurrence of conduits in sparsely connected fracture systems, directly from fracture geometric data. A feasibility study of the application of this methodology showed that this approach is not feasible for the Finnsjön site, due to the nature of the interpreted fracture population, as described in Section 6.1.

Other possible methods exist for deducing CN model parameters from DFN models, but have not been tested within the scope of the Phase 1 feasibility study. These methods are discussed in Chapter 7.

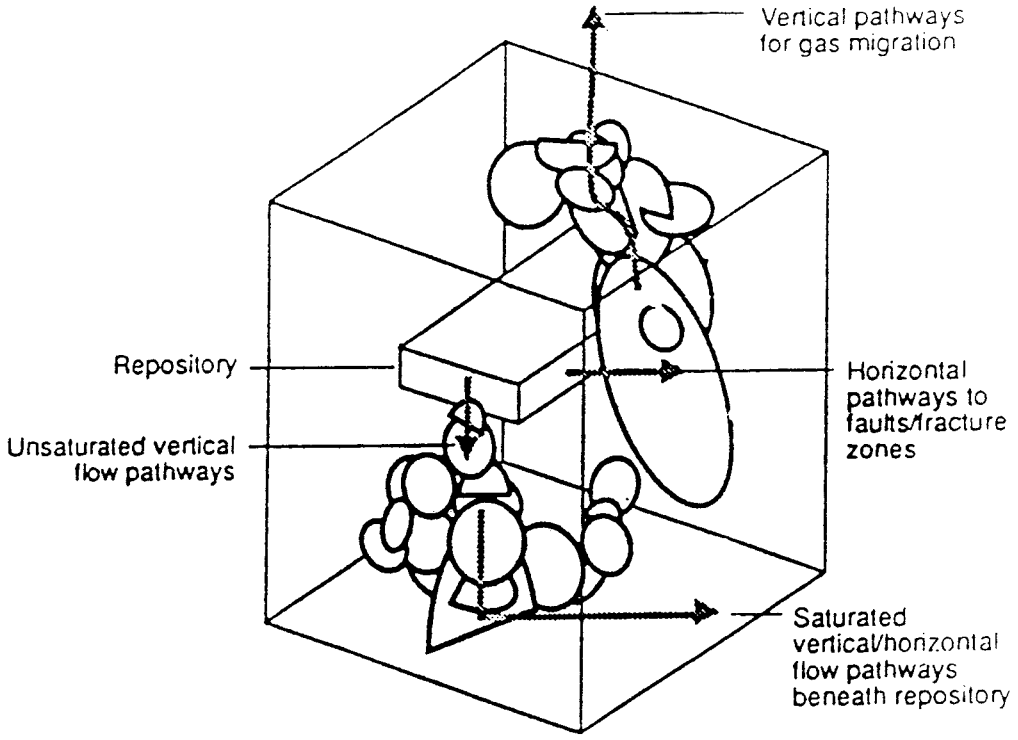

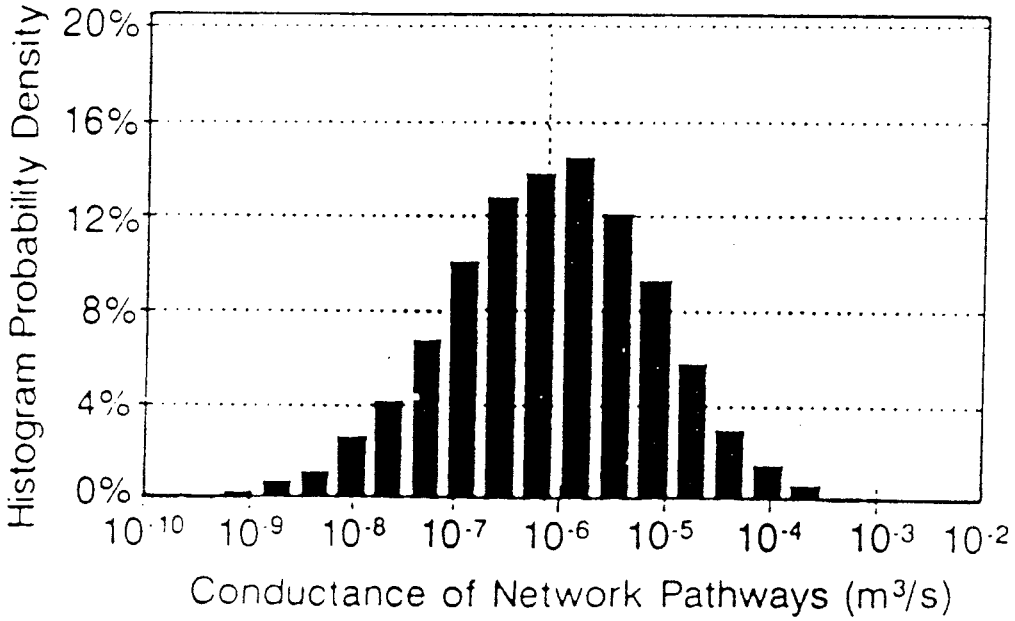

FIGURE 3-3
PATHWAYS ANALYSIS METHODOLOGY

3.2 Modelling Plan

A DFN methodology for achieving the goals of the project has been developed. The methodology is shown schematically in Figure 3-4. The principal components of this methodology are:

- Selection of an appropriate conceptual model for discrete-fracture network geometry.

- Derivation of statistics for fracture properties from site characterization data (outcrop mapping, core logging, and packer test data) to define a **preliminary DFN model** for the rock mass.

- Generalized-dimension flow (GDF) interpretation of transient hydrologic tests to provide **dimensionality** data for model validation, as well as transmissivity and storativity data.

- Simulation of multiple realizations of the fracture geometry within cubes, using the Monte Carlo method. Within each of these cubes, the specific geometry of the fractures is random, but the statistics describing the properties of the fractures match the statistics determined from the field data. Any particular cube is not meant to represent a specific block of rock at the Finnsjön site; rather, it is intended to represent a single **realization** of a possible block within the site. By performing a large number of different realizations, all with the same statistics, the variability of the properties of the blocks (and thus the heterogeneity on the block scale) can be estimated.

- Calculation of the flow field for each simulated fracture network by a finite-element Galerkin approximation of the transient, fully-saturated equations for flow in interconnected, planar fractures.

- Calibration and validation of the derived model by simulation of borehole hydrologic testing and comparison of the simulated dimensionality and transmissivity distributions to the results inferred from GDF analysis of transient packer tests;

- Pathways analysis to determine the probability of a pathway of a given conductance from a repository horizon to a plane at a given distances.

- Simulation of flow through blocks of the calibrated model to determine the minimum scale for equivalent porous medium behaviour, and equivalent conductivity tensors for blocks of rock above that scale. Anisotropy of the rock on the scale of the blocks was assessed in terms of the hydraulic conductivity for any one block in different directions, by simulating flow in response to gradients in the North-South and East-West, and Up-Down directions (Figure 3-5).

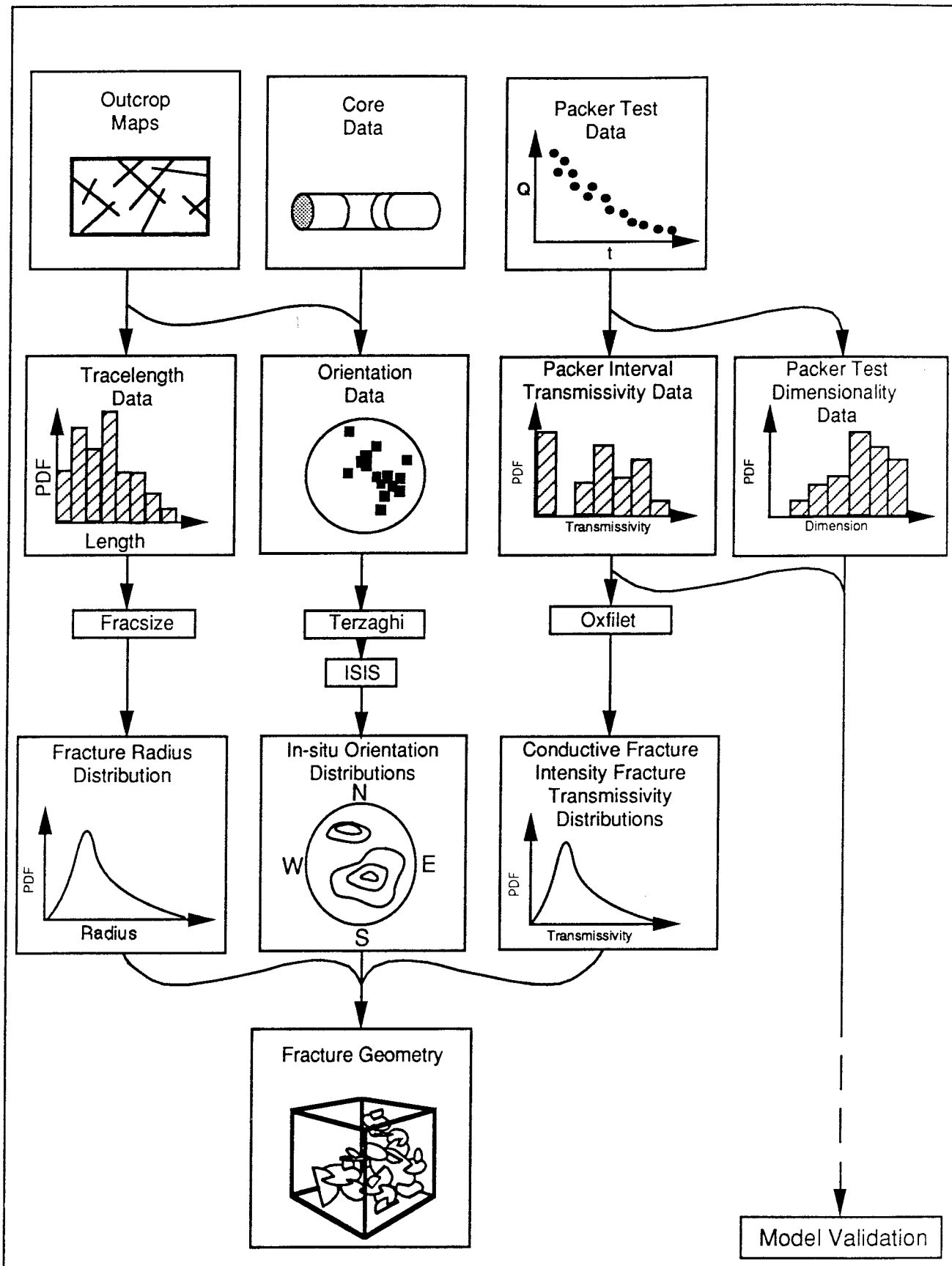

a) **Data Analysis and Conceptual Model Definition**

FIGURE 3-4
OUTLINE OF MODELLING APPROACH

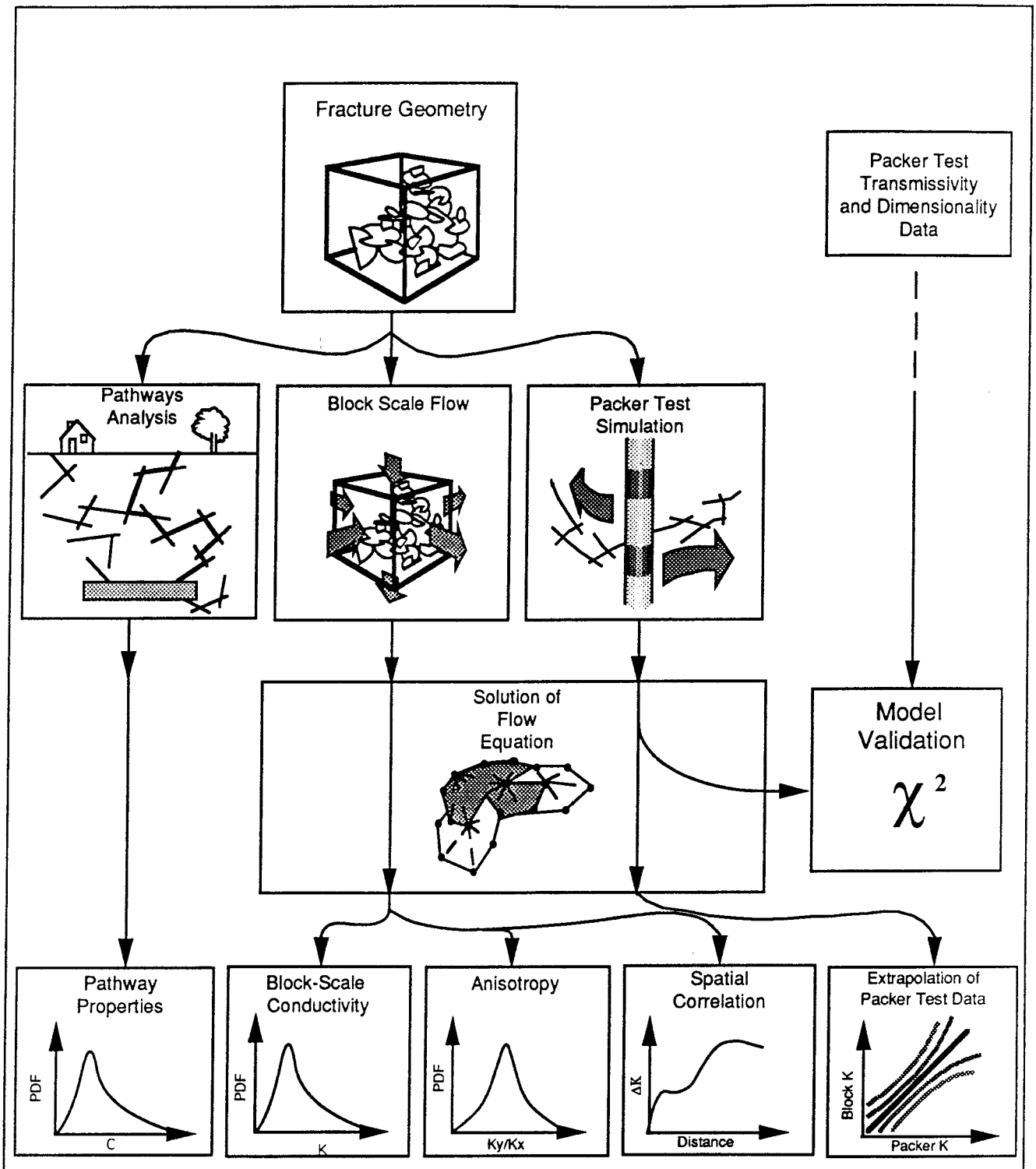

b) Validation and Prediction

FIGURE 3-4
OUTLINE OF MODELLING APPROACH

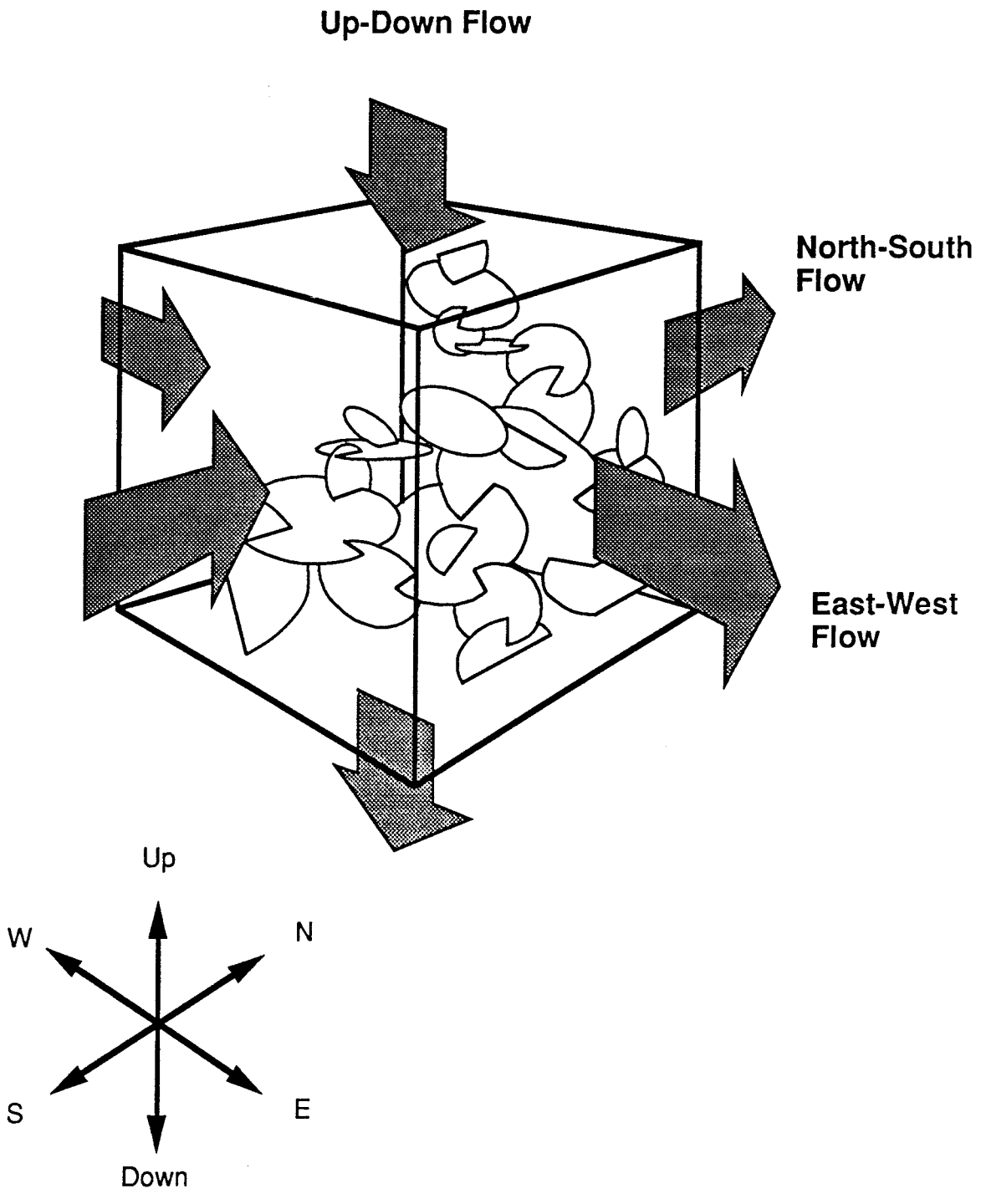

FIGURE 3-5
ROCK-BLOCK ANISOTROPY

- Estimation of spatial correlation among EPM blocks by simulating flow through blocks taken from different locations within a single realization of the fracture population.

- Estimation of the correlation between EPM block conductivity tensors and the results of borehole testing within the blocks or in adjacent blocks.

- Calculation of channel network statistics from block-scale simulations.

Much of the methodology for conceptual model definition was developed previously in a discrete fracture modelling study for the Swedish Hard Rock Laboratory (HRL) site on Äspö Island (Axelsson *et al.*, 1990). The main new developments are the calibration and validation of the model by simulated borehole testing, and the methods for relating DFN results to the specific needs of stochastic continuum and channel network models.

Sections 3.3 through 3.7 describe the components of this methodology in detail. The computer programs that were used to perform these steps are described in Appendix 2. The definition of the model in terms of fracture geometry, conceptual models for flow and transport in the fracture networks, and boundary conditions is described in Chapter 4. The calibration of the model is described in Chapter 5.

This modelling study was planned to consist of two phases, a feasibility study and a full-scale modelling effort. This report describes the results of the first phase, and the implications of these results for the subsequent modelling.

The purpose of Phase 1 was to demonstrate the technology to be utilized in this study, and to determine the suitability of available data on the site for discrete fracture flow modelling. The work performed for Phase 1 included the following:

- Preliminary fracture geometric and data analysis, including fracture flow evaluation of steady state and transient response within packer tests, derivation of cross-fracture transmissivities, and derivation of basic geometric conceptual models and datasets for 25, 50, and 100 meter cubes.

- Demonstration of transient packer test simulations using FracMan and MAFIC, and comparisons of simulated and actual test results.

- 20 rock block simulations for demonstration of the derivation of rock block anisotropy, scale effects, and percolation probability.

- 3 pathways analysis simulations for pathways between a hypothetical repository and two overlying, horizontal fracture zones.

The analysis carried out within Phase 1 provides a clear demonstration of the applicability of discrete fracture technology to the Finnsjön dataset, and with preliminary conceptual models, rock block effective permeabilities, and pathways analyses for confirmation of values used within continuum, stochastic continuum, and safety assessment modelling.

Phase 2 involves full-scale application of the methodologies demonstrated in Phase 1. The envisioned work includes a more rigorous analysis of existing data, and a more thorough verification of hydrologic test interpretations. Additional simulations of flow through rock blocks and pathways analysis are to be carried out within Phase 2, depending upon the needs of the project.

3.3 Discrete Fracture Conceptual Model Definitions

The geometrical and hydrological properties of the fractures used in DFN models are taken from field data. Due to fundamental limitations of site characterization technology, the data needed to model the exact geometries of the fractures in the rock cannot be obtained. Direct observation of fracture geometry and properties is limited to a few boreholes and outcrops. Although a few major conductive features can perhaps be identified within the rock mass by geophysical methods such as borehole radar, the resolution of these techniques is limited by skin-depth effects and interference by lesser features. Since the locations and properties of most of the fractures in the rock cannot be measured by any available means, an approach is needed that is based on some form of statistical characterization of the fracture population.

A discrete-fracture conceptual model is composed of fractures with geometry and hydrology defined in terms of the following characteristics:

- Location
- Shape
- Orientation
- Size
- Intensity
- Transmissivity (single-fracture)
- Storativity

Validation of the model is performed on the basis of aggregate properties of the fracture system, which may include:

- Transmissivity (packer interval)
- Flow dimension (packer interval)

Other properties such as cross-hole hydrological test responses may also be used for validation, when field data are available.

All fracture properties can be viewed as stochastic variables, the **variability** of which is characterized in terms of probability distributions. Because the quantity of data are limited, and because a finite degree of error is associated with any single data measurement, the estimated forms and parameters of the probability distributions for fracture properties have an associated **uncertainty**.

The following sections give definitions for the specific properties comprising the conceptual model.

3.3.1 Location

Location of individual fractures is expressed in terms of a probability density function $f_x(x)$ for fracture centers in 3-D space. The simplest case is the purely random case, referred to as the Baecher conceptual model (Figure 3-6), in which fracture centers are located by a uniform Poisson process in three dimensions, *i.e.*, $f_x(x)$ = constant. The Baecher conceptual model was introduced for rock mechanics applications by Baecher et al. (1977). Other possibilities are defined in terms of particular geometric conceptual models such as:

- Nearest Neighbor -- $f_x(x)$ for "secondary" fractures decreases exponentially with the distance from the nearest "primary" fracture.
- War Zone -- $f_x(x)$ higher in regions bounded by parallel or subparallel polygons, specified either deterministically, or stochastically by identification of subparallel fractures from a set of "primary" fractures.
- Levy-Lee -- Fracture centers located according to a fractal point process, so that $f_x(x)$ is a field of fractal dimension.
- Termination models -- $f_x(x)$ determined implicitly by generation of fractures to match termination statistics.

These conceptual models have been described by Axelsson *et al.* (1990) and by Geier *et al.* (1989). The models describe fracture populations for which the fracture intensity field is locally nonstationary, although the statistical parameters of the models may be spatially homogenous. An exception to this is the deterministic war zone model, which is used to represent observed, large-scale features in site-specific discrete fracture flow models. This particular model is not preferable for interfacing with the stochastic continuum model because it is expected to result in an effective conductivity field that would not be second-order stationary.

For the Phase 1 feasibility study, the only model used was the Baecher model, i.e, the model with $f_x(x)$ = constant. Statistical analysis of tracemap data is planned for Phase 2 to determine which if any of the other models might be applicable. The Phase 2 model for fracture location will be chosen to give the most accurate representation of the system that is possible in the time allotted for simulation.

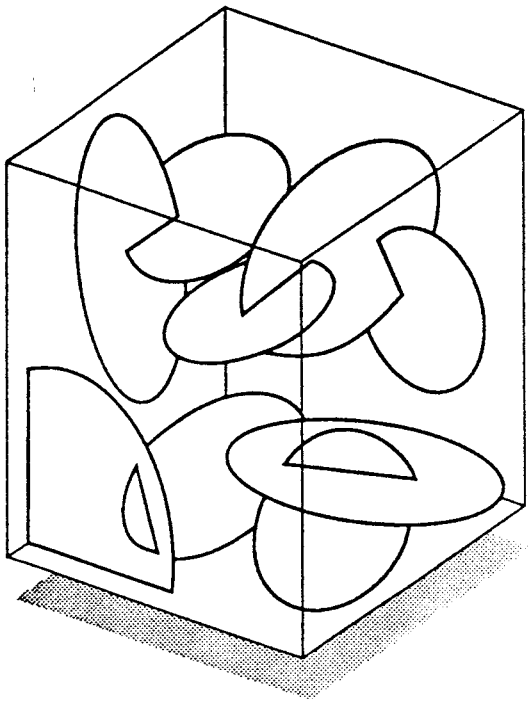

FIGURE 3-6
BAECHER CONCEPTUAL MODEL FOR FRACTURE LOCATION

3.3.2 Shape

In the present model, fractures are assumed to be planar and approximately polygonal. Although curved or undulating fractures are commonly observed in nature, for large populations of randomly oriented fractures, nonplanarity of the fractures is not believed to be of sufficient importance in terms of fracture connectivity to justify the added difficulty of calculating intersections among undulating fractures. Polygonal fractures are used to allow generality in terms of fracture shape. For an isolated fracture, rock mechanics indicates that the shape of fracture should be approximately elliptical, depending upon the stress regime and anisotropy in the rock strength and elastic moduli. When a planar fracture terminates at an intersection with another fracture, the resulting edge is linear. As the percentage of fractures terminating at intersections increases, fracture shape converges to polygonal.

For Phase 1 (the feasibility study), fractures were assumed to be circular. Analysis of fracture tracelength data to obtain fracture size distributions is based on this assumption. Simulated fractures in the Phase 1 model are represented as polygonal (regular hexagonal) approximations to circles. The Phase 2 model may include truncation of fractures at intersections, if this is indicated by analysis of fracture truncation statistics.

3.3.3 Orientation

Fracture orientation is expressed in terms of fracture pole orientations or fracture dip directions. The fracture pole is the direction normal to the plane of the fracture. The variability of fracture orientation can be expressed in terms of either parametric or nonparametric distributional forms for either pole or dip direction. Examples of parametric distributions for orientation are the univariate Fisher distribution (Fisher, 1953), the bivariate Bingham distribution (Bingham, 1964), and the bivariate Fisher distribution (Dershowitz, 1979). Nonparametric characterization of orientation data can be based upon bootstrap or jackknife resampling methods (Efron, 1982).

In both Phase 1 and Phase 2 models, due to the limited amount of orientation information that was available at depth, bootstrap sampling based on a Terzaghi-corrected (to reduce sampling bias) dataset was utilized.

3.3.4 Size

The size of a polygonal fracture is expressed in terms of the "equivalent radius" r_e of the fracture. This is defined as the radius of a circle that has the same area as the polygonal fracture:

$$r_e = \sqrt{\frac{A_f}{\pi}} \tag{3-1}$$

where:

A_f = area of the fracture [L^2]

This definition is suitable for terminated as well as unterminated fractures.

3.3.5 Intensity

The DFN modelling approach is simplified by modelling only the conductive fracture population. In general, only a fraction of the fractures present in the rock are significantly conductive. This is evident from packer tests in borehole intervals that show no measureable conductivity, although core logs show multiple fractures in those intervals. By modelling only the conductive fractures, a realistic prediction can be obtained with considerably less computational effort than would be required to model all of the fractures. For this approach the quantity of interest is the conductive fracture intensity. Using the notation of Dershowitz (1984), this is defined as:

P_{32c} = total area of the conductive fractures in a unit volume of rock [L^{-1}]

This is distinguished from the total fracture intensity:

P_{32} = total area of fractures in a unit volume of rock [L^{-1}]

In principal, P_{32c} can be defined as a probabilistic variable in space, with its value defined in terms of an averaging volume of some specified size. In the Phase 1 feasibility study, P_{32c} was treated as a constant.

The conductive fracture intensity, P_{32c}, is related to the conductive fracture frequency f_c, which is defined as the number of conductive fractures per unit length of line sample (borehole or scanline). The notation CFF is commonly used to denote f_c, but the latter notation is adopted here for convenience.

3.3.6 Transmissivity

The transmissivity at a point ξ on a fracture is defined as the constant of proportionality between flux density and head gradient for two-dimensional, steady Darcy flow in the plane of the fracture:

$$q_i = -T(\xi)\frac{\partial h}{\partial \xi_i} \tag{3-2}$$

where:

q_i	= component of flux per unit width of plane in the direction ξ_i	[L^2/T]
$T(\xi)$	= transmissivity at the point ξ in the fracture plane	[L^2/T]
ξ_i	= ith component of the local coordinate vector ξ	[L]

This is a phenomenological definition in that no particular relationship between transmissivity and the local fracture aperture is assumed. This definition is applicable to fractures with or without infilling. The local transmissivity is assumed to be isotropic (in two dimensions) and independent of the head gradient. The latter assumption may not be strictly true in fractures subjected to high gradients, as in a fracture immediately connected to a packer test interval, in which case turbulent flow may occur at the start of an injection/withdrawal test (Elsworth and Doe, 1986). In such cases, the flow from or to the test interval would be slightly overestimated in the model.

In the simplest model, transmissivity is assumed to be constant throughout any given fracture plane. Examination of single fractures generally indicates that this is not true. Field observations of flow through individual fractures (Abelin *et al.*, 1990) showed that the flow distribution in individual fractures is irregular due to channeling effects. However, the inaccuracy due to this assumption may be slight within the network if details of flow within the fracture can be neglected and the flow between two connected fractures is well characterized by an average, **cross-fracture** transmissivity.

In a more detailed model, transmissivity is considered to vary as a fractal process within the plane of each fracture. Each fracture is recursively discretized into a number of subfractures of approximately equal size (Figure 3-7), and the transmissivity of each subfracture is assigned a distinct transmissivity. This more detailed model is used in the present investigation as a basis for comparing **at-borehole** measurements of transmissivity with cross-fracture transmissivities, in the interpretation of packer test data in fractured rock. This more detailed model may also be applicable for simulation of large-scale channeling within the fracture network.

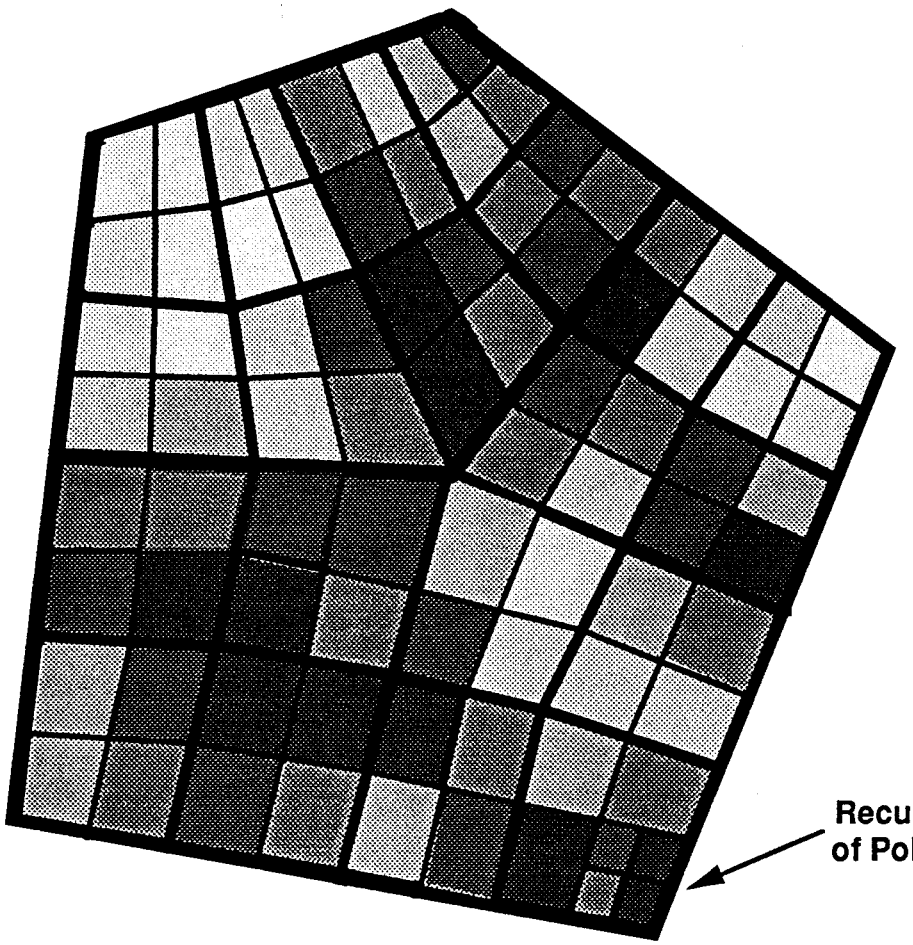

FIGURE 3-7
FRACTAL MODEL FOR VARIABLE APERTURE IN FRACTURES

3.3.7 Storativity

The storativity at a point ξ on a fracture describes the increase in the volume of fluid contained, per unit area of the fracture, in response to a unit increase in pressure

$$S(\xi) = \lim_{A \to 0} \left(\frac{1}{A} \frac{\partial V_w(\xi)}{\partial h(\xi)} \right) \tag{3-3}$$

where:

A	= area in the fracture plane	[L^2]
$S(\xi)$	= storativity at point ξ in the fracture plane	[-]
$V_w(\xi)$	= volume of water contained within an area A around the point ξ	[L^3]

The storativity is related to the fracture normal stiffness, the fluid compressibility, and, if infilling is present, the porosity and compressibility of the infilling material.

3.3.8 Variability and Uncertainty

In hydrological simulations of heterogeneous systems, both the variability and the uncertainty of the model of the system must be recognized.

Variability in the model arises from the natural heterogeneity of the system. In the case of a DFN model, variability is expressed in terms of probability distributions for fracture properties (orientation, transmissivity, *etc.*), the forms and parameters of which can be estimated from field data.

Uncertainty in a model of a heterogeneous system exists whether the simulations are based on a SC, CN, or DFN approach. The uncertainty arises from problems inherent to data collection, such as sample size, sampling bias, sampling accuracy and analysis limitations. In performing risk assessment analysis for a potential repository, each of these problems must be dealt with either by quantifying the resulting uncertainty and including it in the model, or by considering the uncertainty in the interpretation of model results.

- **Sample Size**: The surface exposures used for traceplane mapping, and the boreholes used for packer tests represent a very limited sample of the rock mass. As a result, the true values of the statistics that describe the variability of the rock in-situ may be different from those derived in the data analysis. Sample size limitations can be quantified through sensitivity studies, including techniques for "bootstrap" resampling of the collected data (Efron, 1982). Bootstrap methods allow estimation of the uncertainty in statistical measures by calculating the same statistics for random subsamples of the data, and from these values determining the sensitivity of the statistics to the number of samples.

- **Sampling Bias**: Sampling techniques such as core logging and borehole tests have inherent limitations because they preferentially sample certain ranges of fracture orientations. Theoretical corrections can be applied for biases of this type, when they are recognized. However, such corrections are based on idealized models of the sampling process. Uncertainty due to sampling bias can be quantified only if samples are available at depth for a comprehensive set of sampling orientations.

- **Sampling Accuracy**: Many problems arise from constraints on the resolution of site-characterization methods. The accuracy of transmissivity data is limited by the range and resolution for flux and pressure measurements of the packer testing equipment that is used, as well as the interpretation methods. The accuracy and completeness of fracture data from surface exposures is limited by the methodology and degree of thoroughness that are possible within the scope of the project. Although the data analysis methods used in this study are designed to minimize problems due to sampling accuracy, these problems cannot be eliminated entirely, and they must also be considered in interpretation of the results.

- **Analysis Limitations**: Key assumptions made in analysis can have significant effects on the results of simulations. The effect of these assumptions can, if recognized, be quantified through sensitivity studies. Key assumptions made in the present analysis include the following:

  - Fluxes observed in packer tests represent the sum of the transmissivities of individual fractures intersecting the borehole, and the locations of fractures along boreholes can be described by a stationary, Poisson process.

  - The distributions of properties of conductive fractures (orientation, size, location, shape) are stationary. In particular, it was assumed that the distributions of the geometric properties at depth are not significantly different from those of the fractures observed at surface exposures.

  - Distribution of fracture location can be adequately described by the FracMan conceptual models (Geier *et al.*, 1989).

  These assumptions are discussed in Chapter 4, wherein a description is given of the derivation of parameters for the model.

In a complete analysis such as would be performed in the design of a final repository, these sources of uncertainty could be analysed by quantifying the uncertainties through methods such as bootstrap resampling. Once the uncertainties have been quantified, their effects can be predicted by sensitivity analysis by including the uncertainties as variability in the simulations, or by analytical techniques, as described by Brandstetter and Buxton (1987).

No uncertainty analysis was performed for the Phase 1 feasibility study. However, uncertainty analysis is planned for the Phase 2 modelling. The scope of this analysis should be determined at the outset of the Phase 2 investigation.

3.4 Data Analysis for Preliminary DFN Model

The preliminary DFN model is the model for fracture system geometry prior to calibration. This model is expressed in terms of probability distributions for the discrete fracture properties defined in Section 3.3. This section briefly describes the type of data analysis that must be performed to obtain this information from field data.

A significant benefit of this study is the identification of strengths and weaknesses in the current database for the Finnsjön site, and verification of the interpretation of these data. DFN modelling uses available information directly, including hydrology (single borehole, borehole interference, and regional water balance), solute transport (tracer experiments, geochemistry), and structural geology (regional structure, fracture geometry). When particular information is not available, such as fracture transport porosity, generic assessment of possible values can be used in sensitivity studies to quantify the resulting uncertainty. Table 3.1 summarizes the information necessary for FracMan discrete fracture flow and transport modelling, and the sources that are presently available for that information.

Table 3.1 Data Requirements for Discrete Fracture Modelling

CLASS	FRACTURE PROPERTY	DATA SOURCE
Structural Geology	Set Classification	Lineament and Fracture Maps, Core Logs
	Orientation	
	Conductive Fracture Intensity	Core Logs, and Packer Tests
	Location	Lineament and Fracture Maps
	Size	
	Shape	Fracture Maps, Generic Information
Hydrologic Parameters	Transmissivity	Steady and Transient Packer Test Data
	Dimensionality	Transient Packer Test Data
	Storativity	Transient Packer Test Data, Generic Information
	Transmissivity Variability	Generic Information
Transport Parameters	Lateral Dispersion	Tracer Experiments, Generic Information
	Longitudinal Dispersion	
	Transport Porosity	

Based upon the available datasets, the information on fracture size and orientation at depth is limited. However, within the scope of the SKB 91 project, extrapolation of at-surface data for these properties to depth, and the use of generic information for properties such as transmissivity variability will be sufficient. The following sections outline the methods of analysis for each of the fracture properties. A more detailed presentation of the methodology has been presented by Axelsson *et al.* (1990).

3.4.1 Fracture Orientation Analysis

Three types of data are encountered in fracture orientation data analysis:

- **Complete** orientation data, giving both the strike and the dip of each fracture plane. Examples of complete data include oriented core logs and comprehensive scanline or traceplane maps.

- **Incomplete** orientation data, giving either strike or dip, but not both, for each fracture plane. Examples of incomplete data include unoriented core from vertical holes, and data from horizontal scanlines for which only fracture strike directions are recorded.

- **Uncertain** orientation data, which give neither true strike nor true dip. Examples of this type of data include unoriented core from inclined boreholes, and traceplane data from vertical traceplanes for which only apparent dips are recorded.

Complete orientation data are always preferable, but often due to cost considerations incomplete and/or uncertain data must be utilized. Analysis of incomplete data requires making one of the following assumptions:

- Dips and strikes are independent of each other, or

- The population of fracture orientations can be described in terms of a finite number of probability density functions of some standard form, e.g., the Fisher distribution.

If some complete data are available, these can be utilized in the analysis of incomplete data. Uncertain data can be analyzed by making the latter assumption, or, in the case of unoriented core, by probabilistic extension of the methods described by Hoek *et al.* (1981), by introducing the assumption that any given section of core has been spun a random angle in process of coring and transferral to the core box. The use of probability density functions to deconvolute less-than-complete orientation data is strengthened if some complete data is available.

For both Phase 1 and Phase 2 models, orientations will be simulated using a semi-parametric statistical approach known as the "smoothed bootstrap" resampling technique. This method is a modification of the non-parametrical "bootstrap" resampling technique, which amounts to a random re-sampling of the observed fracture orientations.

The smoothed bootstrap technique is similar to the simple bootstrap technique, except that the measured orientations are assumed to have a slight error, so that the angular distances from the true orientations to the corresponding measured orientations are distributed as a Fisher distribution. The parameter of the Fisher distribution can be estimated from the apparent resolution of the observations (about 5°, for most of the Finnsjön dataset). The smoothed bootstrap method is highly insensitive to whether the orientations are defined in terms of poles or dip directions, if the scatter of the data is large relative to the resolution of the data, as is true of the Finnsjön data.

The orientation dataset used for smoothed-bootstrap resampling is obtained by applying a Terzaghi correction for sampling bias to the data from core logs and cell maps. Incomplete data are combined on the assumption that dip and strike angles are independent. This approach has the advantage of making use of all of the complete data plus all of the incomplete orientation data from at depth, while incorporating only minimal assumptions about the distribution of the orientations.

3.4.2 Fracture Size

Fracture size (radius) probability density functions $f_r(r_c)$ are obtained from fracture and lineament tracelength data. Traces are assumed to represent the lines of intersection between circular fractures and the traceplane (Figure 3-8). The length of these lines may be **truncated** due to the finite extent of the trace plane, or **censored** due to their being overlooked, or due to their being shorter than the minimum length considered by the survey. Analytical methods for deriving $f_r(r_c)$ from tracelength data are available, based upon simplifying assumptions about:

- The form of the distribution (usually assumed to be lognormal).
- The form of the orientation distribution, usually constant or uniform on the sphere.
- The type of censoring (fixed minimum tracelength below which fracture tracelengths are not recorded in the survey.
- Type of truncation at the boundaries of the traceplane (finite width of traceplane, but usually infinite length).

In the present study, a very flexible approach based on simulation is used (Figure 3-9). Equivalent radius distributions are obtained by an iterative, forward modelling approach. Fracture tracelength surveys are simulated using a set of traceplanes having the same orientation and dimensions as the field surveys, and a fracture population that has an assumed size distribution and an orientation distribution simulated by the smoothed-bootstrap technique described above.

Possible fracture size distribution types include lognormal, normal, exponential, uniform, and power-law (defined in Section 4.2) distributions. For each distribution considered, parameters are varied by hand or automatically until an optimal match of the simulated tracelength distribution to the observed distribution is obtained. The "goodness-of-fit" is assessed in terms of Kolmogorov-Smirnov statistics.

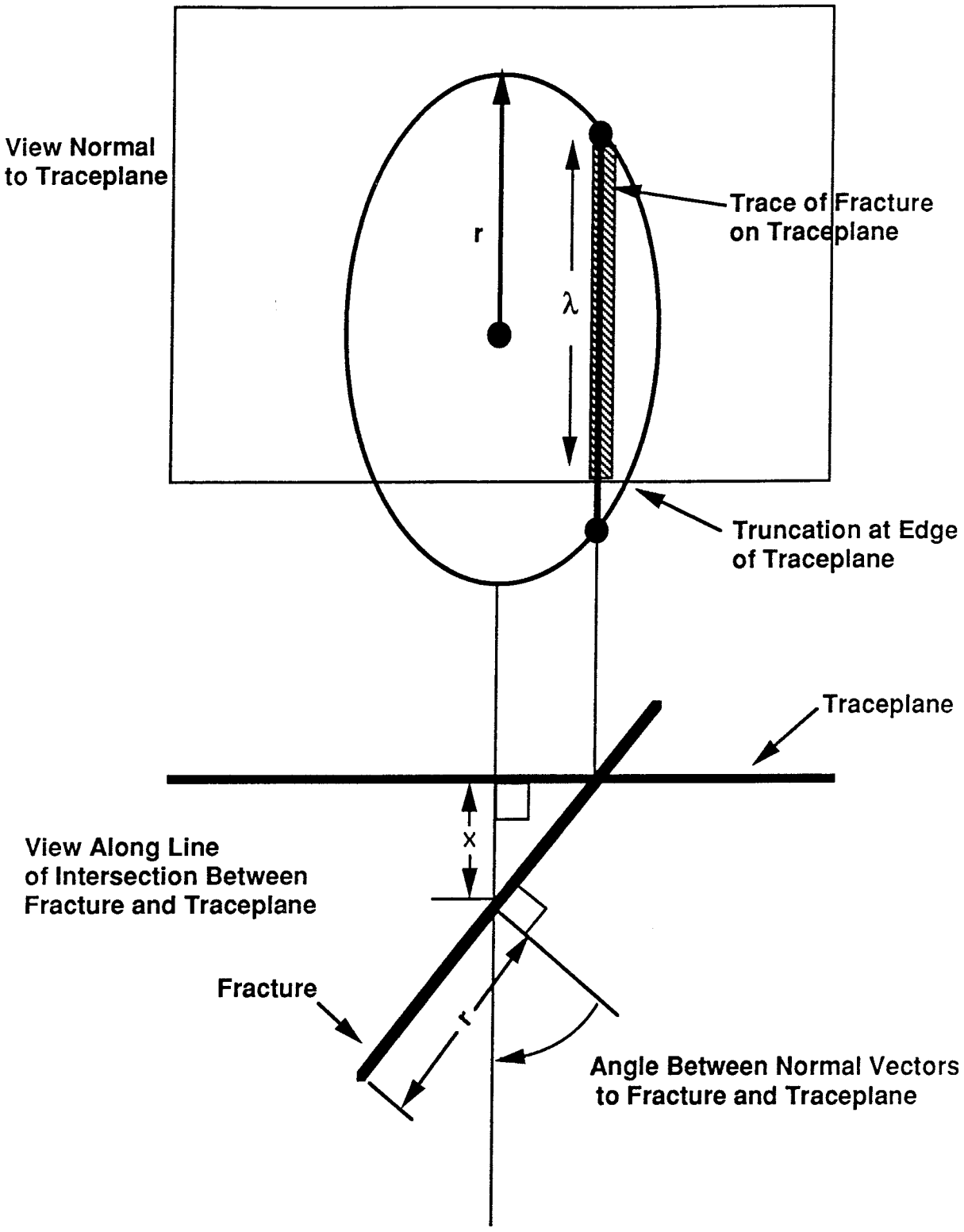

FIGURE 3-8
INTERSECTION BETWEEN
A CIRCULAR FRACTURE AND
A FINITE TRACEPLANE

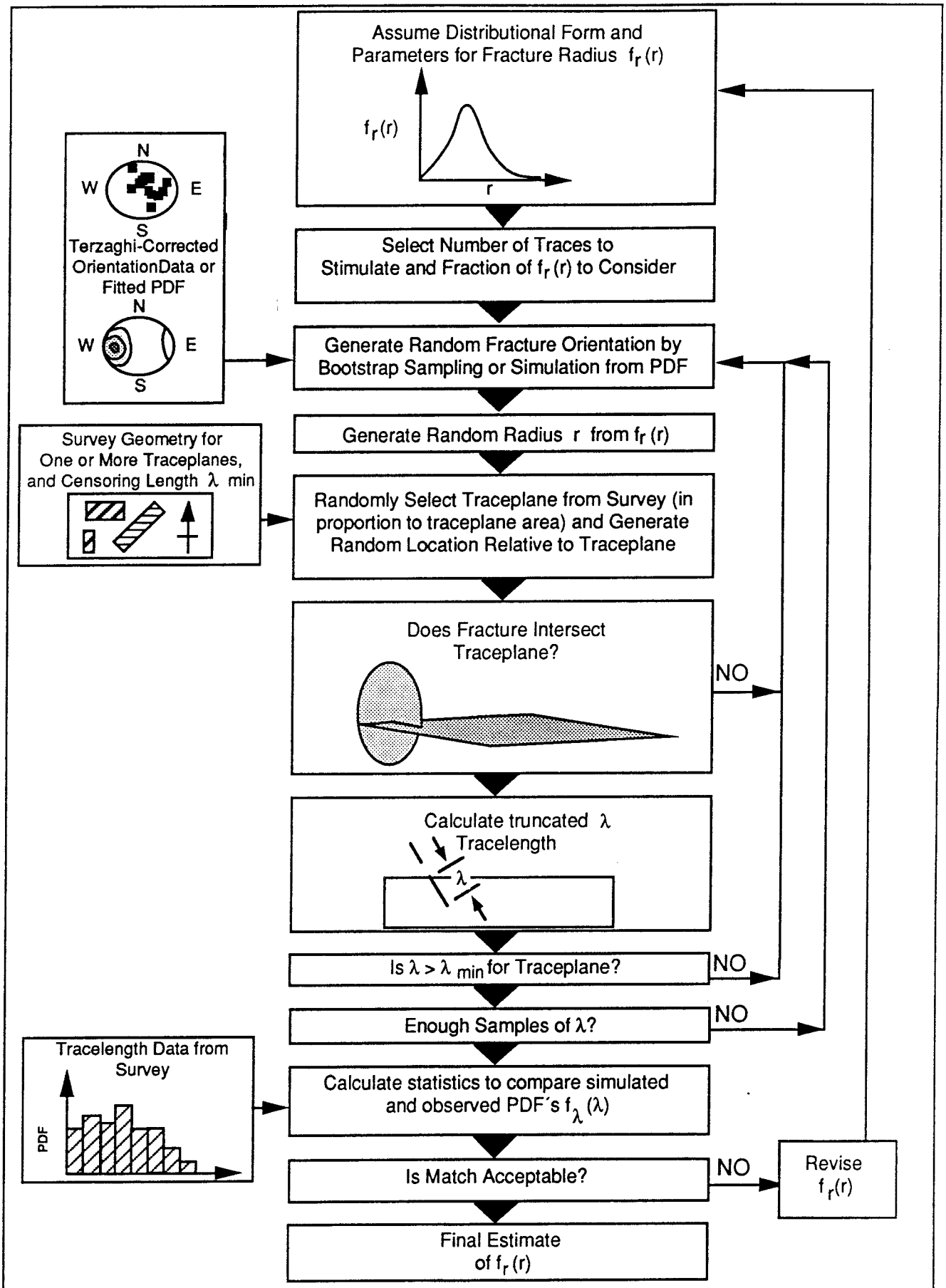

FIGURE 3-9

FRACTURE SIZE ANALYSIS ALGORITHM

This approach explicitly accounts for censoring effects by means of a minimum tracelength that is specified by the analyst. Truncation effects and orientation bias effects are accounted for implicitly by the definition of survey geometry. The derived, parametric distributions (commonly lognormal, exponential, or power-law) are used in simulations of fracture populations for the small-scale model. This analysis is performed using the FracMan module FracSys, described in Appendix 2.

3.4.3 Discrete Fracture Packer Test Interpretation

Hydrologic tests provide information about fracture intensity, transmissivity, and storativity, which can be used to derive the parameters of the preliminary DFN model. Transient test data also provide data on fracture system behaviour that can be used to validate the DFN model, as discussed in Section 3.5. The testing methodology known as "Fixed Interval Length" (FIL) testing, described by Osnes *et al.* (1988), provides the necessary data for statistical derivation of the relevant fracture model parameters.

A discrete-fracture interpretation of FIL packer test results involves three main steps:

- Evaluation of individual packer test results to estimate interval transmissivity (and possibly dimensionality and storativity) for each test.
- Estimation of the effects of within-fracture transmissivity variation (channeling) on borehole measurements of fracture transmissivity.
- Deconvolution of packer interval transmissivity data to estimate the conductive fracture frequency f_c and the single-fracture transmissivity distribution.

These steps are described in the following subsections.

3.4.3.1 Packer Test Analysis

The following discussion applies to the interpretation of single-hole, constant-head (or equivalently, "constant-pressure") tests. The test results that were utilized in the present study came from tests of this type. The advantages of constant-head tests for hydrological characterization of low-permeability, fractured rock have been described by Doe and Remer (1980).

The first step in interpretation of constant-head tests is analysis of the records for flow or pressure *vs.* time to estimate packer interval transmissivities. The simplest approach is to analyze the results according to a steady-state interpretation such as Moye's formula (Moyes, 1967).

Steady-state interpretations are made based on the assumptions that:

- Approximately steady flow has been achieved.
- The flow in all tests is of one regular, simple geometry (spherical, in the case of Moye's formula).

The applicability of the first assumption is generally decided by the personnel performing the test, who terminate the test when the flow appears to have reached steady-state. The applicability of the second assumption is questionable for granitic rock. In a given set of tests in fractured, low-permeability rock, a range of flow geometries may be expected (Karasaki, 1986; Doe and Geier, 1990). Deviations from the assumed flow geometry can be checked by type-curve analysis of the flow *vs.* time records.

The reevaluation of constant-head tests to assess the effects of variable flow geometry, using assumptions appropriate for fractured rock, is an important aspect of the present study. Classical type-curve interpretation methods for constant-head tests generally consider homogeneous aquifers (or fractures) and very simple flow geometries. The three major flow geometries are linear flow, cylindrical flow, and spherical flow (Figure 3-10). The hydraulic response of a single constant-head test in fractured rock may reflect one or any combination of these flow geometries during the test, or a flow geometry intermediate between linear and radial, or radial and spherical.

The interpretation of packer tests is very sensitive to the flow geometry. The present study gives estimates of the errors in interpreted values of interval transmissivity that may result from an incorrect assumption about the actual flow geometry. The issue of flow geometry is of importance in evaluating well tests that provide the basis for SC and/or CN models.

Flow geometry is also of interest for validation of DFN models, because flow geometry is an expression of fracture network connectivity. In well-connected fracture networks, packer tests that affect a large volume of rock will tend to display linear or radial flow in early time, with a transition to spherical flow in later time (Karasaki, 1986). In less well-connected fracture networks, the transition to spherical flow will occur later in the test, or may not be seen at all. In very poorly connected fracture populations, boundary effects due to the termination of a fracture networks may be expected (Doe and Geier, 1990). Section 3.5 describes the use of flow geometry and simulated packer testing as a method for validating DFN models.

The present project follows a generalized approach to packer test interpretation, in which the flow test geometry is not assumed, but rather is viewed as a quantity, **flow dimension** that is measured during the packer test. This approach is based upon a theory of generalized-dimension flow (GDF) that has been developed by Barker (1988). A brief summary of this theory is given in Appendix 3.

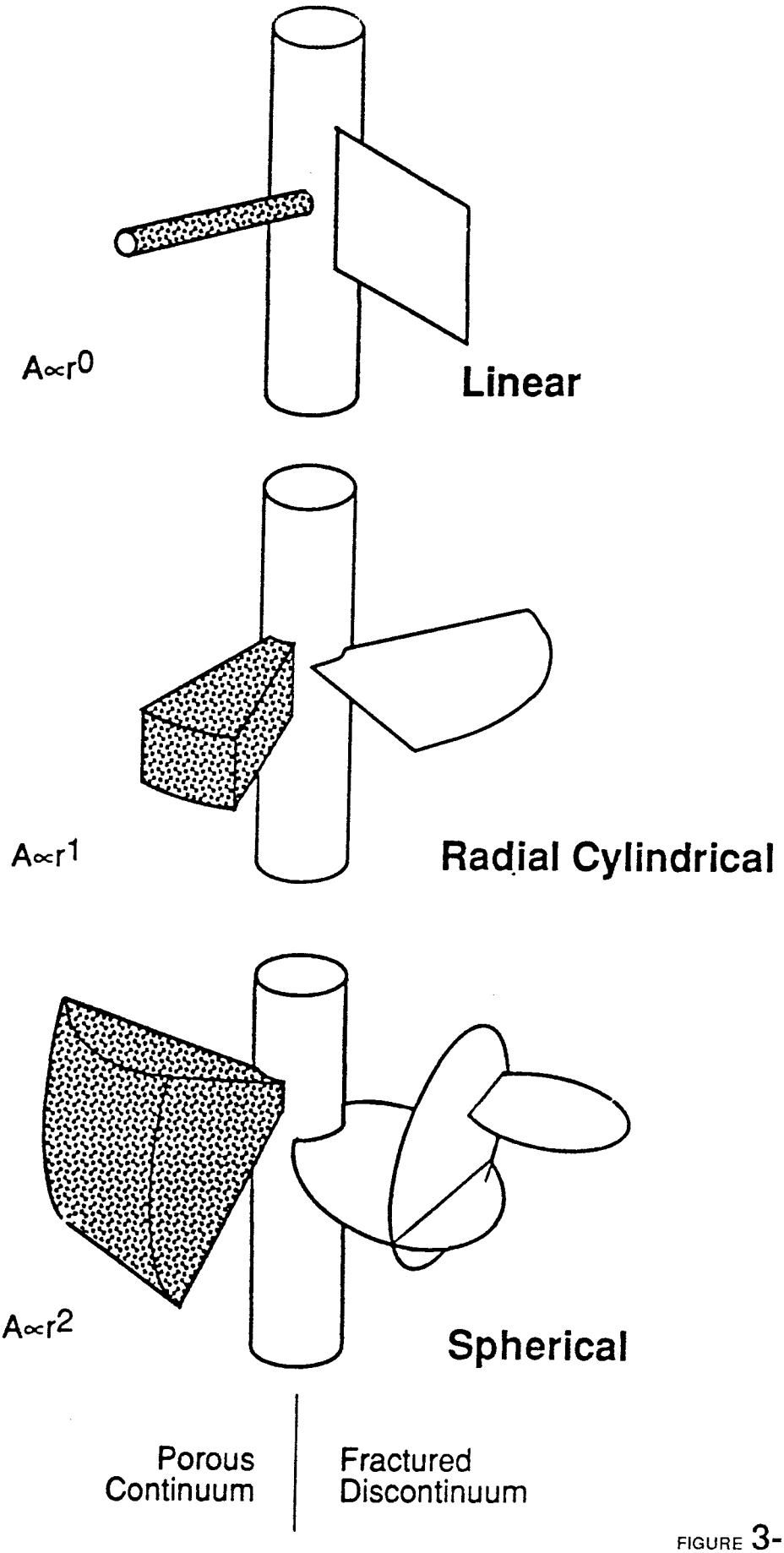

FIGURE 3-10
FLOW DIMENSION IN WELL TESTING

The generalized flow dimension is defined in terms of a conduit for which the product of conductivity and cross-sectional area increases (or decreases) as a power of the distance:

$$\left[K_c(r)A_c(r)\right] \propto r^{D-1} \tag{3-4}$$

where

K_c	= conduit conductivity	[L/T]
A_c	= cross-sectional area of conduit	[L^2]
D	= the flow dimension	[-]
r	= distance from the packer interval	[L]

The cases of integral flow dimension with D = 1, 2, and 3, correspond to the conventional linear, cylindrical, and spherical flow geometries, respectively, for the case of constant K_c. When the flow dimension is not integral (*e.g.*, D = 2.25), the flow geometry is referred to as being of **fractional dimension.**

GFD type-curve analysis for constant-head tests, as described in Appendix 3, produces estimates of interval flow dimension, transmissivity, and storativity. The relative accuracy of the estimates of dimension and transmissivity depends upon the flow geometry. For values of $D < 2$ (*i.e.*, subradial flow), the dimensionality of flow can be estimated quite precisely, while the transmissivity becomes more ambiguous. For higher values of flow dimension, the transmissivity estimates are improved, but flow dimension becomes ambiguous. The issue of accuracy is discussed more thoroughly in relation to actual analyses in Appendix 6.

3.4.3.2 Effects of Channelization on Packer Test Results

A discrepancy exists between borehole measurements of fracture transmissivity and the effective transmissivity of a fracture for flow through a fracture network. This discrepancy arises due to variability in local transmissivity within each single fracture. Single hole hydrologic tests provide the **at-borehole** hydrologic properties of the fracture, *i.e.*, the properties of the fracture that control the steady state and transient response in most hydrologic testing. DFN modelling usually is based on the **cross-fracture** transmissivity, *i.e.*, the properties of the fracture which control flow between interconnected fractures. The relationship between these two values depends upon the scale and structure of the fracture roughness (and infilling, if present).

Probabilistic relationships between at-borehole and cross-fracture transmissivity can be developed by Monte Carlo simulation of the two types of flow in single fractures of variable transmissivity. Preliminary modelling experiments of Kenrick *et al.* (1987) indicated that an approximately logarithmic correlation exists between at-borehole transmissivity T_{fb} and

cross-fracture transmissivity T_f, *i.e.*,

$$T_{fo} = T_f^{c1+\epsilon} \tag{3-5}$$

where:

c_1 = an empirical constant
ϵ = a random term

The precise form of this correlation and the distribution of the "noise" component can be derived by further modelling experiments based on the methodology of Kenrick *et al.* This derivation requires knowledge of the variation of transmissivity of the fractures. Preferably the description of this variation should be based upon fracture roughness or flow channelization data gathered from the site. In the absence of site-specific data, generic fracture roughness data or channelization data can be used, such as the data gathered within the Stripa Project by Hakami (1989) and Abelin *et al.* (1990). A demonstration of this approach is described in Chapter 4.

3.4.3.3 FIL Test Analysis

Interval transmissivities obtained from hydrologic tests analysed by conventional methods or by fractional dimension methods can be used to derive distributions of fracture transmissivity and conductive fracture frequency f_c using the maximum likelihood algorithm, OxFILET (Figure 3-11), described in detail by Axelsson *et al.* (1990). The algorithm uses forward modelling to find the combination of f_c and fracture transmissivity distribution $f_T(T_f)$ that gives the best match to FIL tests.

The analysis of Axelsson *et al.* did not consider the possible discrepancy between at-borehole transmissivity T_{fo} and cross-fracture transmissivity T_f that may be caused by local transmissivity variability or channelization. This discrepancy can be taken into consideration by a slight revision of the OxFILET algorithm, by incorporating the correlation between T_{fo} and T_f (as estimated by single-fracture modelling experiments) in the forward modelling approach as follows:

FIL packer tests are interpreted in terms of assumed or inferred flow geometries to obtain an observed distribution of packer interval transmissivities $f_{Ti}(T_i)$. A Poisson distribution for the number of fractures per test interval is assumed. A distribution type (lognormal or exponential) for cross-fracture transmissivity $f_T(T_f)$ and initial values of f_c and the distribution parameter(s) for $f_T(T_f)$ are assumed.

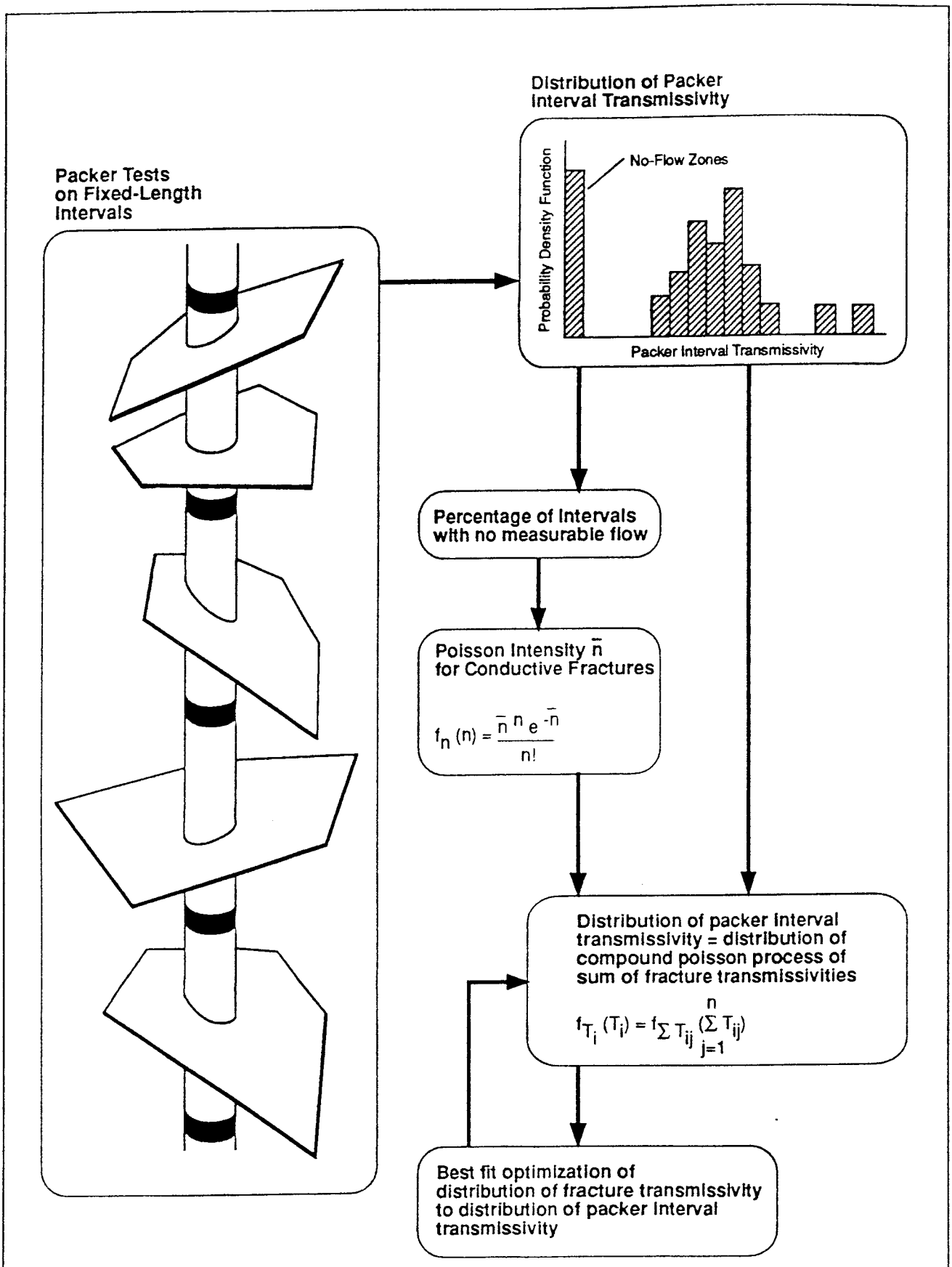

FIGURE 3-11
OXFILET PACKER TEST INTERPRETATION ALGORITHM

Multiple well test intervals are simulated. The transmissivity T_i of each interval is calculated as the sum of a random number N of at-borehole transmissivities:

$$T_i = \sum_{j=1}^{N} T_{fo_j} \tag{3-6}$$

where the T_{fo} are simulated from the compound Poisson process defined by the assumed transmissivity distribution coupled with the correlation between T_{fo} and T_f obtained by the Monte Carlo simulations described above. The value of f_c and the parameter(s) of $f_T(T_f)$ are varied by trial-and-error until a best-fit match is obtained.

This algorithm has several limitations:

- The packer interval transmissivity is assumed to be the sum of independent fracture transmissivities. Thus the approach does not account for the effect of fracture networks; rather, it assumes that fractures act as parallel conduits.

- Flow paths connected to a test interval in general consist of multiple fractures. The OxFILET approach implicitly assumes that the well test response is completely dominated by the first fracture in each flow path intersected. In reality, the test response may be affected by fractures further from the borehole along the flow path, depending on the duration of the test, particularly if the transmissivity of the first fracture is high relative to the fractures that are further from the borehole.

- One-dimensional flow paths, such as fracture channels at fracture intersections have a low probability of intersecting a borehole, and are therefore under-represented in the data.

The significance of these limitations should be assessed in using this technique for a full-scale safety assessment. This can be done through small-scale sensitivity studies, consisting of simulations of the well test sampling process, to estimate the magnitudes of errors thus introduced. The preliminary model validation performed for Phase 1 shows how this can be done. If these limitations are found to be significant for a fracture population similar to that at Finnsjön, the OxFILET algorithm should be generalized to remove or reduce the limitations.

The Phase 1 analysis used an interpretation approach that was simplified in two respects:

- Interval transmissivities estimated from continuum analyses were used, due to the limited number of tests that could be analyzed by application of the fractional-dimension approach.

- The assumption was made that T_{fo} and T_f are identical, because single-fracture modelling to estimate the form of the correlation between T_{fo} and T_f had not yet been performed.

These simplifications can be removed in the Phase 2 analysis.

3.4.3.4 Conductive Fracture Intensity

The conductive fracture intensity P_{32c} is related to the conductive fracture frequency f_c determined from the OxFILET analysis, by a factor C_p:

$$P_{32c} = C_p f_c \tag{3-7}$$

C_p is constant for a given orientation distribution and set of borehole orientations. This factor can be calculated analytically for a few special cases of orientation distributions; for the general case it can be obtained by simulation of borehole sampling using smoothed bootstrap resampling of the orientation distribution. This analysis can be performed using the FracMan module FracWorks, described in Appendix 2.

3.4.4 Storativity

The storativity of single fractures S_f is truly difficult to determine from single-borehole measurements, due to the confounding effect of uncertain flow geometry (Doe and Geier, 1990). Cross-hole packer tests provide information about the storage capacity of the fracture networks between boreholes, but are impossible to interpret in terms of single-fracture storativity because of the large number of fractures that may be affected by a single test.

Realistic values of S_f are needed for transient predictions using DFN models. In particular, for the present study reasonable storativity values are needed for simulations of packer testing, which are used in the validation and calibration of the present model. The problem of storativity is not an issue in the interpretation of tests for which only steady-state data are available.

Calibration of the fracture storativity distribution is possible by simulation of cross-hole testing using discrete fracture modelling. However, this approach suffers from the problem of non-uniqueness. Many different distributions for storativity may give approximately the same simulated cross-hole test results. Thus some assumption must be made about the form of the single-fracture storativity distribution.

One possibility is that storativity is correlated in some fashion to transmissivity. For a planar fracture with uniform aperture the transmissivity is proportional to the cube of aperture, while storativity is proportional to aperture (Doe and Osnes, 1985). Therefore for ideal planar fractures the relationship between transmissivity and storativity may be expressed as:

$$S_f = A_1 T_f^{-1/3} \tag{3-8}$$

where A_1 is a proportionality constant related to the viscosity and density of the fluid.

This suggests a possible form for a correlation between transmissivity and storativity:

$$S_f = A_1 T_f^{A_2 + A_3 \epsilon} \tag{3-9}$$

where:

A_2, A_3 = dimensionless constants

ϵ = a random, Gaussian deviate with zero mean and unit standard deviation

Other forms of correlation are of course possible. The identification of a proper form may be possible from a compilation of laboratory data on single-fracture normal stiffnesses and transmissivities, but this would go considerably beyond the scope of the present modelling study. The quantity and quality of transient test data available for the present study are very limited (as discussed in Appendix 7), and therefore the effort required for such a compilation is not justified.

The form of correlation given in Equation 3-9 is, at least, not implausible, since it reduces to the correct form for ideal, parallel-plate fractures when A_2 = 1/3 and A_3 = 0. For non-ideal fractures, also, the idea that storativity increases with transmissivity seems likely, due to the effects of both fracture stiffness and water compressibility. Since more transmissive fractures contain more water, the fraction of storativity due to water comressibility is expected to be higher for more transmissive fractures. Also, since higher-transmissivities tend to have less contact area (Walsh, 1981; Tsang and Witherspoon, 1983), the normal stiffness of more transmissive fractures is expected to be lower, and thus the fracture-stiffness component of storativity is expected to be lower as well.

A rough estimate of the parameters of this relationship can be made by performing a log-linear regression on interpreted values of interval storativities S_L versus T_L for packer test data. This approach is crude in that it does not account for the possibility of multiple fractures, or for the possibility of large errors in the evaluation of S_L. However, preliminary sensitivity studies show that, for the packer test simulations used in the Phase 1 calibrations, the results are not highly sensitive to a variation of the correlation coefficients within an order of magnitude. The nature of the sensitivity can be quantified by more extensive sensitivity studies in Phase 2.

3.4.5 Fracture Shape

Fracture shape is determined by analysis of termination statistics. Termination statistics can be expressed in the following forms:

$$t_p = t_{fi}/I_i$$

$$t_{\%} = t_{fi}/(t_{fi}+t_{ri}) \cdot 100\% = t_{fi}/(2P_{32}) \cdot 100\%$$

$$t_v = (t_{fi}+t_{ri})/(2P_{32})$$

where

t_p	=	Termination probability
t_{fi}	=	Number of fracture terminations at fracture intersections per unit area mapped
t_{ri}	=	Number of fracture terminations in intact rock per unit area mapped
I_i	=	Number of fracture intersections per unit area mapped
$t_{\%}$	=	Percentage of terminations mapped which occur at fracture intersections
t_v	=	Percentage of possible fracture terminations which were recorded in area mapping survey.

For the Enhanced Baecher and Nearest-Neighbor models FracMan utilizes termination probability t_p as the measure for fracture shape. For the Baecher model with terminations at intersections, FracMan uses the termination percentage $t_{\%}$. In order to properly simulate all FracMan geometric conceptual models, it is necessary to map both termination modes (t_{fi} and t_{ri}), and fracture intersection intensity I_i.

For the Phase 1 model, the ordinary Baecher model with circular fractures was used, so termination statistics were not compiled. However, a large number of terminations are visible on the trace maps from the Finnsjön site, and hence termination statistics should be developed for the Phase 2 model.

3.4.6 Location

In the Phase 1 simulations described in this report, only the simplest model for fracture location, the Baecher model was used. In this model, fracture location is assumed to be uniformly, randomly distributed in space according to a stationary, Poisson process. Thus fracture location is specified entirely by the P_{32}, intensity, calculated as described in Section 3.4.3.4.

3.5 Conceptual Model Calibration and Validation

Application of the procedures outlined in Section 3.4 produces a preliminary DFN model. This model can be validated, and, if need be, calibrated by comparing the reponse of the model to the observed results of transient packer testing. This is carried out as follows:

- Multiple realizations of the DFN model, including variation of fracture transmissivity on the fracture plane (i.e., "channeling"), are produced by Monte Carlo simulation.

- Constant-pressure, FIL packer tests are simulated within these realizations.

- The simulated FIL tests are analyzed in terms of arbitrary-dimension flow geometry. The analysis of simulated packer tests yields simulated distributions of interpreted flow dimension ${}^{s}f_{DL}(D_L)$ and interval transmissivities ${}^{s}f_{TL}(T_L)$ for the given packer interval length L.

- The simulated distributions are compared to the observed distributions of interpreted flow dimension ${}^{o}f_{DL}(D_L)$ and interval transmissivities ${}^{o}f_{TL}(T_L)$, obtained by analysis of actual FIL test data according to the same techniques.

- If the match between simulated and observed packer test responses is adequate, the preliminary DFN model is considered to be validated. If not, model must be calibrated. This can be done by modifying the underlying parameters of P_{32} and $f_{Tf}(T_f)$ iteratively, to match the observed and simulated distribution.

In conventional SC methods, type curves are used to derive effective parameters that match the observed behavior of the individual fractures tested. These effective parameters are then applied to the rock blocks. It is not possible to validate this approach by simulation, since the same parameters are used in both observation and modelling. The approach described above is in some ways a more credible validation, because the tests are used to derive more fundamental properties of fractures, and these fractures must then be re-aggregated within the conceptual model to predict the test response.

In Phase 1, only a small selection of FIL tests were chosen for arbitrary-dimension analyses; all of these tests were for 2m interval lengths. Also, variability of transmissivity within fractures was not included in the DFN model. The following extensions of this procedure should be performed for the Phase 2 DFN model validation and calibration:

- Arbitrary-dimensional interpretation of all transient FIL tests for which reasonably good data is available.

- Simulations of 2m and 20m packer tests centered in rock blocks simulated from the preliminary fracture geometric model, including variable transmissivity within the fracture plane.

- Validation/calibration of the model by comparing the simulated ${}^{s}f_{DL}(D_L)$ and ${}^{s}f_{TL}(T_L)$ with the observed ${}^{o}f_{DL}(D_L)$ and ${}^{o}f_{TL}(T_L)$ for L = 2m and L = 20m.

The inclusion of variable aperture within the fracture plane, in particular, is necessary to make the validation/calibration procedure consistent with the extended OxFILET algorithm.

3.6 Discrete Fracture Pathways Analysis

The DFN model derived and validated as described above can be used to quantify the occurrence and properties of preferential pathways, by the methodology of pathways analysis. The properties of these pathways may be related to CN model parameters.

Pathways analysis (Dershowitz and Black, 1990) is the study of the occurrence of hydrologically continuous pathways between a **source** and any number of defined **targets**. An example of the application of this analysis is shown in Figure 3-3, in which the source is a repository and the target is the plane representing the surface environment. Pathways may be formed by individual faults or fractures, or by networks of interconnected features, possibly including short bridges through intact rock. **FracMan** includes routines which search through all fractures within a geologic realization to identify possible pathways and their properties, using a dynamic programming methodology (Figure 3-12).

Examples of output from this analysis are:

- Distributions for the probability of occurrence of pathways which exceed established flux or solute transport guidelines,
- Distributions of pathway conductance, transport porosity, and reactive surface area,
- Spatial distribution of pathways, as an input to the design of a repository which avoids pathway locations.

Note that this analysis does not require flow modelling, and does not address issues of radionuclide dispersion or retardation. Instead, it addresses the existence of preferential pathways for radionuclide migration, and the properties of those pathways.

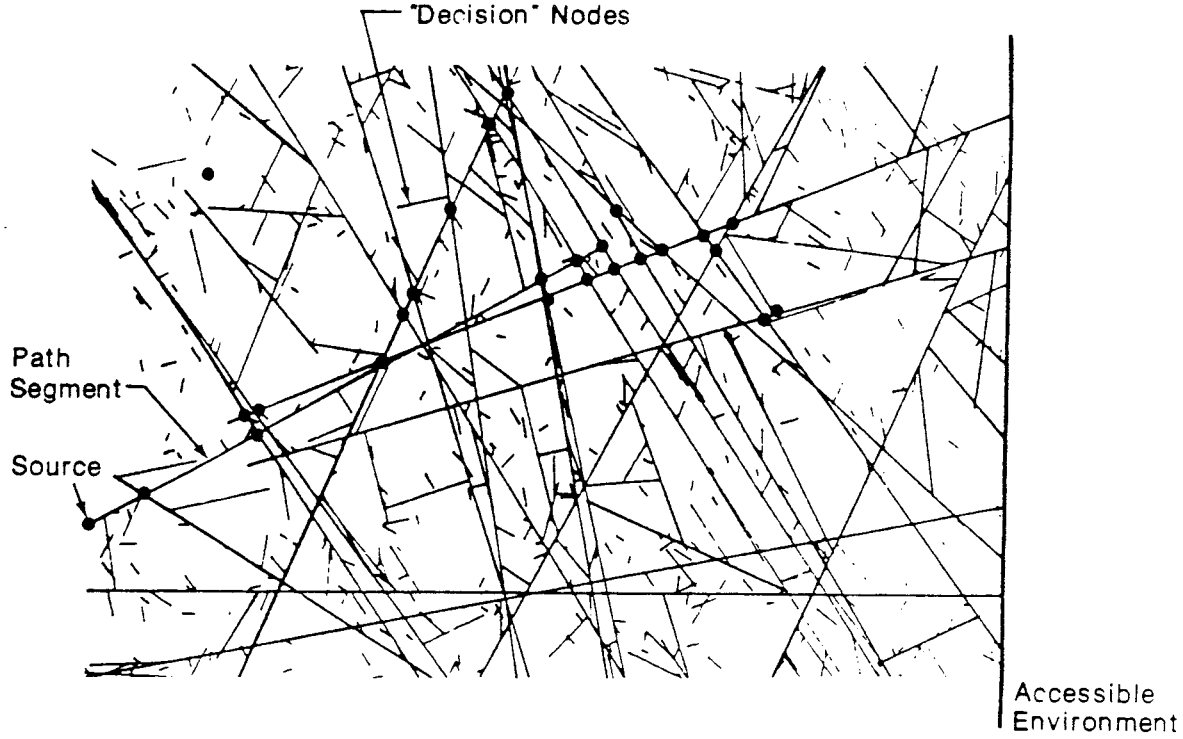

Dynamic Programming Goal: Search Routes for route which minimizes travel time to Accessible Environment, given constraints of network topology, and velocity in each segment.

FIGURE 3-12
FRACTURE NETWORK ANALYSIS

In Phase 1, an example of the application of pathways analysis was demonstrated which gives a rough prediction of the number of pathways between a rectangular "repository" and a plane representing a major fracture zone such as Zone 2, using an adaptation of the Phase 1 DFN model. The analysis gives the distribution of **pathway conductance**, defined as the geometric mean of the effective conductances of each fracture comprising a given pathway, where the effective conductance C_e is estimated as:

$$C_e = T_f L_e \tag{3-10}$$

where L_e is the effective length of the fracture within the pathway, defined as the mean distance between the two line segments of intersection between the fracture and the two fractures that it intersects in the upstream and downstream directions. In addition, this analysis gives the total storage for each pathway, defined as the sum of the products of storativity and area for all fractures in the pathway. Other properties of the identified pathways can be easily claculated by adaptation of the algorithms for postprocesing the results of the pathways analysis.

The pathways analysis demonstration in Phase 1 showed that the methodology was not efficient for the specific geometry of the Phase 1 DFN model, due to a high degree of interconnection among fractures, as discussed in Chapter 5.

3.7 Equivalent Porous Medium Characterization

A validated DFN model can be used to support SC modelling by providing information on the variability, anisotropy, and heterogeneity of rock mass effective hydraulic conductivity. The basic approach is to generate fracture populations within rock blocks of a given scale *s*, and to simulate the response in terms of flow within the blocks to various configurations of boundary conditions. Analysis of the simulated flow response for a well-chosen set of boundary conditions will provide information about the appropriateness of a SC model on that scale. The appropriateness of a SC model is assessed in terms of the adequacy of Darcy's law for explaining the flow response of the blocks to a variety of head gradients. If appropriate, estimates of the variability and anisotropy of the effective hydraulic conductivity on that scale can be obtained.

Analysis of the nature of the heterogeneity (*i.e.*, spatial structure) of these properties requires simulation of blocks much larger than the target scale, and flow simulations of blocks on the target scale, taken from within those larger blocks (Figure 3-13). The heterogeneity of flow properties on the target scale can then be described in terms of covariograms, by analysis of the spatial variation of flow properties with respect to separation distance between blocks.

The simplest way of estimating the hydraulic conductivity of target-scale SC blocks with DFN models is the **permeameter method**. In this approach, flow is simulated through a cube of rock by imposing head gradients in each of three orthogonal directions x_i (i = 1,2,3) corresponding to North-South, East-West, and Up-Down. The total flux Q_i flowing from the downgradient side of the cube is divided by the cross-sectional area of the cube to a permeameter estimate of the conductivity tensor, ${}^{p}K_{ii}$ in each direction x_i.

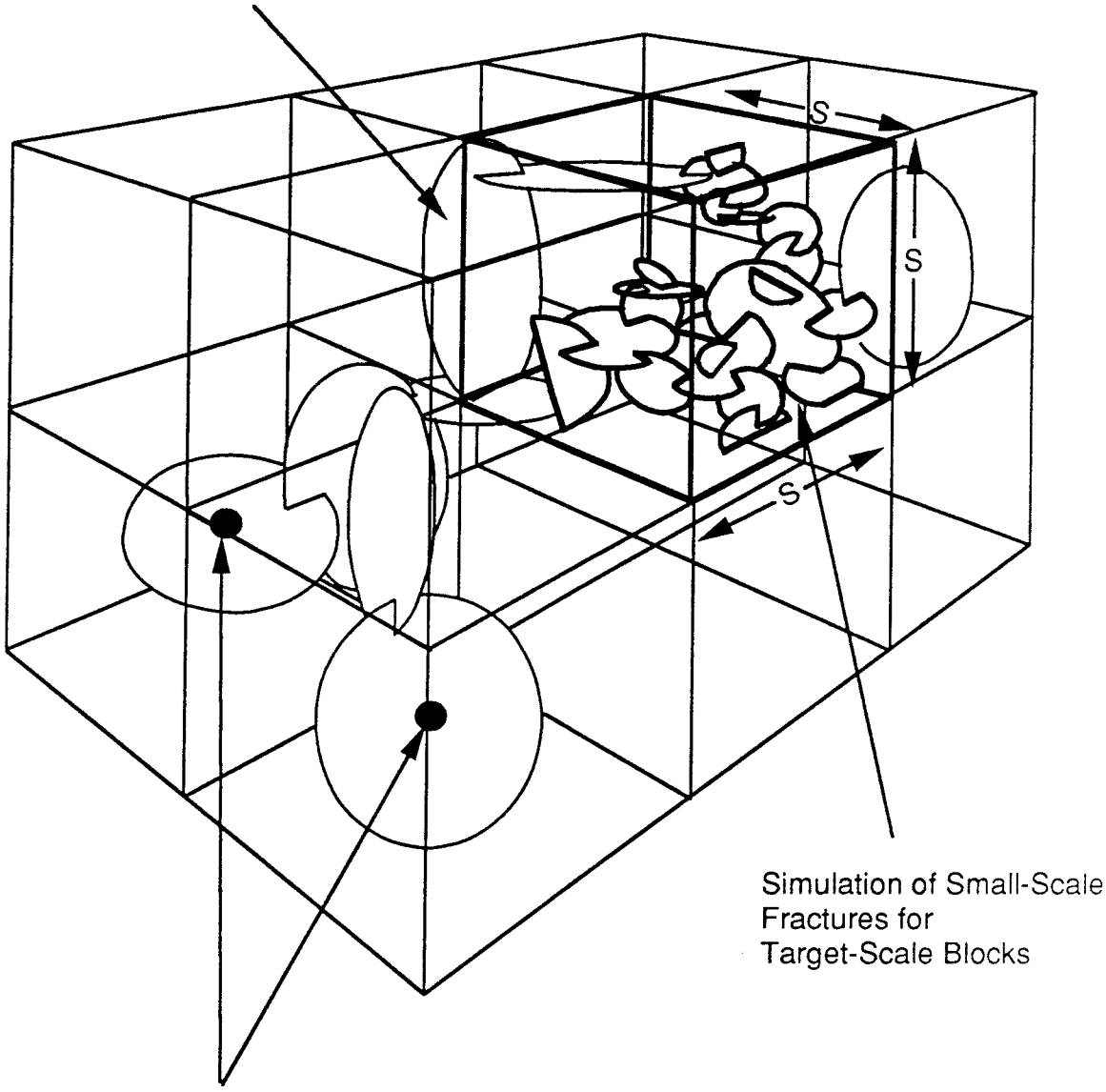

FIGURE 3-13
CONCEPTUAL MODEL FOR SPATIAL CORRELATION AMONG BLOCKS

For each block, flow is simulated in three directions parallel to the coordinate axes, using no-flow boundaries on the sides parallel to the flow direction (Figure 3-14). This type of boundary can result in network truncation at the edges of the model region, potentially ***reducing*** the flux through the fracture system.

The principal alternative to this choice of boundary conditions is to impose constant-head boundary conditions, and thereby simulate a permeable medium on the edge of the model region. This has the potential to ***increase*** the flux through the fracture system. Constant-head and no-flow boundary conditions on the boundaries parallel to the flow direction can thus be seen as upper and lower bounds on the effects of boundary conditions. The Phase 1 feasibility study considered only the no-flow boundary conditions, because this boundary condition was known to be most sensitive to percolation threshold from previous work by Axelsson *et al.* (1990).

The problem of boundary conditions can be mitigated by applying the boundary conditions to a somewhat larger region than the scale of interest. The permeability at the desired scale is then calculated for a measurement volume within the simulation region, by dividing the net flux across the region by the average gradient (the average head difference between ends divided by the region length) in the direction of flow. Non-porous media behaviour is indicated by large differences between the flow that enters the measuring volume on the upstream end, and the flow that emerges on the downstream end. This approach was not followed in Phase 1 because it required development of an additional post-processing code to calculate the fluxes and average head values on the boundary of the measurement volume.

Extension of the permeameter approach to estimation of the off-diagonal components of the equivalent permeability tensor requires a considerable amount of additional computational effort, because of the need to generate additional finite element meshes at different orientations.

An alternative approach (personal communication, S. Norman, 1990) is to use a fixed mesh for the simulation region (which is larger than the scale of interest), and to apply an arbitrary set of boundary conditions at different fracture intersections with the boundary. By computing the gradient of an average head, $\nabla\langle h\rangle_f$ and an averaged velocity $\langle \boldsymbol{u}\rangle$ for an averaging volume on the scale of interest, for each case of boundary conditions, the EPM assumption can be tested by multivariate analysis to estimate the conductivity tensor K_{ij} such that:

$$\langle \boldsymbol{u}\rangle \; = \; -\mathbf{K}\nabla\langle h\rangle_f \qquad (3\text{-}11)$$

where

$\mathbf{K}$ = the conductivity tensor with components K_{ij} [L/T]

The average head gradient and velocity in this case are defined in terms of weighted averages taken over the areas of all fractures within the averaging volume. This approach provides for greater generality, without increasing the number of finite element meshes that must be produced. Hence this method should be considered in the continuation of the DFN modelling.

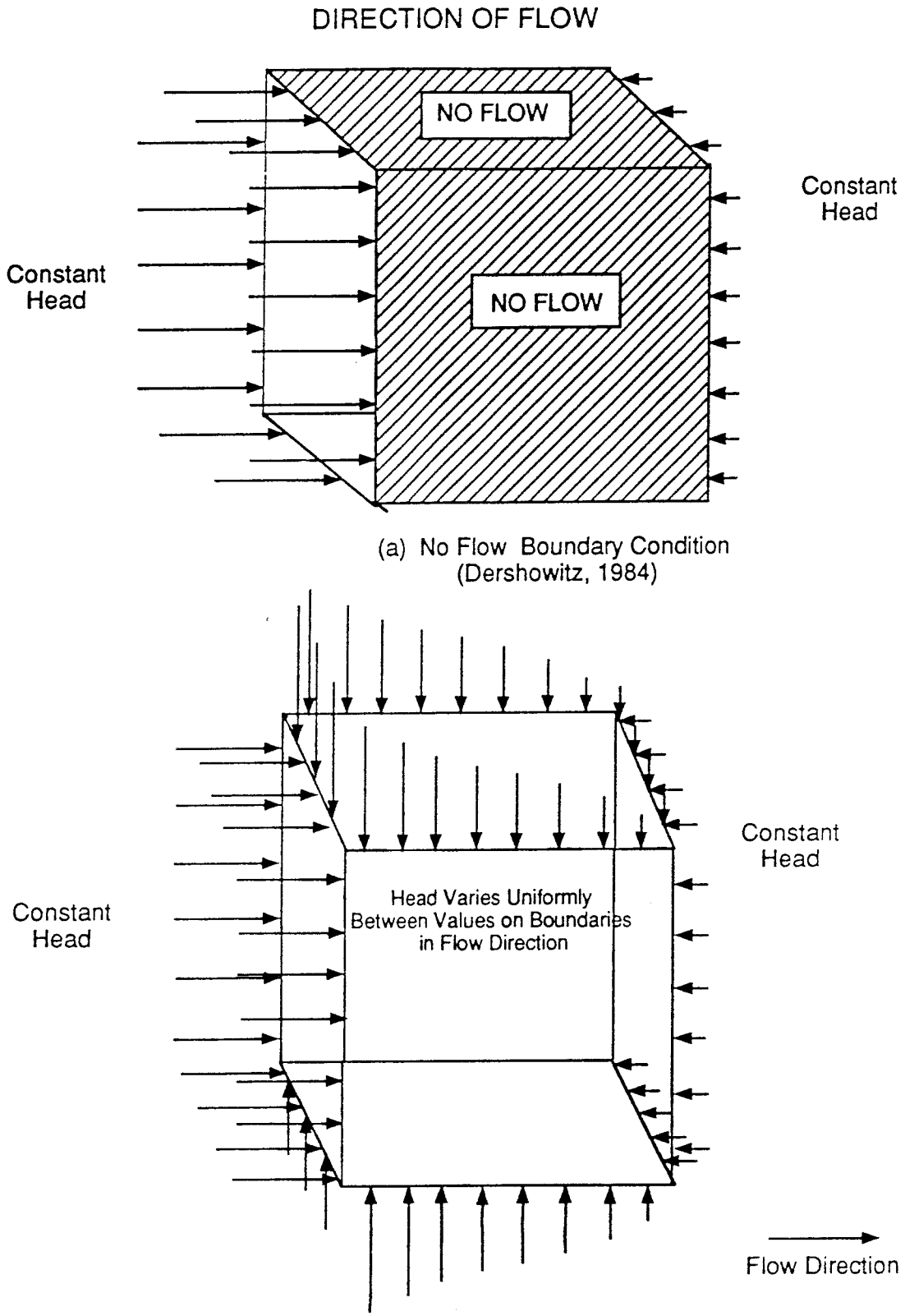

FIGURE 3-14

BOUNDARY CONDITIONS FOR DFN MODEL USING PERMEAMETER APPROACH

4. DERIVATION OF DISCRETE FRACTURE MODEL PARAMETERS

The data available for the Finnsjön site is sufficient for derivation of a DFN model suitable for the SKB 91 project. The following sections give a summary of the derivation of the statistical parameters for a preliminary DFN model, according to the methodology described in Section 3.4.

Several portions of the dataset are less complete than would be desired for a full-scale repository safety assessment. For example, the lack of oriented core from at depth requires making some rather bold assumptions about the distribution of fracture orientation. However, formulation of a preliminary DFN model based upon the available data is worthwhile, as it provides opportunity for identifying deficiencies in the data.

Like any type of modelling, DFN modelling is an evolutionary process that requires iterative adaptation to site-specific conditions. The data analysis carried out in the Phase 1 Feasibility study must be seen as preliminary. Many aspects of the analysis, as noted in the following sections, involved *ad hoc* assumptions and rather cursory analysis. Preliminary analysis is a necessary step in building a DFN conceptual model. It provides a working model that hopefully represents the main statistical features of the fracture population in an approximate manner. Such a model provides a basis for sensitivity analyses to identify which components of the model require a more thorough analysis in subsequent phases of the safety assessment.

4.1 Orientation

The types of fracture orientation data available have been described in Section 2.1. No complete orientation data (*i.e.*, data containing both strike and dip) were available from within the Finnsjön block below Zone 2. The only complete data came from cell maps and scanlines taken from a rather limited, detailed-mapping area 1 m × 100 m. Figure 4-1 shows stereoplots of the original orientation data from scanlines and cell maps.

In addition to the complete data from the detailed mapping, incomplete orientation data were available from earlier scanline surveys (strikes only) and unoriented, vertical core (dips only). The earlier scanline data were not used in the Phase 1 model. Data from inclined boreholes was also not utilized in Phase 1 because the scope of the feasibility study did not justify applying the complex data analysis procedures required for uncertain orientation data. Appendix 4 gives the dataset used in the Phase 1 analysis.

The incomplete orientations from core from vertical boreholes were combined with the complete data from surface maps based on the assumptions that fractures at the surface have an orientation distribution identical to those below Zone 2. This assumption was adopted based upon the rough similarity between plots of the dip distribution for core and outcrop data (Figure 2-8).
It was desirable to add core data to the outcrop data, because the outcrop data probably undersample the subhorizontal fracture population more severely than can be compensated for by applying Terzaghi's correction.

An *ad hoc* procedure based on bootstrap resampling was developed to produce a combined dataset for bootstrap simulation of orientations, according to the following procedure:

1. A Terzaghi weighting factor to correct for directional sampling bias was calculated for each fracture record from the scanline and cell mapping near KFI 11. Trend and plunge angles were calculated for the pole (normal vector) to each fracture plane. The trend, plunge, and weighting factors for these two data sets are given as the listings of the files SCANORS.wN and CELLORS.PRN in Appendix 4.

2. The scanline and cell map orientations with Terzaghi correction factors were combined into a single dataset containing all complete fracture orientations from surface, and sorted according to plunge of the pole vector.

3. The fracture dip angles from the boreholes KFI 06 and KFI 11 was extracted from the raw data, and recorded in the two files KFI06ORS.PRN and KFI11ORS.PRN (Appendix 4).

4. A short FORTRAN program MAKEORS (listed in Appendix 4) was used to combine fracture pole azimuths with the fracture dip angles, by bootstrap sampling of the fracture orientations from surface. In this program, for each core dip angle ϕ_d,the plunge ϕ_p for the corresponding, upper hemisphere pole direction was calculated from the formula:

$$\phi_p = 90^\circ - \phi_d$$

A fracture pole azimuth θ_p for each ϕ_p was selected randomly from the subset of surface orientations having plunges within $\pm 5^\circ$ of ϕ_p. The probability of selecting any single surface orientation record from within this subset was proportional to the Terzaghi correction factor for that orientation record. For each core fracture, a number of orientation records (in proportion to the Terzaghi correction factor) were written to the bootstrap sampling file ALLORS.ORS. Multiple records were also written for each surface orientation, in proportion to its Terzaghi correction factor, to form the complete, Terzaghi-corrected dataset for bootstrap sampling.

This procedure was designed to preserve (in a non-parametric fashion) any correlations among trend and plunge that may be present within the surface data, while using the core data to produce a somewhat less biased distribution of plunge directions. A more rigorous procedure making use of oriented core data would be highly preferable. However, assuming that the fractures below Zone 2 are similar to those mapped at the surface, this *ad hoc* approach can be expected to provide an orientation dataset that, however crudely, reflects the main features of the actual orientation distribution. This should be sufficient to give a preliminary indication of the degree and type of anisotropy that is to be expected, so that the importance of including anisotropy in SC models can be assessed.

Figure 4-2 shows a stereoplot of the complete, Terzaghi-corrected dataset. This dataset was used in all subsequent data analysis, including size analysis and the calculation of the conductive fracture intensity-frequency ratio C_p, as well as the final simulations.

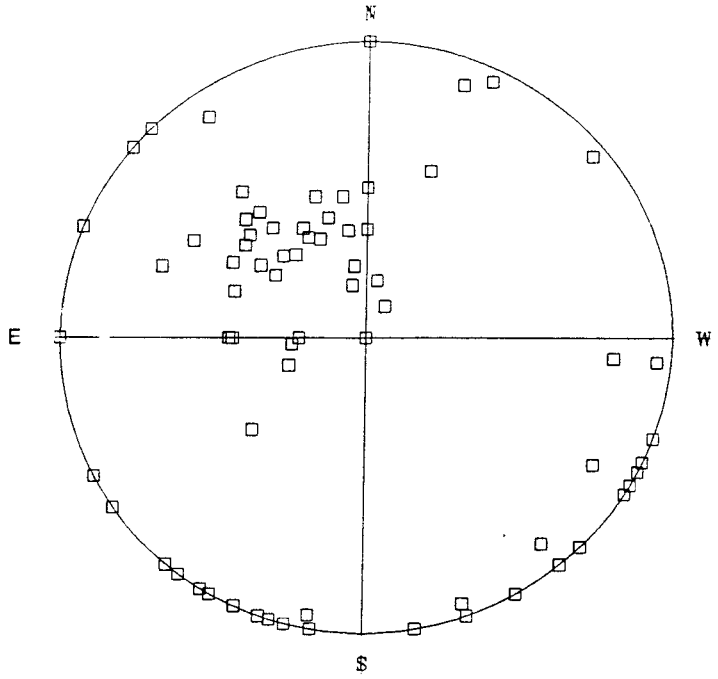

a) Scanline Data

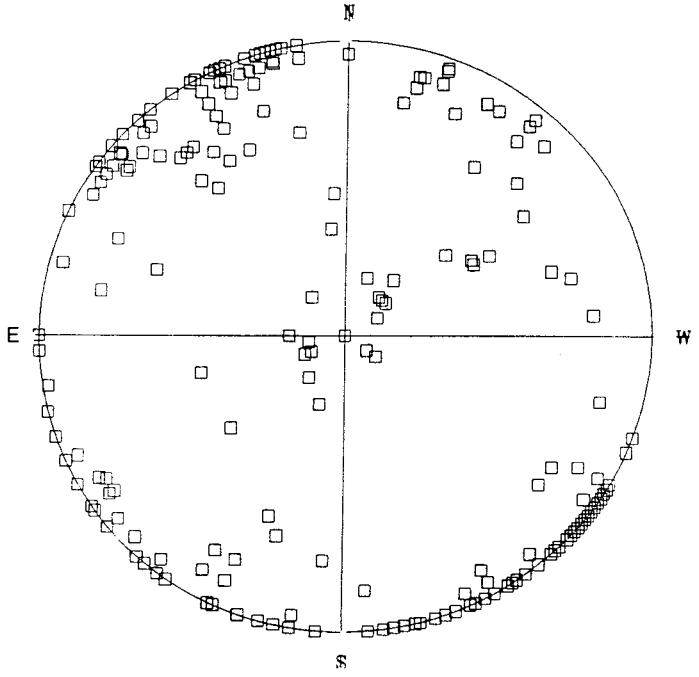

b) Cell Map Data

Schmidt Projection
Lower Hemisphere Fracture Poles

FIGURE 4-1
STEREONET PLOTS OF ORIENTATION DATA FROM SCANLINES AND CELL MAPS

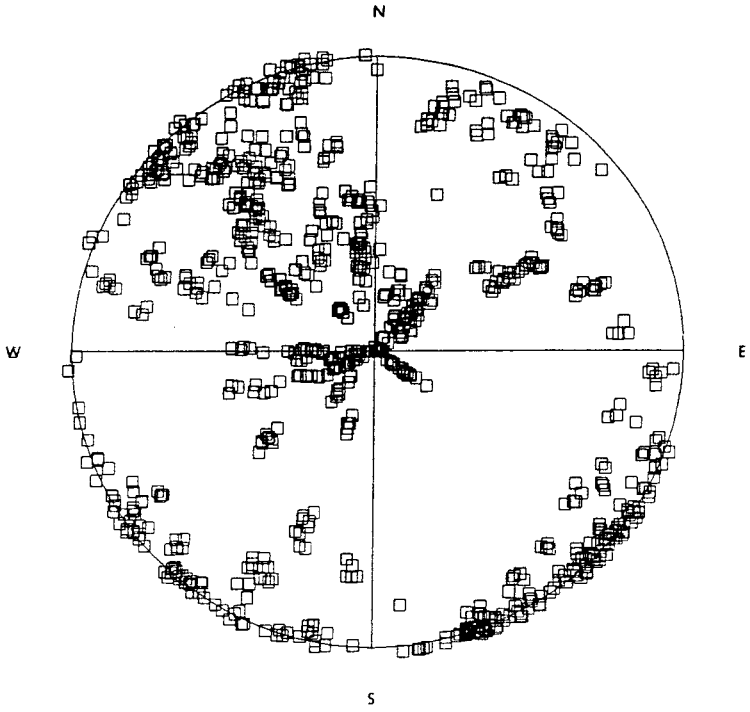

Equal-Area Projection
Fracture Poles

FIGURE 4-2
TERZAGHI-CORRECTED DATASET FOR FRACTURE ORIENTATION

4.2 Fracture Size

The fracture size distribution was analyzed using the **FracMan** module FracSys (Appendix 2). Constant, normal, exponential, and lognormal distributions of fracture radius were used to simulate tracelength samples on traceplanes having the same geometry as the cell maps and lineament maps (The data sets utilized are listed in Appendix 5). The Terzaghi-corrected orientation dataset ALLORS.ORS was used for bootstrap simulation of the orientations of fractures intersecting the simulated trace maps. For each distribution, simulations were performed for alternative values of the distribution parameters. Goodness-of-fit between the simulated and observed tracelength distributions was measured by calculating the Kolmogorov-Smirnov (K-S) statistic for each simulation.

Because of the large differences in tracelength censoring levels of the surveys on different scales, it was necessary to perform separate analyses for each scale (cell maps, and local, semiregional, and regional lineaments). Preliminary analyses showed that none of the standard distributions (normal, lognormal, or exponential) gave even approximate fits (Kolmogorov-Smirnov statistics of less than 0.25 or so) on more than one scale. Hence it was necessary to consider other possibilities for size distributions.

As noted in Section 2.1.1, there is an apparent similarity among the tracelength distributions observed for different sampling scales (Figure 2-6). This suggests that the tracelength population may be self-similar on different scales, *i.e.*, that fracture tracelengths behave as a fractal process. This possibility was investigated by calculating the total trace length measured per unit area, as a function of censoring length. Figure 4-3 shows a log-log plot of the normalized total tracelength versus the minimum measured tracelength for the four sampling scales, which indicates a loglinear relationship with a log slope of approximately negative one. Some basic calculus shows that this relationship corresponds to a probability density function (PDF) for tracelength λ in the form of a power law:

$$f_{\lambda}(\lambda) = C_1 \lambda^{-C_2} \tag{4-1}$$

where C_1 is a normalization factor and C_2 is approximately three. Figure 4-4 shows a plot of tracelength frequency versus log tracelength. A least-squares fit to the data gives $C_2 = 2.78$. As the fracture tracelength approaches the censoring lengths of the cell maps and the local-scale lineament maps, the frequency does not fit this model very well. However, this may be due to censoring effects, if in the mapping process the probability of not noticing a fracture increases as the tracelength approaches the censoring limit.

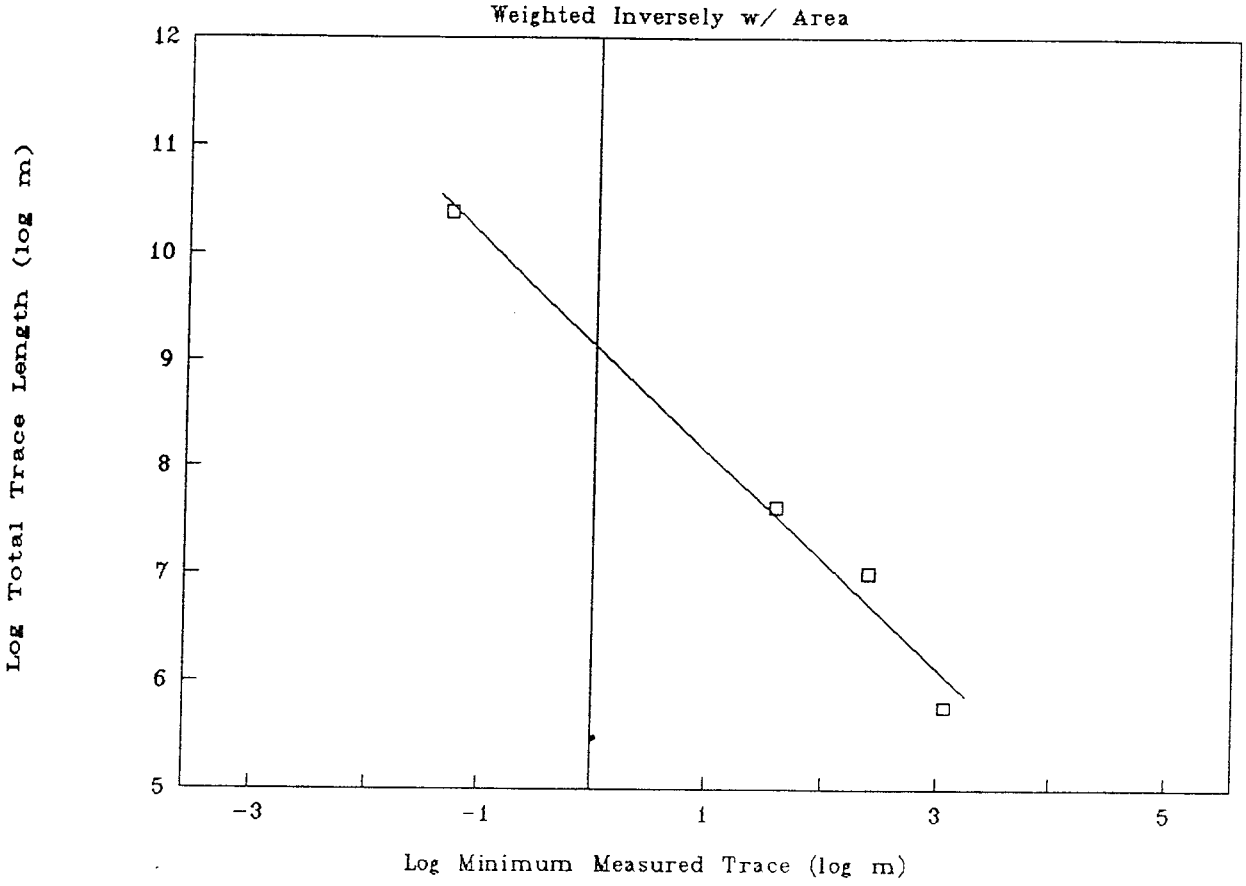

FIGURE 4-3
NORMALIZED TRACELENGTH DISTRIBUTION

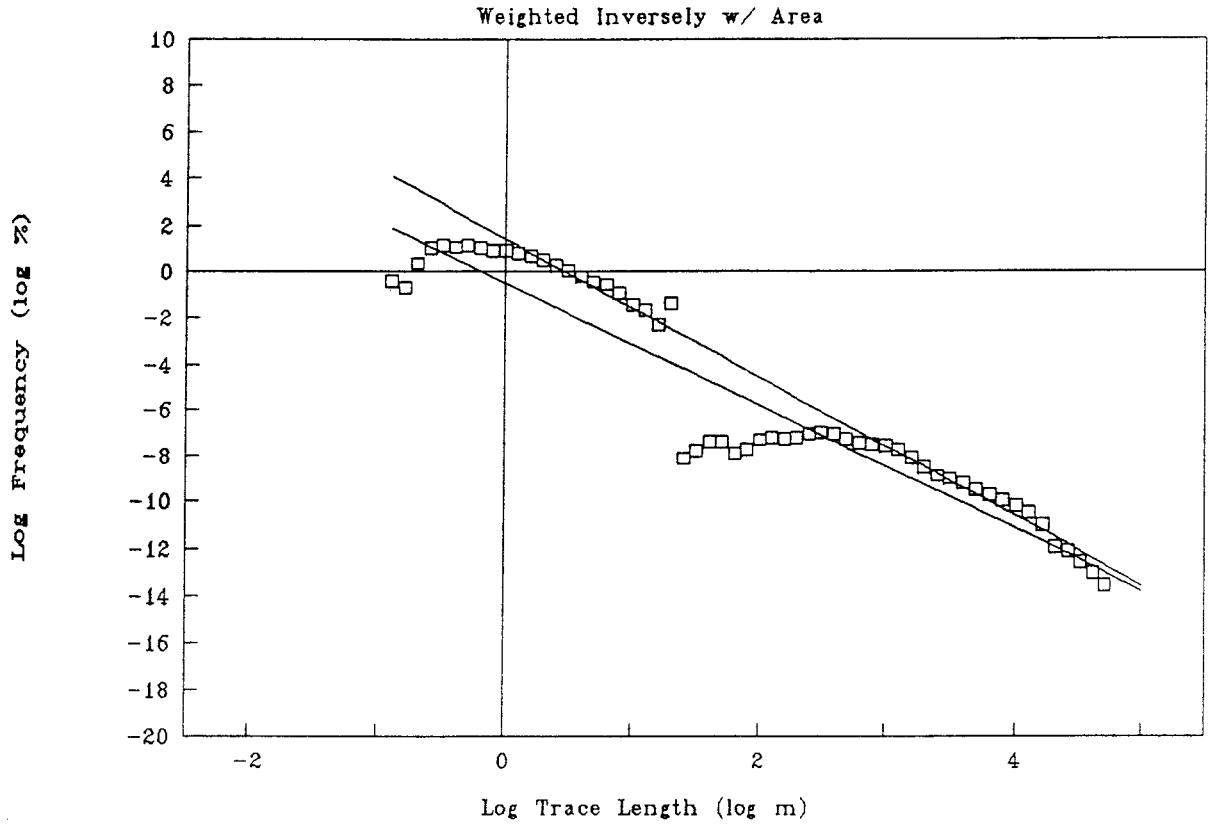

FIGURE 4-4
FRACTURE FREQUENCY *VS.* LOG TRACELENGTH

The approximately power-law form of the observed PDF for tracelength suggests that (assuming circular fractures) the underlying fracture radius distribution may be of the same power-law form. This hypothesis was tested by adding a power-law distribution for radius to the FracSize module, defined as:

$$f_r(r_e) = \frac{b-1}{r_{min}}\left(\frac{r_{min}}{r_e}\right)^b, \qquad r_e \geq r_{min} \tag{4-2}$$

where:

b	= the power-law exponent	[-]
r_{min}	= the minimum value of r_e	[L]

The lower bound on this distribution is introduced to facilitate simulation because the $f_r(r_e)$ goes to infinity as r_e goes to zero. It is not interpreted as a physical limit on the smallness of fractures. Indeed, it seems likely that, at least in some rocks, the number of fractures per unit volume increases as fracture size decreases, all the way down to microcracks at the grain scale or smaller (Jaeger and Cook, 1977).

The power law distribution differs from distribution types more commonly employed in statistical analysis, such as the normal distribution, in that the first and second moments (mean and variance) for the distribution become infinite for $b < 2$ and $b < 3$, respectively. This is of course impossible for distributions of real fractures, since an upper bound must exist — the fractures cannot be larger than the earth's crust! However, the maximum lineament size observed at the site is over 50 km in length, which is extremely large in relation to the simulation scale (no more than a few hundred meters), that one can say that the upper bound is effectively infinite.

FracSize analysis indicated that a value of b in the range 1.85 to 1.9 gave adequate fits to both cell map and local lineament data (Figure 4-5). The value $b = 1.89$ was chosen for preliminary model simulations as it gives the best fit to the cell map data, which are closer to the scale of fractures within block simulations (25 to 100m) than the local lineament map data.

It should be noted that the uncertainty in the value of b is fairly high (on the order of $\pm$ 0.1), as is evident from these figures. Trial simulations of fracture geometry indicate that the interconnectivity of the fracture network is very sensitive to this parameter, as discussed in Section 5.1. More restrictive limits on b (*i.e.*, reduced uncertainty) may be obtained by treating the estimation of b as a global optimization problem, rather than by analyzing the data for each scale separately. Such an analysis could not be carried out within the time frame of Phase 1, but should be seen as a necessary component of the Phase 2 analysis.

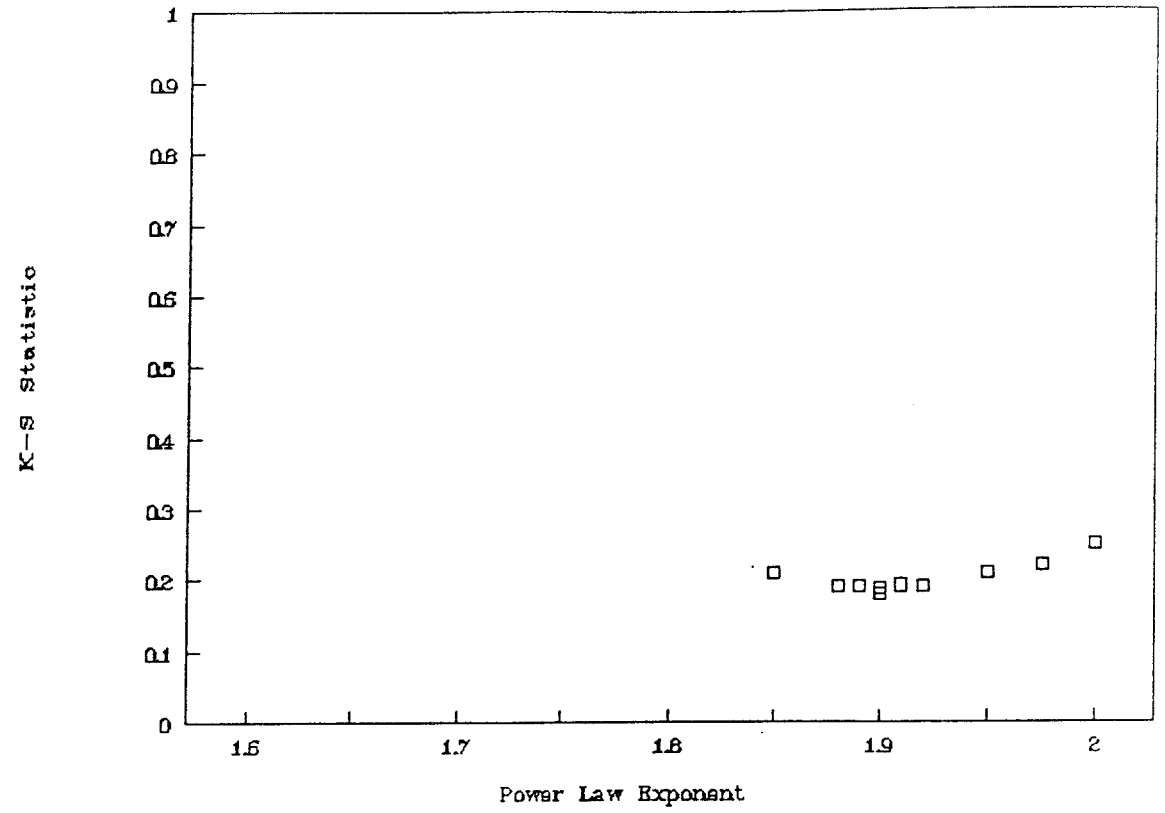

a) Cell Map Data

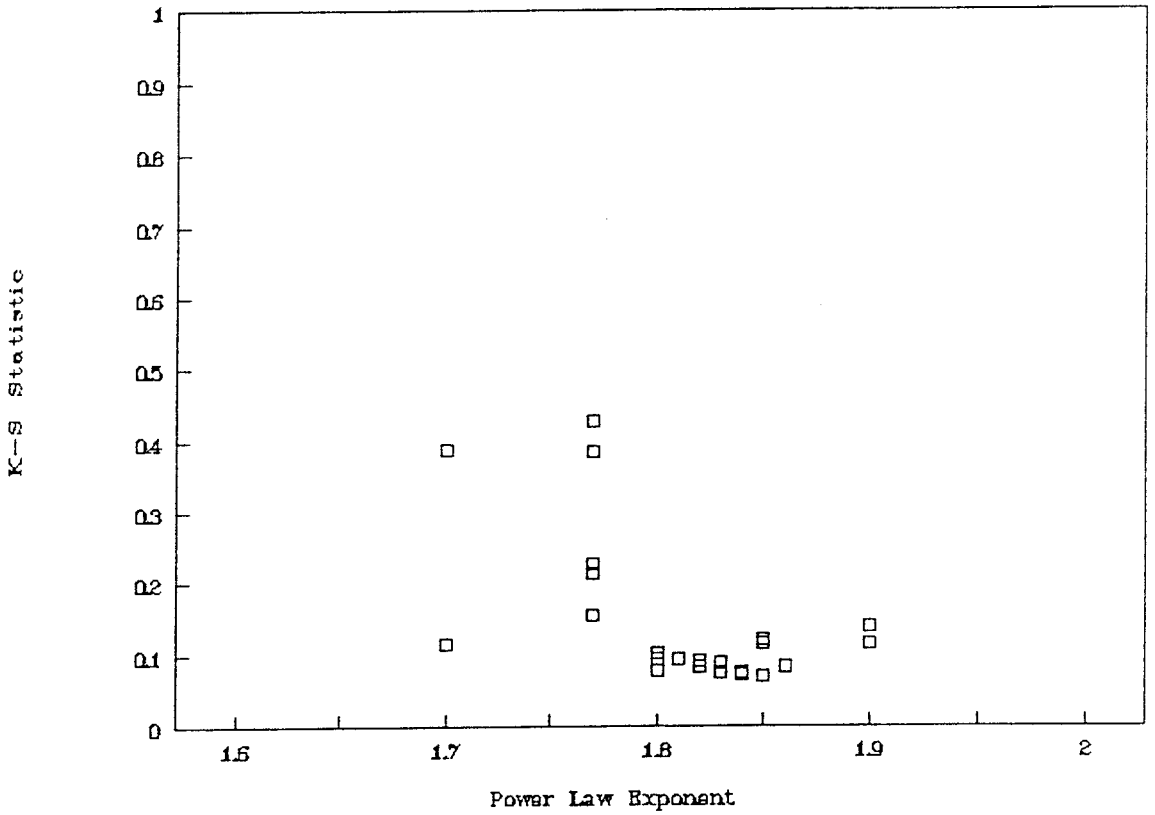

b) Local Lineament Data

FIGURE 4-5
FRACSIZE ANALYSIS OF TRACELENGTH

4.3 Packer Test Interpretation

The interpretation of transient data from constant-head packer tests according to the theory of generalized-dimension flow (GDF) was demonstrated in the Phase 1 study. A limited sample of transient FIL test data was selected from the results of the testing program in the boreholes BFI 01-02. Thirteen separate tests were included in this sample. Details of the type-curve analyses are described in Appendix 6.

Because only a limited number of tests were analyzed in this way, the transmissivity values obtined from the GDF analysis were not used for derivation of the single-fracture transmissivity distribution according to the methodology described in Section 3.4.3.3. However, the transmissivity and dimensionality values obtained from this analysis *were* used within the validation methodology described in Section 3.5.

The selection of test data was not random; tests with relatively good data (low "noise" level) were preferentially selected. A few of the test records were selected because they looked interesting; that is, they showed markedly non-radial behaviour that was apparent from visual inspection. The selection of relatively good data probably means that the sample is biased toward more conductive zones, since a high noise level suggests that the flowrate during the test was near the lower limit of the flowmeter range.

Because of the small size and non-random nature of the sample, this analysis should be seen simply as a demonstration of the methodology. The results of the analyses show a portion of the range of behaviour that occurred within the full suite of packer tests in these holes, but not necessarily the entire range. Application of the results of these analyses to validation and calibration of the DFN model in Chapter 5 is also simply for demonstration purposes. Fractional-dimension analysis of the full suite of tests during Phase 2 of the present study will make more meaningful application of the results justifiable.

4.3.1 Comparison of Moye's Formula and Generalized-Dimension Flow Interpretations

A principal reason for performing this analysis is to determine how serious the errors are that result from use of steady-state interpretations of packer test data for the DFN, SC, and CN models. Figure 4-6a compares Moye's-formula and GDF interpretations of the conductivity values for the sample of thirteen test intervals. The size of each hexagonal symbol in the plot is proportional to the interpreted flow dimension D, which ranged from 1.13 to 2.75.

The line in the figure indicates an exact match of conductivity values. The GDF conductivities in this plot have been normalized to account for the fact that, in the GDF analysis, an effective section thickness L = 0.005 m was assumed, whereas the Moye's conductivities are based on an effective L equal to the packer spacing, approximately 2 m. The smaller L was used for the GDF analysis to obtain a more reasonable estimate of the conduit thickness at the wellbore, *i.e.* it is assumed that only a fraction of the wellbore surface is conductive. The GDF conductivities were multiplied by a factor of (0.005m / 2m), so that the conductivities are expressed in terms of an equivalent section conductivity.

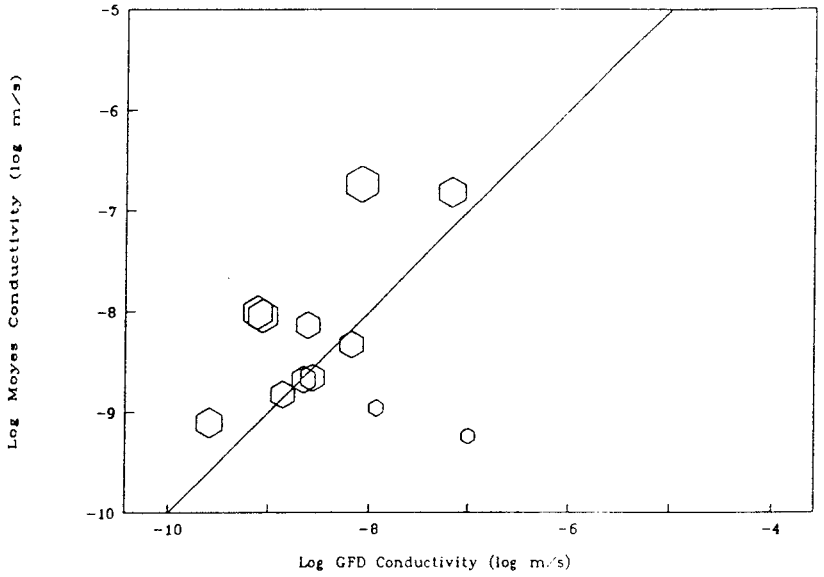

a) Conductivity

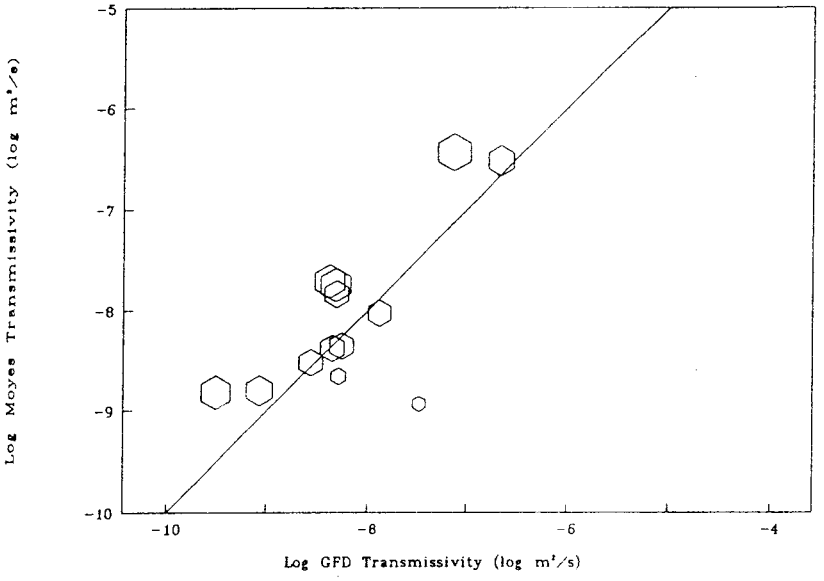

b) Transmissivity

○ Dimension = 1 ⬡ Dimension = 3

FIGURE 4-6
COMPARISON OF MOYE'S FORMULA AND GENERALIZED- DIMENSION FLOW INTERPRETATIONS OF CONSTANT-HEAD TESTS

This plot shows that, for the test intervals with higher flow dimension ($D > 2$), the interpreted Moye's conductivities are generally high relative to the normalized GDF conductivities, whereas the test intervals with lower flow dimension ($D < 2$) are low relative to the normalized GDF conductivities. The greatest magnitude of discrepancy (3 orders of magnitude) occurs for the interval with the lowest flow dimension. A comparison of GDF generalized transmissivities (defined in Appendix 6) with Moye's transmissivities (Moye's conductivity times section thickness) shows a similar pattern (Figure 4-6b), although the discrepancies between the two approaches are reduced considerably.

These comparisons show that interpreted values of K or T obtained from the two methods for individual tests may differ significantly, in a manner that is highly dependent on the flow dimension. The aggregate influence of interpretation method on the distributions of interpreted values cannot be quantified from such a small sample, but clearly the aggregate influence will depend upon the relative proportions of high-dimension and low-dimension tests in the dataset. If $D > 2$ for most of the tests, the Moye's interpretation will give a conductivity distribution that is skewed toward lower K values relative to the distribution obtained from the GDF interpretation.

A surprising result is that the interpretation approaches are generally in good agreement for cases of approximately cylindrical flow, but not for cases of more nearly spherical flow. This is surprising because Moye's formula is based on the assumption of spherical flow. Perhaps this implies that Moye's formula incorrectly estimates the radius of the effective spherical source in fractured rock similar to that around the test intervals, due to non-EPM behaviour on the scale of the packer test. However, there is also uncertainty in the GDF approach regarding an appropriate choice of conduit cross-sectional area at the source, as discussed in Appendix 6. The question of the sensitivity of GDF analysis to this choice could be addressed by a detailed analysis of packer test simulations using a DFN model.

Due to the limited number of tests for which moderately good transient data are available, it will be necessary to use steady-state test interpretations in the calibration of SC, DFN, and CN models in the present study. The results of this limited investigation suggest that, although the interpretations of individual tests may be strongly affected by flow dimension, for nearly all of the tests the two methods of interpretation are in agreement within an order of magnitude, which is probably not much greater than the precision of the interpretation methods. The discrepancy is greater for low D flow, but there appear to be fewer conduits of low D. Since the discrepancies corresponding to high and low D are in opposite directions, the Moye's formula interpretation should give transmissivity values for the FIL tests that are reasonably correct in some average sense. However, measures of the **variability** of the system that are estimated from the Moye's formula interpretations are likely to be different from those estimated by the GDF approach. This effect may be important in the estimation of autocovariances (for conditioning of SC models) and the characterization of distribution tails (for CN models), as well as for derivation of discrete fracture transmissivity distributions (for DFN models). The small number of tests analyzed in Phase 1 is too few for assessment of this effect.

4.4 Derivation of at-Borehole vs. Cross-Fracture Transmissivity Relationship

The Phase 1 preliminary model did not account for variability of transmissivity within the individual fractures. Specifically, the data analysis for the model did not account for the distinction between at-borehole transmissivity T_{fb} and cross-fracture transmissivity T_f. However, techniques for deriving the probabilistic relationship between T_{fb} and T_f were developed, and preliminary analysis was performed to demonstrate the methodology, which is based upon the numerical experiments of Kenrick *et al.* (1988).

The approach is based upon numerical simulations of transient packer tests and steady-state, cross-fracture flow in single fractures with variable aperture. In the present study, the methodology of Kenrick *et al.* was extended to use real fracture data in two complementary ways:

- **Replicated Geometry**: Simulation of flow through replicated fracture geometries, taken directly from maps of single fracture aperture variation.
- **Simulated Geometry**: Simulation of flow through simulated fracture geometries, based upon measurements of the fractal dimension of fracture roughness profiles or single-fracture conductivity profiles.

The demonstration of these two approaches is described in Appendix 7. Only one replication of fracture geometry was performed to demonstrate the first approach; many more would be necessary to adequately define the relationship of at-borehole to cross-fracture transmissivity. A major problem with the replicated-geometry approach is that the available aperture maps are very small compared to fractures on the scale of interest. A second problem is that a very large quantity of data would be required to characterize the relationship between T_{fb} and T_f.

The simulated-geometry approach was found to be more easily implemented, because it utilizes information from fracture profiles rather than two-dimensional aperture maps. The demonstration of this approach, described in Appendix 7, used an assumed fractal model for transmissivity variation, to predict the consequent relationship between T_{fb} and T_f. Larger-scale fracture conductivity profiles are available from the Stripa Project (Abelin *et al.*, 1990) that can be used in Phase 2 to derive a valid fractal model for this approach.

4.5 Conductive Fracture Frequency and Transmissivity

OxFILET analysis was performed using hydraulic conductivity data from 2 m packer tests. Hydraulic conductivity values based upon steady-flow interpretations of FIL tests were provided for all boreholes in ASCII format by SGAB (Appendix 8). Only data from the boreholes BFI 01-02 and KFI 11 were used. These boreholes, together with KFI 09 and KFI 10, contained the best data (in terms of conductivity resolution) for below Zone 2. The data from KFI 09 and KFI 10 were not included in the dataset for the Phase 1 analysis. For this reason, the dataset contained only 62 of the 94 higher-resolution measurements (conductivity measurement limit of 1.0×10^{-10} m/s) below Zone 2. Thus the sample used in the statistical analysis represented only about 66% of the available data.

Only 2 m intervals were used the Phase 1 analysis, because in general the resolution (minimum detection limits) was better for the 2 m tests than for the 3 m tests. Including the 3 m tests would add significantly to the quantity of data, but would be detrimental to the analysis (due to the poorer resolution) unless a more complicated analysis approach were used. This could be done in the latter phase of the study, but would have been excessively complicated for the scope of the Phase 1 feasibility study.

The data were separated into four categories based upon the locations of fracture zones as defined on the basis of core evidence and borehole geophysics by Andersson *et al.*, 1990:

- Above Zone 2.
- Within Zone 2
- Within Zone 5.
- Below Zone 2 (excluding Zone 5).

The data from above Zone 2 were not used. The data from within Zones 2 and 5 were not considered in the Phase 1 analysis, but will be considered in Phase 2. The data from below Zone 2, excluding Zone 5, were assumed in the Phase 1 analysis to be representative of conductivities for the "average rock" outside of major fracture zones, within the Finnsjön block at depth.

Approximately 25% of the conductivity values were below the theoretical detection-and-analysis limit for the packer tests, which was estimated as 1.0×10^{-10} m/s for all three holes. This corresponds to a transmissivity measurement limit of 2.0×10^{-10} m^2/s. The interpreted hydraulic conductivities were transformed to transmissivities simply by multiplying the conductivity values by the packer separation of 2 m. The minimum transmissivity actually seen in the data was 2.05×10^{-10} m^2/s, so this value was used as an estimate of the actual measurement limit. Intervals below the measurement limit were assigned a transmissivity value of 2.05×10^{-10} m^2/s.

The data were analyzed using the OxFILET algorithm (Section 3.4.3.3). Lognormal, normal, and exponential distributions for fracture transmissivity were evaluated. Of these distributions, only the lognormal distribution provided a reasonable fit for the observed packer interval transmissivity distributions. Two distinct sets of distributional parameters were found to produce the nearly equivalent matches to the data for the rock below Zone 2. These sets of parameters are given in Table 4.1. Figure 4-7 provides a comparison of observed and simulated

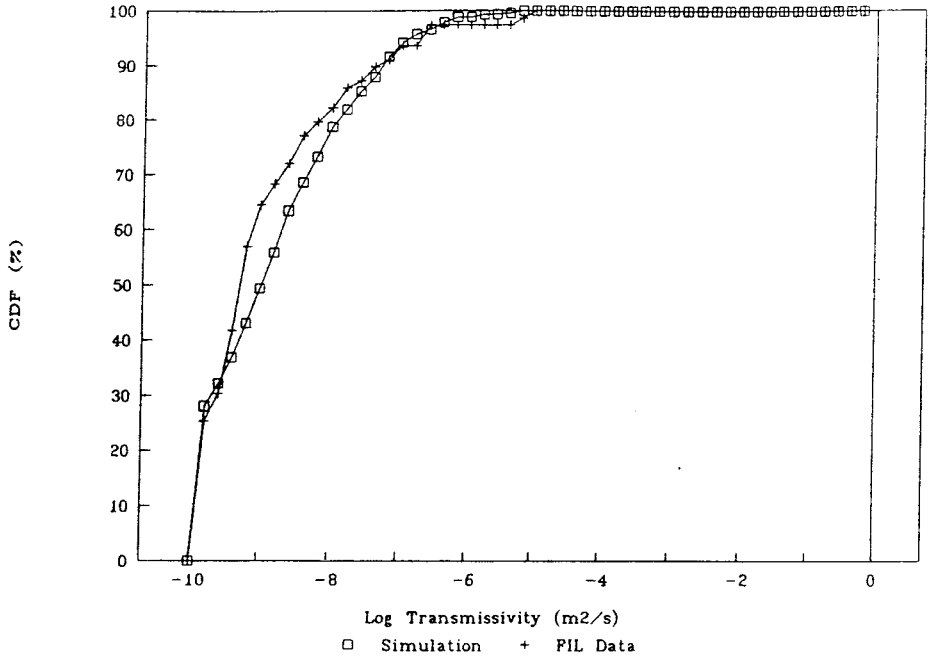

a) Cumulative Density Function

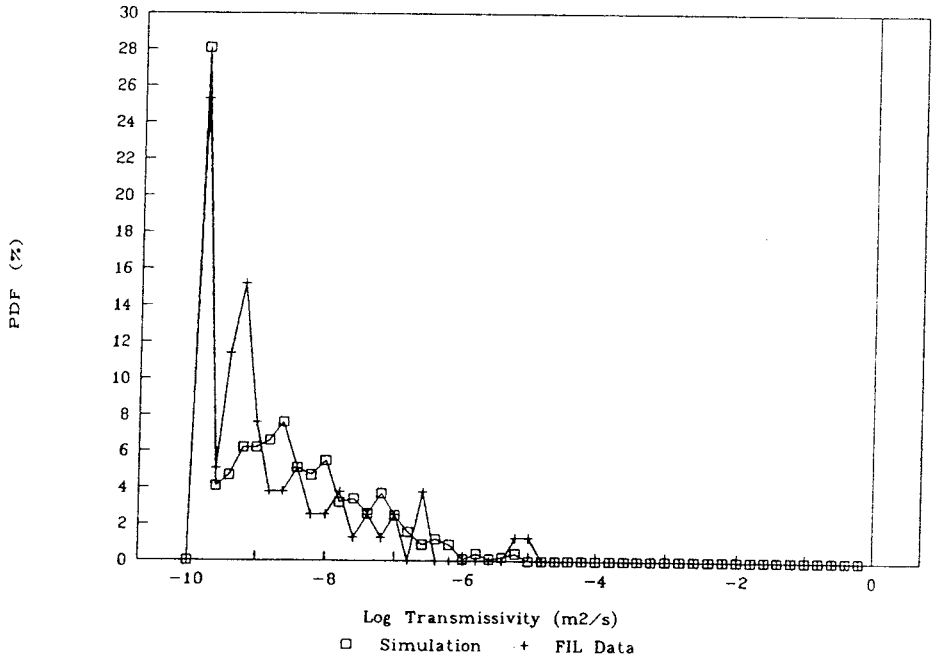

b) Probability Density Function

FIGURE 4-7
TRANSMISSIVITY DATA ANALYSIS - COMPARISON OF SIMULATED AND OBSERVED DISTRIBUTIONS FOR BEST-FIT PARAMETERS

distributions for the parameters that gave a marginally better fit, as measured in terms of the K-S statistic and percentage of nonconductive intervals. The non-uniqueness problem arises from the fact that a large number of the test intervals are very near to the measurement limit.

Table 4.1 Best-Fit Parameters for Conductive Fracture Frequency and Transmissivity

Fracture Frequency (m^{-1})	3.29	1.50
Mean of Log_{10} Transmissivity (log m^2/s)	-11.3	-10.0
Standard Deviation of Log_{10} Transmissivity (log m^2/s)	2.1	1.2
Nonconductive Intervals (%)	28.	29.
Kolmogorov-Smirnov Statistic	0.08	0.09
Kolmogorov-Smirnov Probability (%)	69.7	61.0

The set of parameters in the left-hand column of Table 4.1 was adopted for subsequent analysis in Phase 1, based upon the marginally superior match to the FIL data. The estimated conductive fracture frequency, f_c = 3.29 m^{-1}, is higher by a factor of 4 to 6 than the values of f_c calculated by Andersson *et al.* (1988). Indeed, this value of f_c is of the same order as the total coated fracture frequency! However, it should be noted that the log mean of the transmissivity distribution is well below the measurement limit for 2 m test intervals; approximately 78% of the fractures in this distribution are below the measurement limit. If only fractures with transmissivity above the measurement limit of the equipment are considered, the corresponding, "effective" f_c is about 0.72, which is close to the estimate of Andersson *et al.* (1988).

Neither set of parameters provides a very precise fit to the data, in comparison with results achieved elsewhere in granitic rock in Sweden (Axelsson *et al.*, 1990; Geier *et al.*, 1990); this suggests that a unimodal lognormal distribution is not necessarily the correct distribution. A better fit could possibly be obtained with a bimodal or trimodal distribution. this possibility was investigated by performing a bimodal OxFILET analysis of a partial dataset early in the analysis, but this was not carried out for the full set of FIL data during Phase 1.

In any case, this analysis must be regarded as preliminary, since it does not consider the distinction between at-borehole and cross-fracture transmissivity. Furthermore, the assumption is made that the rock below Zone 2 contains a single, statistically homogeneous population of fractures. The possibility of spatial variability in the dataset should be considered in subsequent analysis. This can be accomplished by grouping borehole datasets according to location, and comparing the f_c and $f_{TL}(T_L)$ thus obtained from the different groups, and different boreholes within groups, to estimate the significance of any spatial trends in the fracture population relative to the variability within any given cluster of boreholes.

4.6 Conductive Fracture Intensity

The conductive fracture intensity P_{32c} was calculated from the best-fit OxFILET estimate of f_c = 3.29 by using the FracMan module FracWorks to simulate borehole sampling of a fracture population having the same orientation distribution as the fractures *in-situ*. The fracture orientation dataset derived as described in Section 4.1 was used for bootstrap simulation of a population of fractures having a fixed effective radius r_e = 60 m. This artificially large radius was used to accelerate the simulated sampling process. Provided that there is no correlation between fracture orientation and fracture size (a basic assumption in the Phase 1 analysis), the ratio of P_{32c} to f_c obtained from borehole sampling is independent of the fracture size distribution.

The simulation was performed using an assumed value of P_{32c} = 1.0, since the "true" value of P_{32c} was unknown. A total borehole length of 1000 m was simulated in 200 m sections, with an average f_c of 0.680, giving the ratio:

$$C_p = \frac{f_c}{P_{32c}} = \frac{(0.68\ \mathrm{m}^{-1})}{(1.0\ \mathrm{m}^3/\mathrm{m}^2)} = 0.68 \qquad (4\text{-}3)$$

Thus the value of P_{32c} for the actual fracture population can be estimated as:

$$P_{32c} = \frac{f_c}{C_p} = \frac{3.29\,\mathrm{m}^{-1}}{0.68} = 4.84\,\mathrm{m}^{-1} \qquad (4\text{-}4)$$

Trial simulations of the fracture population using this value of P_{32c} together with the size distribution derived in Section 4.1 showed that, to make simulation tractable on block scales up to 100 m, the number of fractures in the population would need to be reduced by truncating the fracture radius distribution at about r_{min} = 1 m, and by truncating the fracture transmissivity distribution at approximately $T_{min} = 3.16\times10^{-9}$ m²/s (equivalent to a minimum log T of -9.5). The effective value of P_{32ce} for this truncated fracture population was calculated as P_{32ce} = 0.487 m^{-1}.

4.7 Storativity

The storativity of the fractures was assumed to be correlated with the transmissivity, as discussed in Section 3.4.4. The parameters of this correlation A_1 and A_2 were estimated by a simplistic analysis based upon the assumption that the transmissivity and storativity values interpreted from any given conductive interval are dominated by the most conductive single fracture intersecting that interval. This assumption is not entirely consistent with the OxFILET interpretation approach, but seems reasonable in view of the very low probability of two fractures in the same interval having transmissivities of the same order of magnitude, and well above the measurement limit.

Based on this assumption, the correlation coefficients can be estimated from a simple, loglinear correlation of FIL storativity to transmissivity. This was done using the interpreted hydraulic properties from the fractional-dimension type curve analysis in Section 4.3. The major weaknesses of this approach are:

- The error in storage estimates for the FIL tests is believed to be large.
- The error in storage estimates may be systematically related to interval transmissivity.
- The sample of 13 tests was not randomly chosen, and may not be representative of the entire suite of FIL tests.

More trustworthy data could perhaps be obtained from single-fracture experiments *in-situ* or in the laboratory, but no applicable data of this nature were available at the time of this study. For lack of appropriate data, this simple approach was adopted based on the assumption (verified by preliminary packer tests simulations) that, for the limited purposes of using storativity for transient packer test simulations in the present study, the approach is relatively insensitive to the storativity values.

Figure 4-8 shows a scatter plot of storativity versus transmissivity. The line in the plot indicates the model estimated by log-log correlation. The values of the correlation parameters thus estimated were:

$A_1 = 1.0$
$A_2 = 0.686$

for the form of the relation of storativity to transmissivity specified in Equation 3-9. Zero noise was assumed (*i.e.*, $A_3 = 0$).

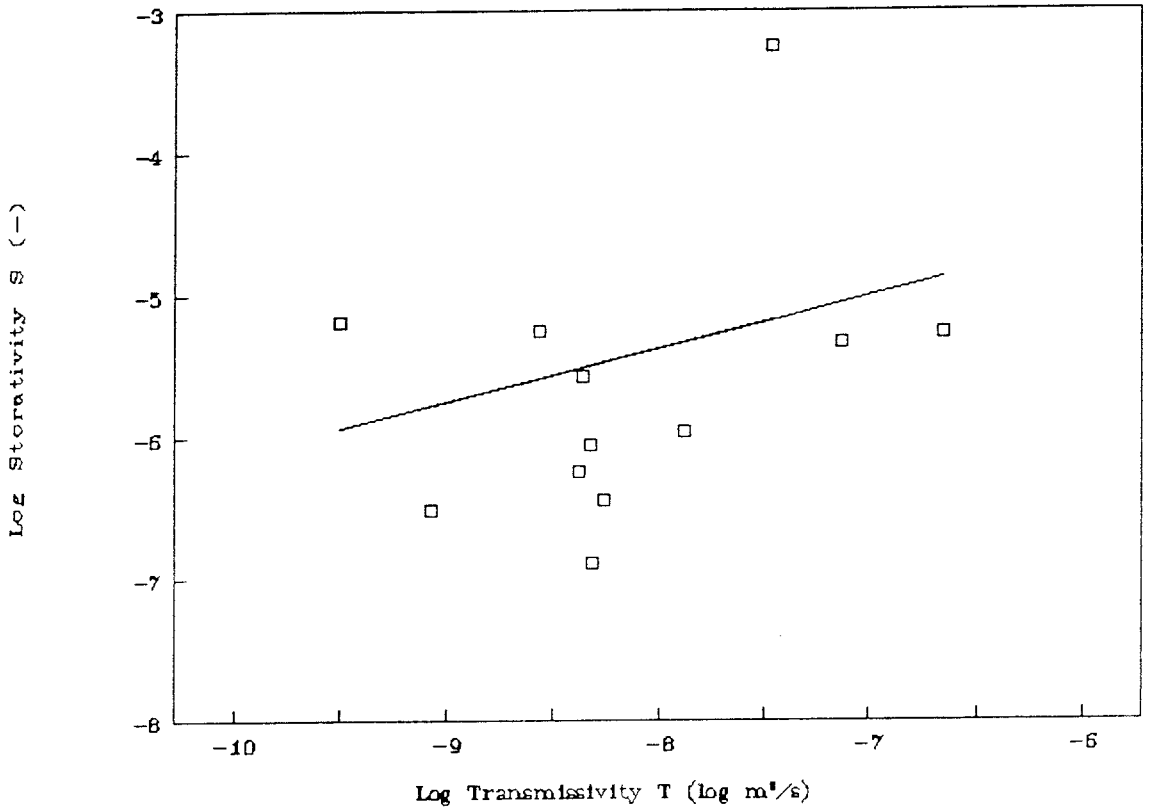

FIGURE 4-8
CORRELATION OF STORATIVITY TO TRANSMISSIVITY

5. CALIBRATION AND VALIDATION OF THE MODEL

The preliminary Phase 1 DFN model is defined on the basis of the discrete fracture properties derived in Chapter 4. This analysis is simplistic in many respects, but it provides an adequate basis for demonstrating the feasibility of the methodology.

The preliminary DFN model can be validated and/or calibrated by simulating the response of the discrete fracture model to various types of hydrological testing. The possibility of validating the model arises from the fact that the dataset is deduced from the obsereved properties of discrete components of the system, but the hydrological response depends upon network effects, *i.e.*, how the components act together as a system. In particular, the observed flow geometry in transient packer tests is an excellent basis for validation, since this information is not used in a direct way in the analysis (The observed transmissivities, on the other hand, are more applicable to calibration, since these data have been used more directly in the OxFILET analysis).

In the Phase 1 study, the preliminary DFN model was found to be reasonably well validated by comparison of simulated and observed FIL test results. Hence calibration of this model was not carried out. However, discussion of calibration procedures is included in the following sections, in anticipation of the likelihood that some calibration of the final safety assessment model will be required.

5.1 Preliminary Conceptual Model Dataset

The Phase 1 preliminary DFN model is defined in terms of a Baecher conceptual model for fracture properties, expressed in terms of probability distributions. Table 5.1 gives a summary of this model. This model is applicable to simulation of cubical regions ranging in scale from 25 m to 50 m. A FracMan macro file for generating 50 m cubes based on this model is listed in Appendix 9. Application of this model to regions much smaller than 25 m cubes may require reducing the minimum fracture radius r_{min} to take smaller fractures into account (These fractures are not expected to be important on a larger scale because of the well-connected nature of the fracture population, discussed below). Application of this model to regions much larger than 50 m will require increasing r_{min} and/or the minimum transmissivity; for a 100 m cube, a minimum transmissivity of 10^{-9} is required to keep mesh generation times within allowable limits for Monte Carlo analysis (No more than 30 minutes CPU time on the SKB Convex).

Figure 5-1 shows an example of a fracture population simulated in a 100 m cube using a truncated version of this conceptual model (only the fractures having $T_f > 10^{-7.5}$ and $r_e > 5$ m are included). The salient feature of the model is the very large number of large fractures, up to the size of the cube and beyond. This results in a fracture network that is very well connected. Many fractures have intersections with dozens of other fractures.

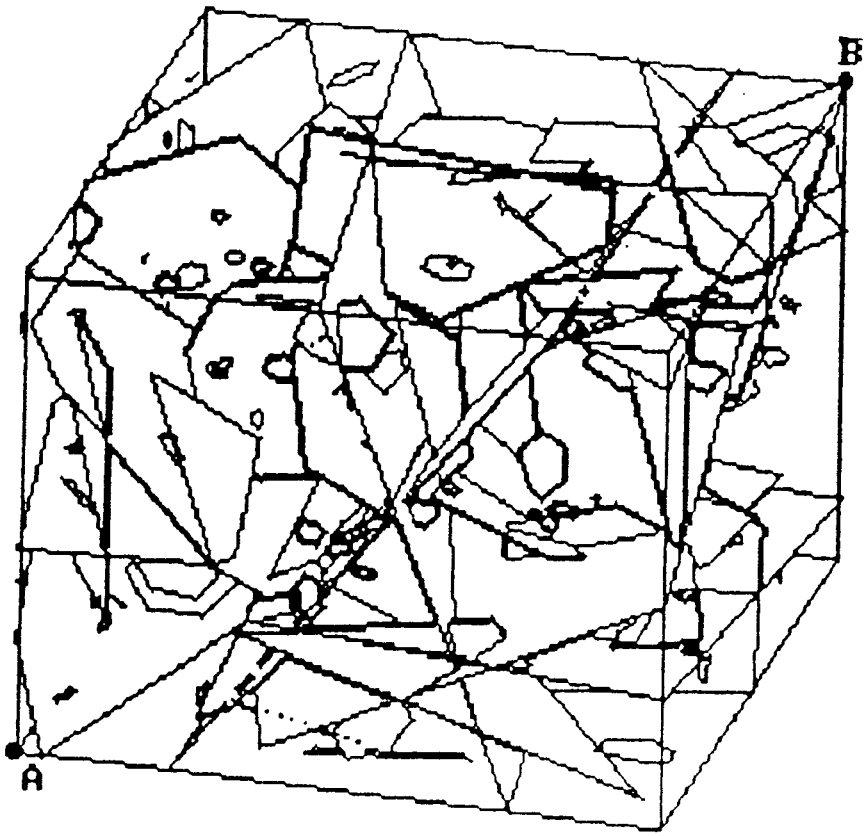

FIGURE 5-1
FRACTURE POPULATION SIMULATED FROM MODEL

Table 5.1 Preliminary Discrete Fracture Flow Model for Phase 1 Feasibility Study

Property	Type of Descriptor	Descriptor Value
Location	Distribution Type	3-D Poisson process
Orientation	Distribution Type	Smoothed Bootstrap
	Concentration κ	10.
Size	Distribution Type	Power Law
	Power Law Exponent b	1.89
	Minimum Radius r_{min} (m)	1.0
Transmissivity	Distribution Type	Truncated LogNormal
	Logarithmic Mean μ_{logw} (m^2/s)	-11.3
	Logarithmic Std. Dev. $\sigma_{log\,T}$ (m^2/s)	2.1
	Log Minimum (m^2/s)	-9.5
	Log Maximum (m^2/s)	-3
Storativity	Correlation Type	Log Linear with T_f
	Constant Factor	1
	Exponent	0.686
Shape	Termination Percentage	0.
Intensity	Distribution Type	Constant
	Effective P_{32c} Intensity	0.487

The high number of intersections per fracture is illustrated by Figure 5-2, which shows a representative horizontal cross section through a 50 m cube for the full fracture population in Table 5.1. The number of intersections per fracture is likely to be even higher in three dimensions than is apparent in such a cross section. The percolation probability of blocks (the chance of a pathway across the blocks) over a wide range of scales is expected to be high, although the conductance of most pathways is expected to be very low.

Subsequent refinement of the analysis during Phase 2 may result in modifications of this model, but the well-connected nature of the simulated fracture population is not likely to be substantially changed. The connectivity was so extreme that it caused a practical problem in terms of extremely slow finite-element mesh generation. This problem was obviated by an enhancement to the mesh generator. With the enhanced mesh generator, finite element meshes for cubes of scales up to 50 m could be produced in less than 15 minutes of CPU time on the SKB Convex.

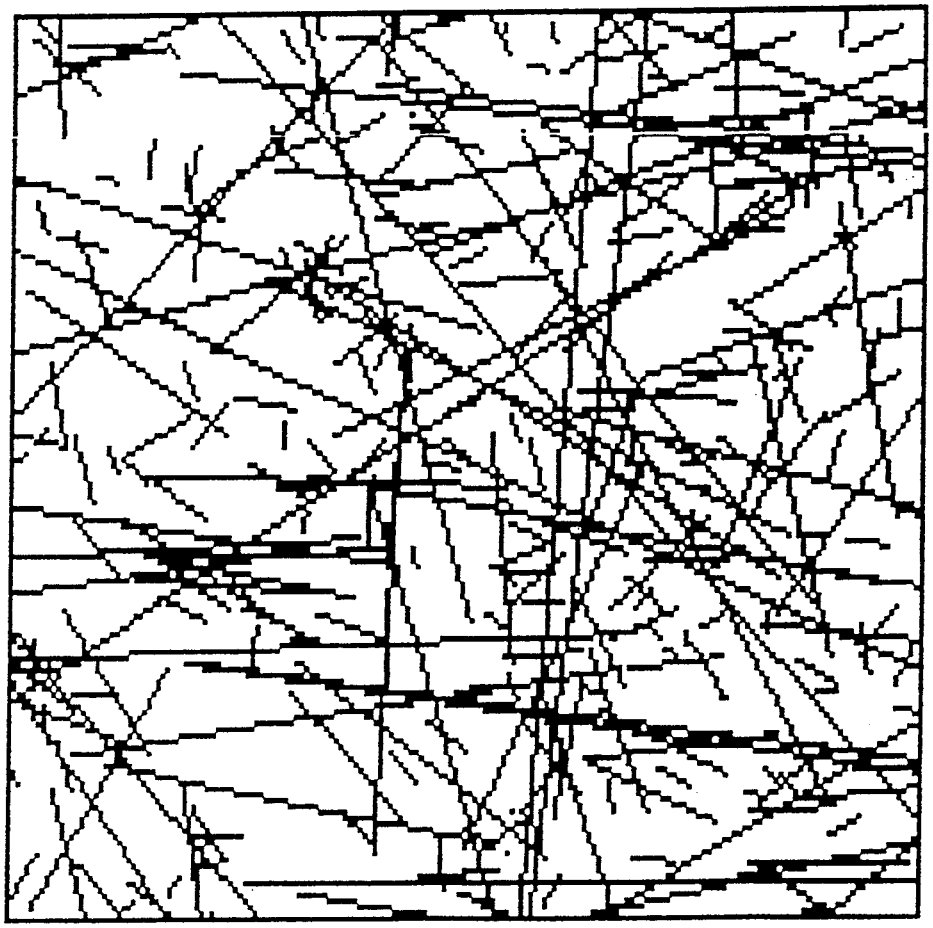

FIGURE 5-2
CROSS-SECTION THROUGH SIMULATED FRACTURE POPULATION

5.2 Description of Validation and Calibration

A rough validation of the Phase 1 DFN model was carried out by simulating transient packer tests in vertical packer intervals, approximately in the center of 50 m cubes. The simulated packer test results were analyzed by the same fractional-dimension type curve matching procedure used for the analysis of transient data in Chapter 4.3.

The geometry of the boundaries for these tests were as shown in Figure 5-3. A vertical borehole through the center of each block was simulated by five 2 m "packer intervals," separated by 1 m sections of intact rock. These 1 m sections were intended to represent packers. The behaviour of these sections may differ slightly from actual packers, since fractures passing through these sections can still conduct flow; however, this difference is most likely negligible since for a fracture larger than the hole diameter, the flow would most likely simply pass around the packer.

Only the three intervals nearest the center of the block were used for flow simulations. A separate flow simulation was run using MAFIC for each of the three intervals. In each simulation, an increase in head of 20 m over the background head of zero was applied to the active interval. The remaining intervals were modelled using a group flux boundary condition, with a net flux of zero into each interval. Transient simulation of constant-head injection was performed, with flow and head calculated for timesteps from 5 to 1000 seconds after the start of injection. The flowrate as a function of time from the packed-off interval produced flux vs. time curves.

Figure 5-4 gives log-log plots of the flowrate versus time for the conductive intervals in the first ten intervals tested. Four of the ten intervals (40%) were nonconductive (no intersections with fractures), in comparison with 25% nonconductive intervals in the full FIL dataset. However, the use of a truncated transmissivity distribution with a minimum value $T_{min} = 10^{-9.5}$ m^2/s means that the measurement limit of these tests was significantly higher than for the original dataset, which had a measurement limit of only about 10^{-10} m^2/s. The percentage of FIL tests with transmissivities less than $10^{-9.5}$ was about 36%, as seen in Figure 4-7.

The results of type-curve analyses of the curves in Figure 5-4 is shown in Table 5.2. Figure 5-5 shows a comparison of the dimensionality and transmissivity distributions for the simulated tests and the sample of tests analyzed in Appendix 6. Based upon this limited sample, the simulated tests are seen to have approximately the same range of dimensionality as the sample analyses. The transmissivity distributions are also roughly similar, although the logarithmic mean simulated transmissivity is about half an order of magnitude less than logarithmic mean of the sample analyses.

Given the many limitations of the analysis on which the Phase 1 model is based, the degree of agreement between these small samples of simulated and actual tests is rather remarkable — and probably mostly a matter of luck. The non-random selection of the dataset for comparison may make this comparison misleading — although the expected effect of the sampling bias would be to **increase** the average transmissivity of the test sample, and thus worsen the match.

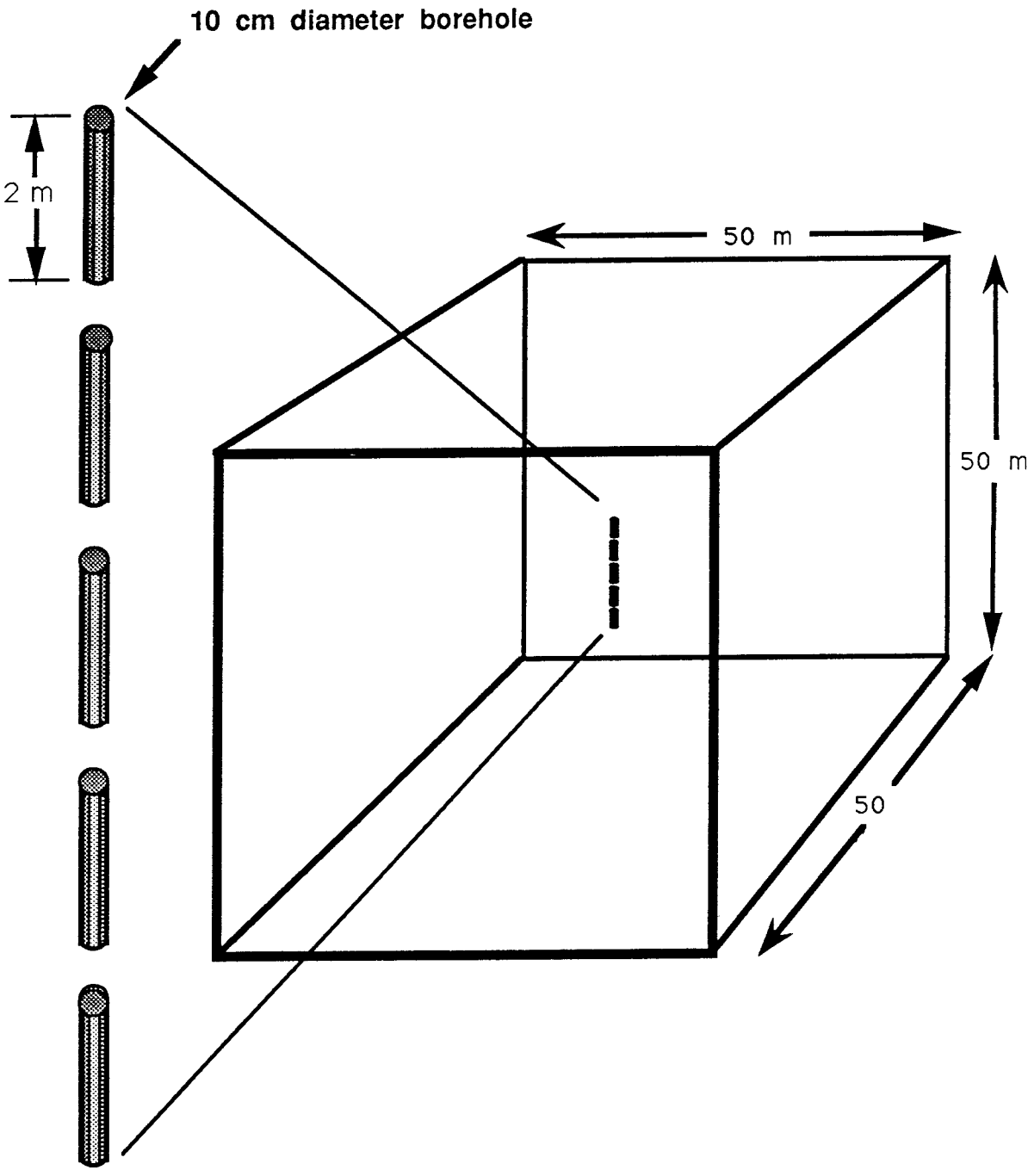

FIGURE 5-3
GEOMETRY FOR PACKER TEST SIMULATIONS

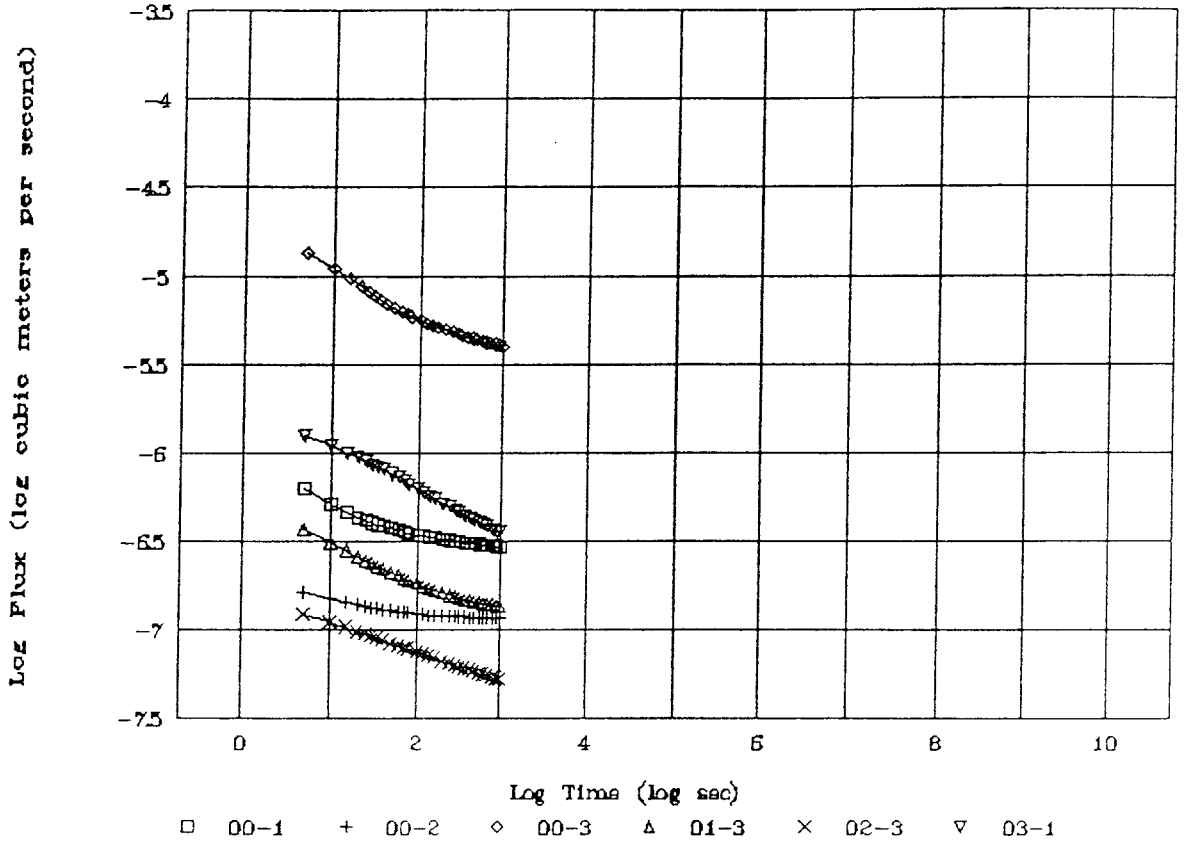

FIGURE 5-4
TYPE CURVES FROM PACKER TEST SIMULATIONS

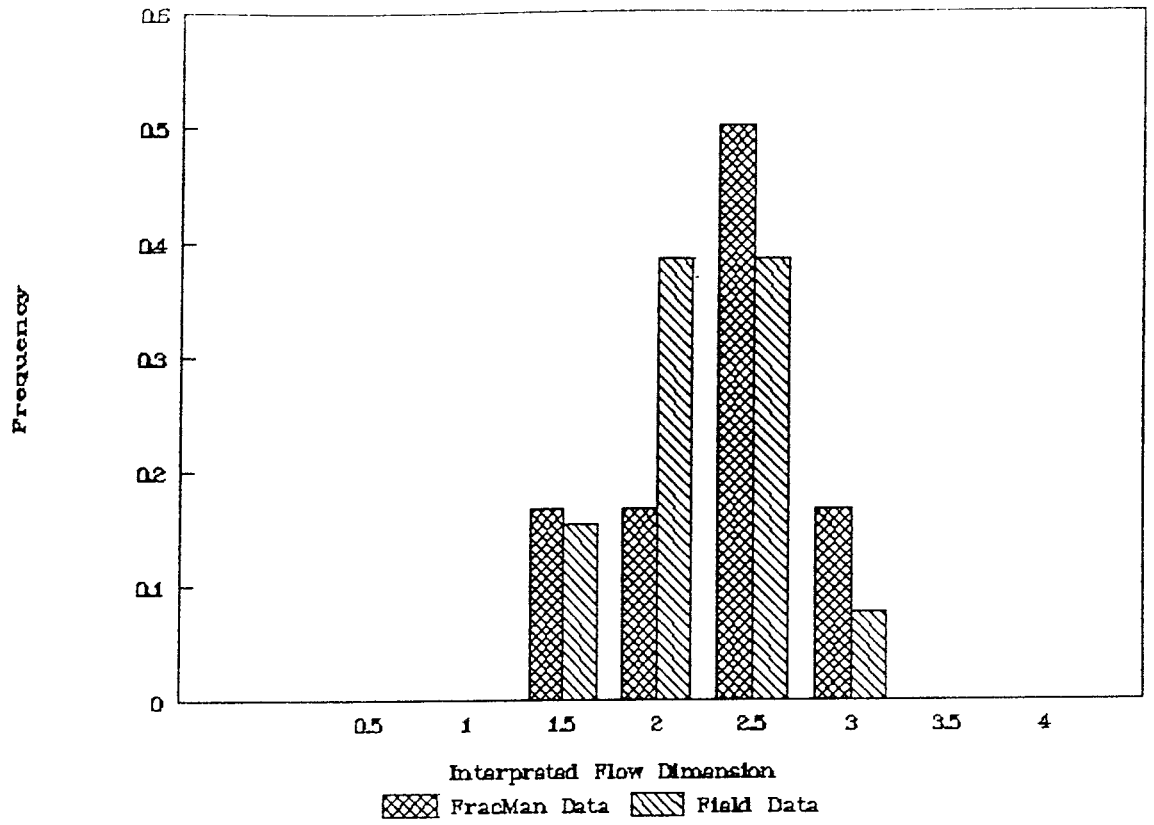

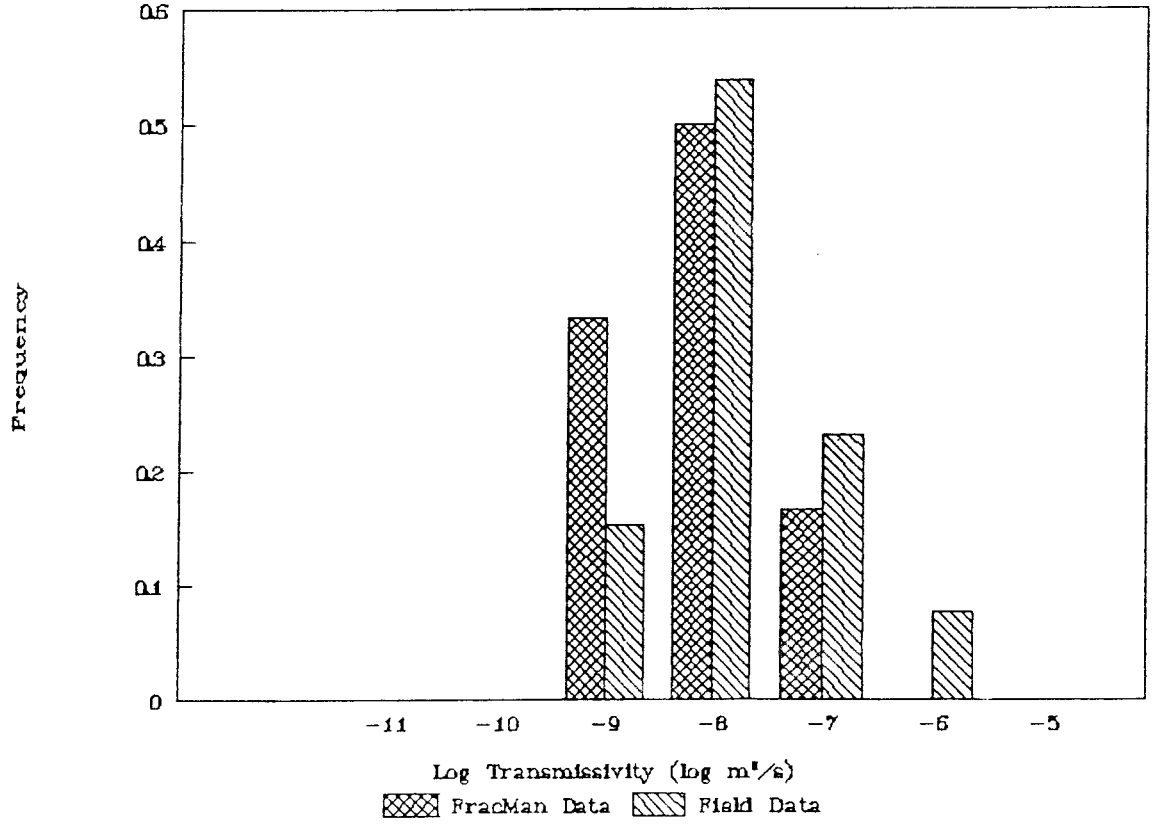

FIGURE 5-5

VALIDATION OF MODEL WITH PACKER TEST SIMULATIONS

Table 5.2 Generalized-Dimension Flow Analysis of Constant Head Test Simulations

Radius of well	r_w	0.05 m
Effective length	L	0.005 m
Head in zone	h_{w0}	20 m
Match point	t_{Dmatch}	1 s
	Q_{Dmatch}	1 m^3/s

Simulation Number	Zone No.	Flow Dimension D	Match Point		Conductivity K (m/s)	Specific Storage S_s (1/m)	Transmissivity T (m^2/s)
			Log t_{match} (s)	Log Q_{match} (m^3/s)			
D2ABT00	1	3.0	1.35	-6.6	2.00×10^{-8}	1.79×10^{-4}	9.99×10^{-11}
D2ABT00	2	2.5	0.5	-6.9	4.31×10^{-8}	5.46×10^{-5}	2.16×10^{-10}
D2ABT00	3	2.5	1.8	-5.3	1.72×10^{-6}	4.33×10^{-2}	8.59×10^{-9}
D2ABT01	1	-	-	Nonconductive			
D2ABT01	2	-	-	Nonconductive			
D2ABT01	3	2.5	1.35	-6.72	6.53×10^{-8}	5.85×10^{-4}	3.26×10^{-10}
D2ABT02	1	-	-	Nonconductive			
D2ABT02	2	-	-	Nonconductive			
D2ABT02	3	2.0	0.1	-6.7	3.18×10^{-7}	1.60×10^{-4}	1.59×10^{-9}
D2ABT03	1	1.5	-0.75	-5.15	5.81×10^{-5}	4.13×10^{-3}	2.91×10^{-7}

As the match between simulated and actual FIL tests is quite good, considering the crudeness of the Phase 1 analysis, there is no point in refining this preliminary model further by calibration. If all available transient test data had been analyzed and compared with at least 20 simulated FIL tests, and if a discrepancy of half an order of magnitude in the mean of log T_L were still seen, then the transmissivity distribution $f_{Tf}(T_f)$ would need to be calibrated.

For results similar to the present case, a small increase in $\mu_{\log T}$ would be tested first. Since the variance of the simulated test results is greater than the observed variance, the parameter $\sigma_{\log T}$ might also be reduced, particularly if the OxFILET analysis indicated (as it does in the present case) that the sensitivity of the K-S statistic to a change in the parameters of $f_T(T_f)$ is least if $\mu_{\log T}$ is increased and $\sigma_{\log T}$ are decreased simultaneously. The philosophy of the calibration procedure is to avoid adjusting model parameters so far that the revised fits to the field data become unacceptable. If the model cannot be calibrated within reasonable limits for goodness-of-fit to field data for all stages of analysis, the basic conceptual model must be re-examined.

5.3 Phase 1 Discrete Fracture Conceptual Model

Given the small quantity of transient FIL test interpretation available for comparison, the preliminary Phase 1 DFN model is considered to be adequately validated. Thus the dataset for the Phase 1 DFN model is exactly as given in Table 5.1. This model forms the basis for simulations of block-scale flow and pathways analysis.

6. PHASE 1 SIMULATIONS

This chapter describes pathways analysis and simulation of block-scale and packer test conductivity evaluations, based upon the DFN conceptual model derived in Chapter 4 and validated in Chapter 5. These analyses were originally proposed to demonstrate the interfacing of the DFN model to the CN and SC models. However, during Phase 1 the plans for this interface were revised extensively during consultations with the other modelling groups participating in the SKB 91 safety analysis. In some cases, the proposed plans for the interface between models require effort beyond that envisioned at the outset of the Phase 1 feasibility study, as described in Sections 3.6 and 3.7.

The analyses described in the following sections are thus simplistic in comparison to the work foreseen in the remainder of the SKB 91 project. However, these analyses provide an indication of the larger-scale behaviour of the DFN model, which may be valuable to SC and CN modellers in devising test data sets. As illustrations of the DFN approach, these analyses may help to clarify the relationships among the various models.

6.1 Pathways Analysis

Only three pathways analyses simulations were performed as illustrations of the method. The objective of the simulations was to determine the number and conductance of pathways from a 100 m × 100 m "repository" to either of two hypothetical, horizontal "fracture zones" located 50 m and 100 m above the repository, respectively. Figure 6-1 shows the geometry of the FracMan model for this scenario, with the lower plane representing the repository, and the upper and middle planes representing the two fracture zones.

An attempt was made to perform pathways analysis for this problem using the full data set in Section 5.1. However, due to the very large number of fractures in the model, and the extremely well-connected nature of the fracture population, trial simulations ran for several hours on an 80386-based computer without producing a solution.

To reduce the time needed for the simulations, the fracture population was reduced by increasing the minimum radius to 5 m, and increasing the minimum transmissivity to $10^{-7.5}$ m^2/s. This reduced the number of fractures in the simulated population to less than 1500, and made it possible for FracMan to identify pathways within about an hour. However, the connectivity of the network was severely reduced by these very high truncation limits, as indicated by trace plane samples. As a result, the outcome of the pathways analyses was not very interesting — in each simulation, a single large fracture was found that connected all the way across the region. Table 6.1 gives an example of the output from one of these runs.

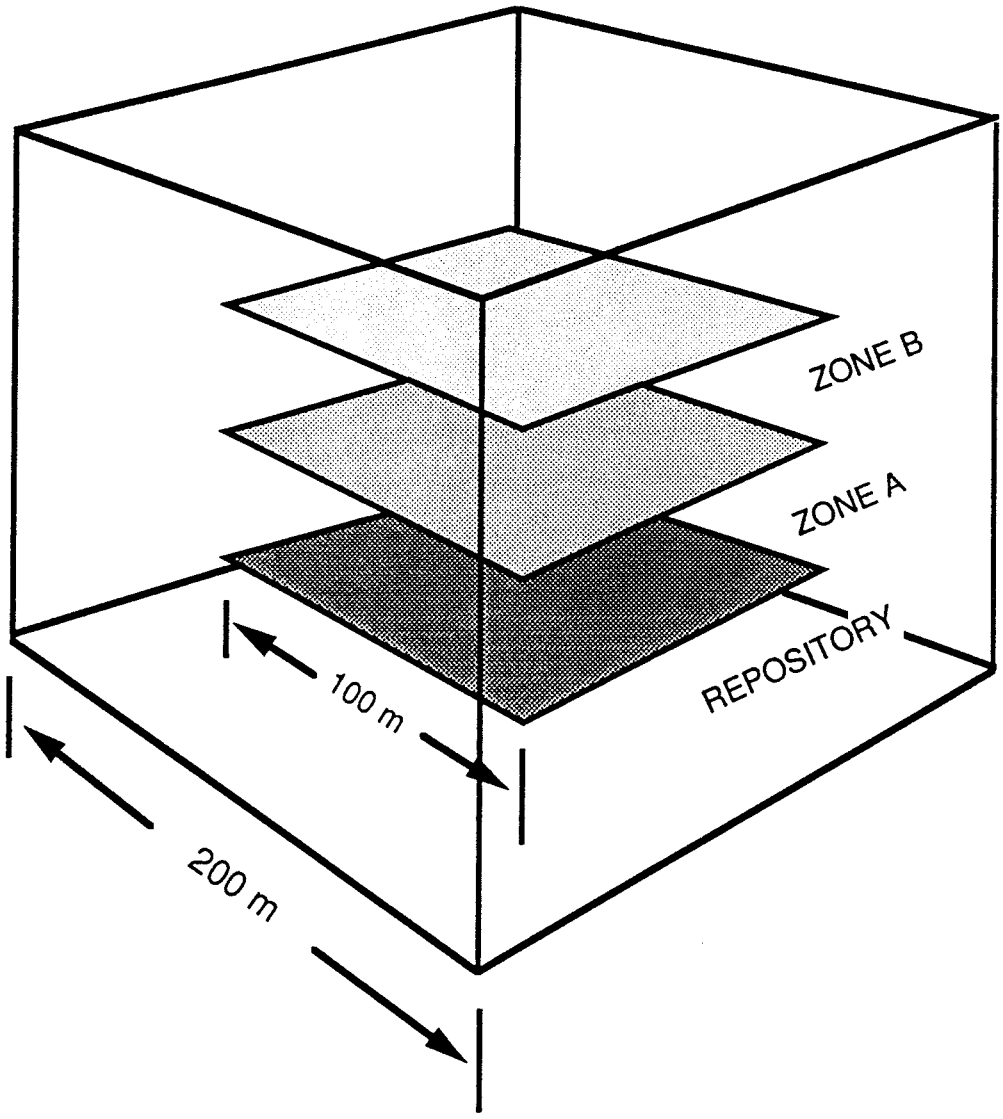

FIGURE 6-1
GEOMETRY FOR PATHWAY ANALYSIS DEMONSTRATION

Table 6.1 Example of Output from Pathways Analysis

No. of Fractures = 1387	Source = T1	Minimum Conductance = 1.0×10^{-14}

Network No.	Source/ Target	Pathway Minimum Transmissivity (m^2/s)	Pathway Effective Conductance (m^3/s)	Pathway Total Storage (m^2)
1	S-->T2	1.50×10^{-7}	1.50×10^{-5}	1.16×10^{-4}
2	S-->T3	1.50×10^{-7}	1.50×10^{-5}	1.16×10^{-4}

Total No. of Pathways: 2	Total Conductance: 3.00×10^{-5}

For each pathway found, from the source to each of the targets, FracWorks gives the following information:

- Minimum transmissivity (the transmissivity of the least conductive fracture on the pathway)
- Conductance (the approximate, effective conductance of the pathway, calculated as the harmonic mean of the conductance of the fractures comprising the pathway).
- Storage (the sum of the products of storativity times fracture area for all fractures in the pathway).
- Number of fractures in the pathway.

In the example shown, the only pathway found consists of one fracture.

As a rule, pathways analysis is most effective for finding pathways in fairly sparse fracture systems, or fracture systems in which most fractures have only a few connections. For such systems, pathways analysis provides a much more efficient method for characterizing the most conductive paths than does a full solution of the flow equation. However, for highly connected fracture systems such as the dataset from Section 5.1, the method becomes inefficient due to the high number of intersections per fracture, which results in an enormous number of possible pathways that must be searched.

The utility of pathways analysis for CN models using the present dataset is doubtful, because the idea of such large fractures having constant aperture seems unlikely. The method may be more realistic with the addition of variable aperture, but the efficiency of the method is likely to be poor due to the high degree of interconnection, unless the size and transmissivity distributions are drastically truncated.

For very well connected fracture populations such as the Phase 1 DFN model, highly conductive pathways can be identified more efficiently by applying boundary conditions and solving the flow equation. Major flow conduits can be distinguished by calculating the flux passing through each triangular element from the finite element solution, and identifying those elements that carry the major quantities of flow (Figure 6-2). This type of analysis was not carried out in the Phase 1 study.

6.2 Block-Scale Simulations

Multiple cross-block flow simulations were performed for scales of 25 m and 50 m. Ten blocks were simulated on each scale. Finite element meshes for both of these scales were created from the same realizations of the DFN model, produced using a 56 m × 56 m × 56 m fracture generation region.

The meshes for the 25 m simulations were generated from the center of the 56 m cubes. For the 50 m simulations, the same finite element meshes were used as for the packer tests simulations. In the 50 m block simulations, the simulated packer intervals were "sealed" by imposing a zero-flux (no-flow) boundary condition on the intervals.

For each block, flow was simulated in three directions parallel to the coordinate axes, using no-flow boundaries on the sides parallel to the flow direction. Declining-head boundary conditions were not performed. Prior experience with the two sets of boundary conditions indicated that the no-flow boundary conditions in general required more time for solution, and hence represented a more severe test of the model for the feasibility study.

The boundary conditions that were applied to all faces were of the form:

$$H = H_1x_1 + H_2x_2 + H_3x_3 + H_o \qquad \text{Fixed head (m)}$$

$$Q = Q_1x_1 + Q_2x_2 + Q_3x_3 + Q_o \qquad \text{Fixed flux (m}^3\text{/s)}$$

where x_1, x_2, and x_3 represent coordinates in a system with axes in the South, West, and Up directions, respectively. The coefficients used in fixed-head and no-flow boundary conditions are shown in Table 6.2.

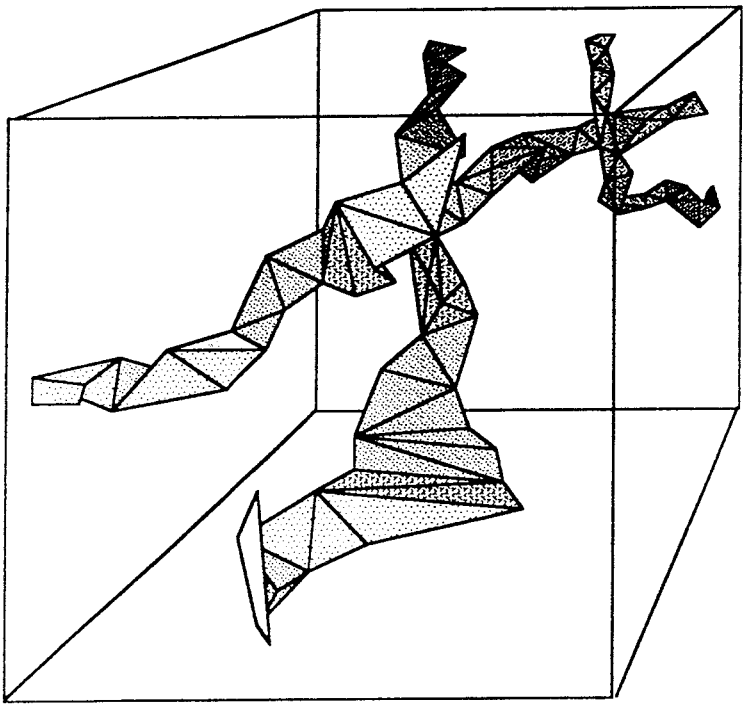

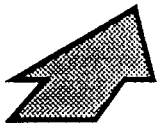

Flow Direction

FIGURE 6-2
IDENTIFICATION OF PRINCIPAL CONDUITS
WITHIN BLOCK-SCALE FLOW SIMULATIONS

Table 6.2 Boundary Conditions for the Phase 1 Block-Scale Simulations

	Head Cofficients				Flux Coefficients			
	H_1 (-)	H_2 (-)	H_3 (-)	H_o (m)	Q_1 (m^2/s)	Q_2 (m^2/s)	Q_3 (m^2/s)	Q_o (m^3/s)
North-South Flow								
North and South faces	-1	0	0	0	--	--	--	--
East and West faces	--	--	--	--	0	0	0	0
Top and Bottom faces	--	--	--	--	0	0	0	0
East-West Flow								
North and South faces	--	--	--	--	0	0	0	0
East and West faces	0	-1	0	0	--	--	--	--
Top and Bottom faces	--	--	--	--	0	0	0	0
Up-Down Flow								
North and South faces	--	--	--	--	0	0	0	0
East and West faces	--	--	--	--	0	0	0	0
Top and Bottom faces	0	0	-1	0	--	--	--	--

6.2.1 Accuracy of Simulations

For each cross-block flow simulation, the results obtained were the effective hydraulic conductivity on the scale of the block, for North-South, East-West Flow, and Up-Down flow. The effective hydraulic conductivities of blocks were calculated from the flux values across the boundaries that were calculated by **MAFIC**. Accuracy of the numerical solutions was checked to ensure that minimal global and nodal mass-balance criteria were satisfied. The nodal mass balance ratio ϵ_ℓ was calculated as:

$$\epsilon_\ell = \frac{\max_i |\Delta q_i|}{\sum_i \Delta q_i} \qquad (6\text{-}3)$$

where:

Δq_i = the flux imbalance calculated at the ith node [L^3/T]

For the present study, the nodal mass balance criterion was $\epsilon_\ell \leq 10^{-7}$. The global mass balance criterion ϵ_g was calculated as:

$$\epsilon_g = \frac{\sum_{i=1}^{6} Q_i}{\max_i |Q_i|} \tag{6-4}$$

where:

Q_i = the flux across the ith boundary of the cube [L^3/T]

For all simulations the values of ϵ_g satisfied the criterion $\epsilon_g \leq 10^{-5}$.

6.2.2 Block Scale Hydraulic Conductivity

The effective hydraulic conductivities were calculated from the fluxes across the faces of the cubes:

$$K_{11_s} = \frac{Q_{south} - Q_{north}}{2s^2} \tag{6-5}$$

$$K_{22_s} = \frac{Q_{east} - Q_{west}}{2s^2} \tag{6-6}$$

$$K_{33_s} = \frac{Q_{up} - Q_{down}}{2s^2} \tag{6-7}$$

where:

Q_{north} = flux northward out of the cube (m^3/s)
Q_{south} = flux southward out of the cube(m^3/s)
Q_{east} = flux eastward out of the cube (m^3/s)
Q_{west} = flux westward out of the cube (m^3/s)
Q_{up} = flux upward out of the cube (m^3/s)
Q_{down} = flux downward out of the cube (m^3/s)

For each scale s, an average block-scale conductivity K_s was calculated as the mean of the directional conductivities:

$$K_s = \frac{1}{3}\left(K_{11_s} + K_{22_s} + K_{33_s}\right) \tag{6-8}$$

Statistical summaries of the preliminary results for average hydraulic conductivity of 25 m and 50 m blocks are given in Tables 6.3. Figure 6-3 shows histograms of the average conductivity values calculated for the two scales. The measured conductivities show a fairly tight distribution on a log scale, suggesting that the heterogeneity on these scales is rather low. The differences between the conductivity distributions on the two scales can be assessed on the basis of the χ^2 statistic to determine whether the scale effect is significant between these sizes of blocks.

Table 6.3 Statistical Summary of Block-Scale Conductivities

	25 m Cubes		50 m Cubes	
	K_s (m/s)	log K_s (log m/s)	K_s (m/s)	Log K_s (log m/s)
Mean	1.92×10^{-8}	-7.87	1.97×10^{-8}	-7.87
Standard Deviation	1.72×10^{-8}	0.36	2.26×10^{-8}	0.34
Median	1.05×10^{-8}	-7.98	1.16×10^{-8}	-7.94

6.2.3 Block-Scale Anisotropy

The anisotropy of the blocks was characterized in terms of the ratios:

$$\kappa_{ii} = \frac{K_{ii_g}}{K_s}, \qquad i = 1,2,3 \tag{6-9}$$

for each block. The distributions of the ratios κ_{ii} are plotted in Figure 6-4.
These results show that, on average, the blocks are approximately isotropic. However, significant anisotropy is predicted to exist, as indicated by κ_{ii} values ranging over two orders of magnitude. Slight differences are apparent among the plots for the different flow directions, but given the variance observed for each ratio, the number of blocks simulated is insufficient to justify any definite statement about differences among the three directions.

6.3 Packer Test Simulations

The simulations of packer tests that were performed for model validation and calibration are also useful for estimating the probabilistic relationship between packer test conductivities observed within a block and the large-scale behaviour of the block. This relationship is needed for conditioning of SC models based upon packer test results.

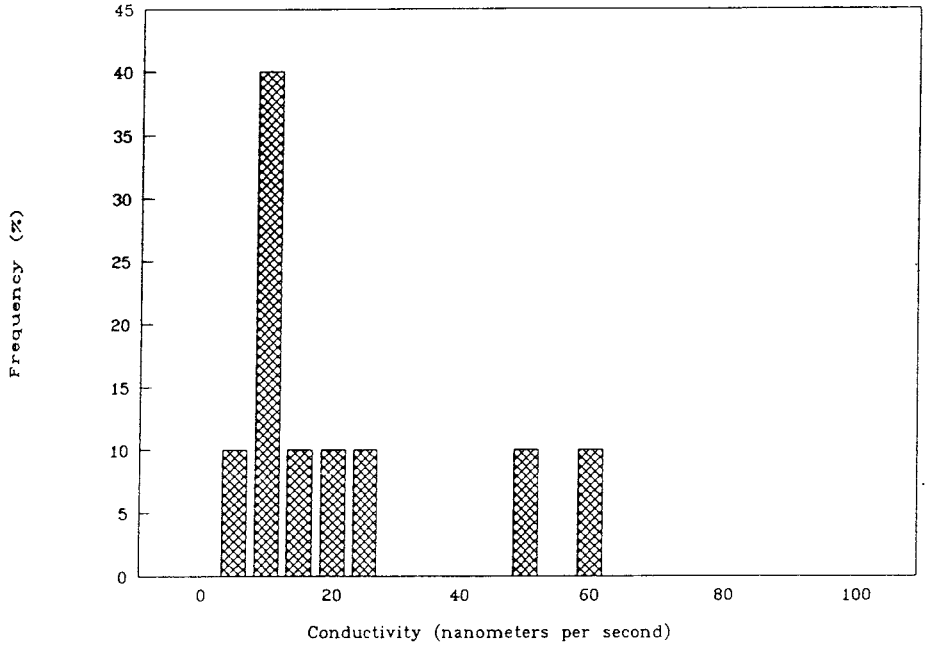

a) 25 m Cubes

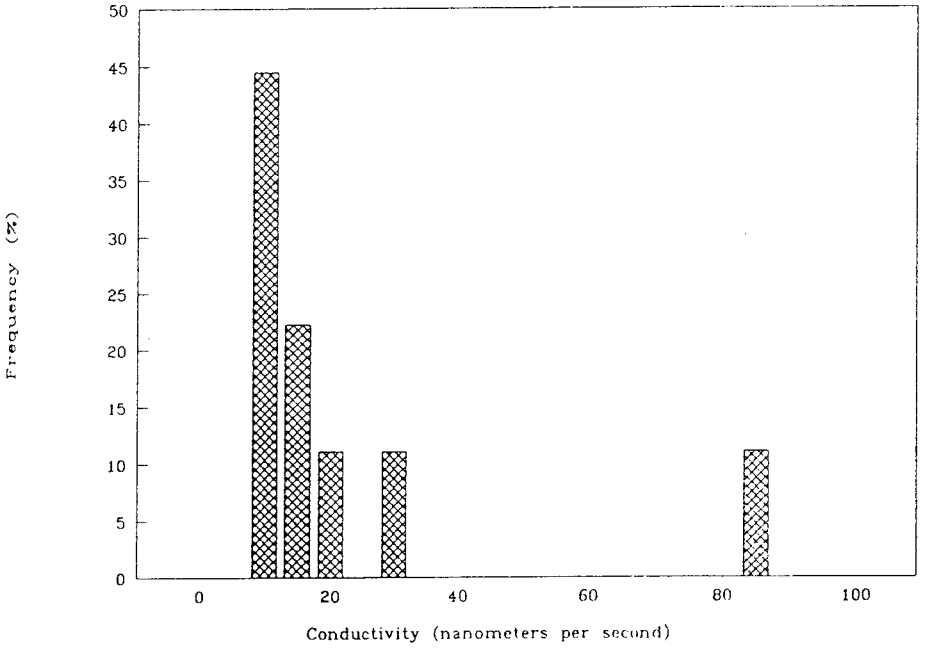

b) 50 m Cubes

FIGURE 6-3
BLOCK-SCALE CONDUCTIVITY FOR
25 m AND 50 m BLOCKS

25 m

50 m

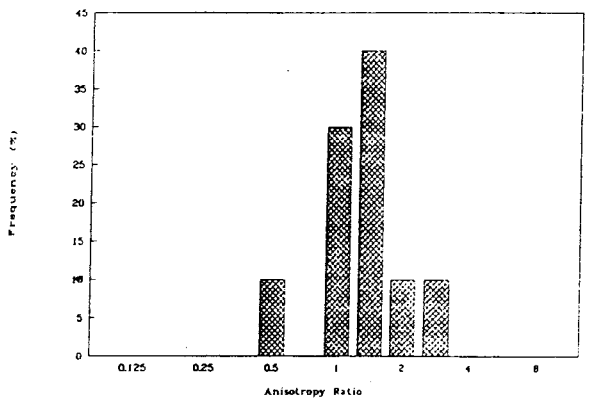

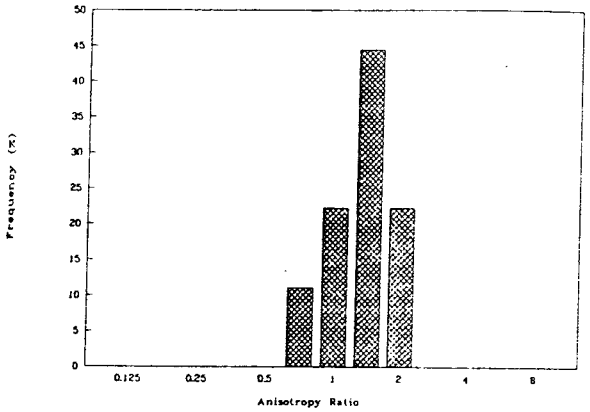

a) K_{11} / K_S

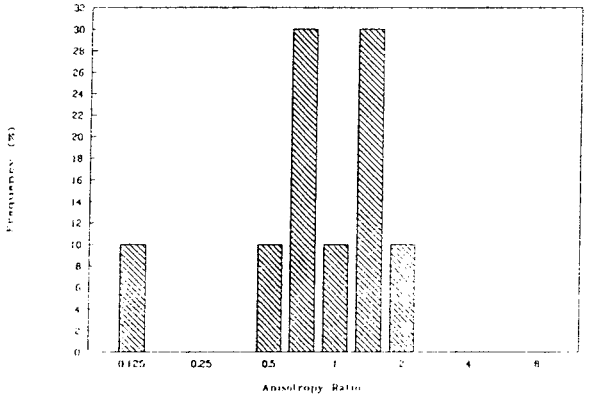

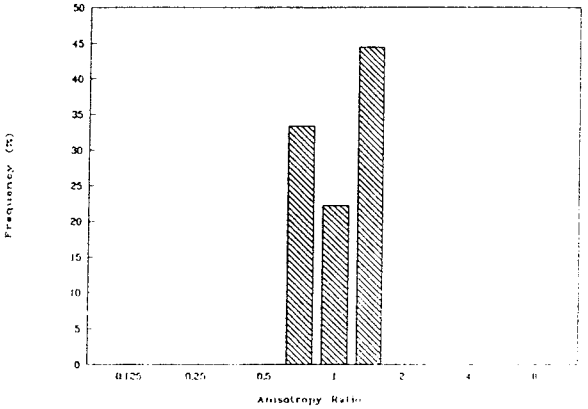

b) K_{22} / K_S

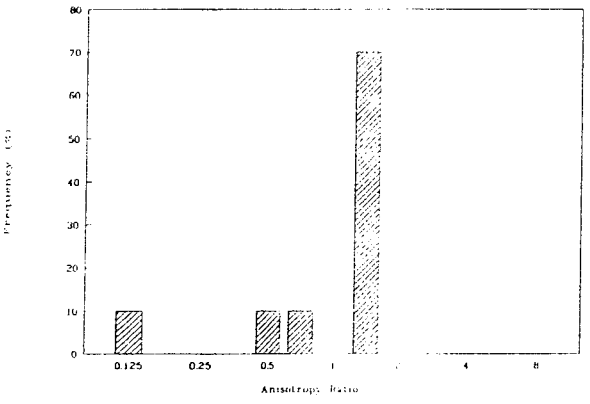

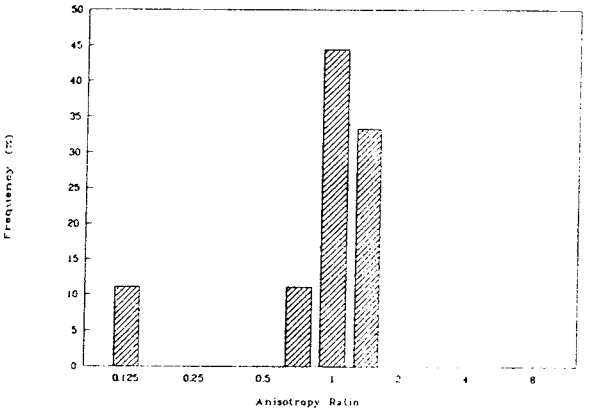

c) K_{33} / K_S

FIGURE 6-4
BLOCK-SCALE ANISOTROPY RATIOS
FOR 25 m AND 50 m BLOCKS

Figure 6-5 shows plots of interpreted well test conductivities from Table 5.2, plotted as a function of K_s for the corresponding blocks, for 25 m and 50 m scales, respectively. The position of the test intervals is indicated by number:

1. 2 m test centered in block.
2. Test interval 2-4 m above center of block.
3. Test interval 2-4 m below center of block.

A large number of simultaneous block-scale/packer-test simulations such as these would provide a basis for estimating the statistical relationships between test results in different locations (in this case, either centered in the block or slightly above or below center) and block conductivity. For SC simulation from data that have been analyzed in other fashions, the method of interpretation for the simulated tests should correspond to that used to analyze the field data.

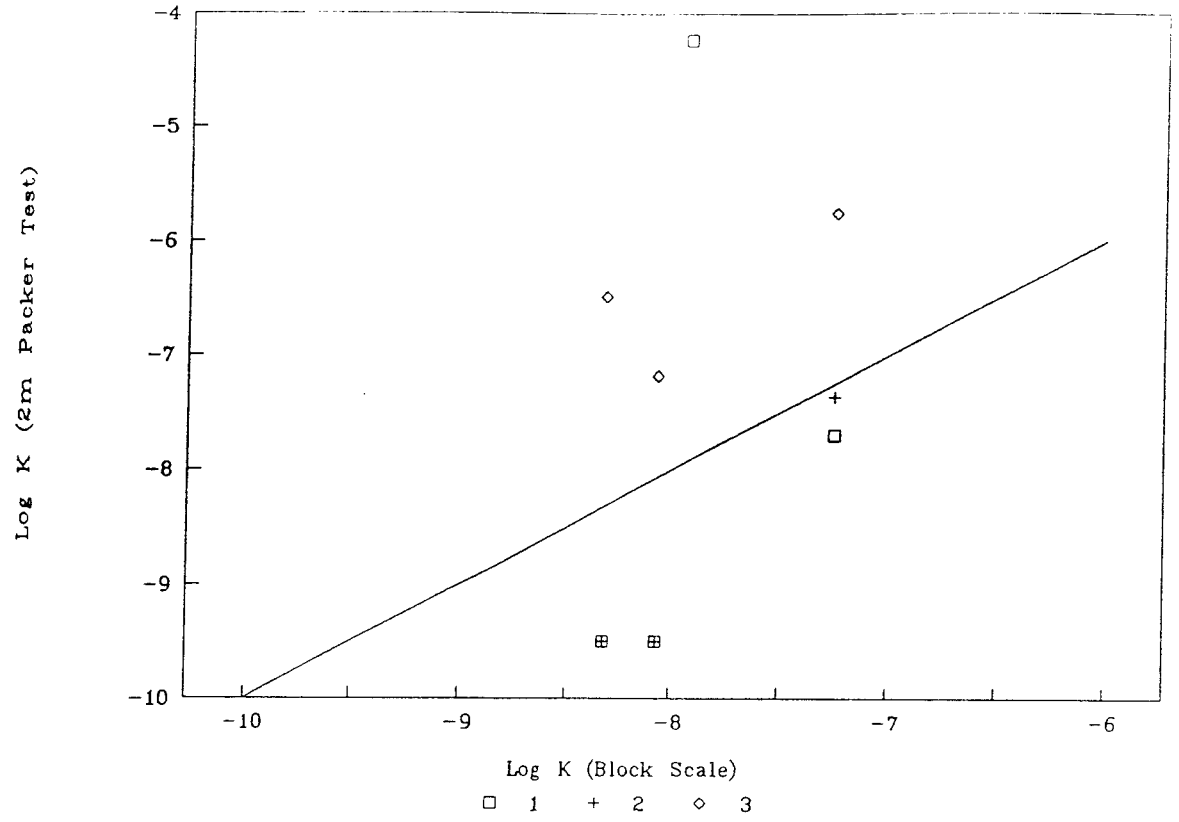

a) 25 m Cubes

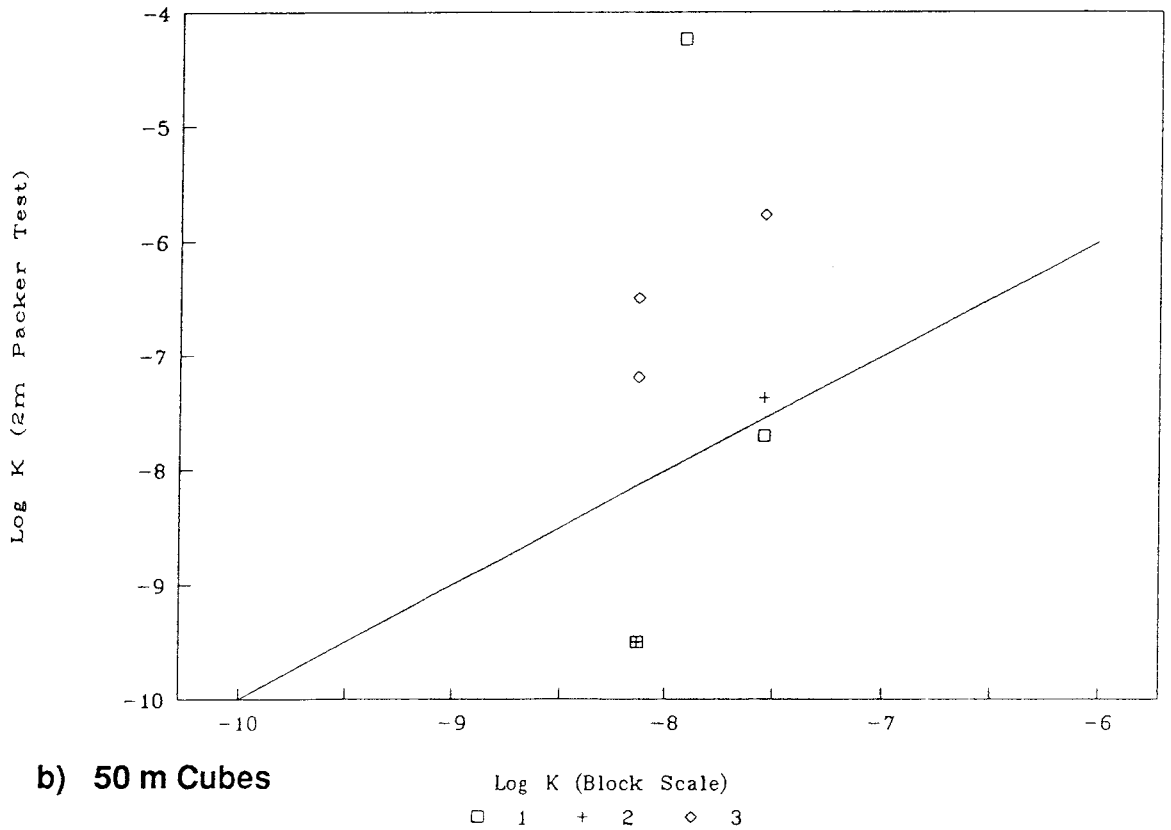

b) 50 m Cubes

FIGURE 6-5
PACKER TEST CONDUCTIVITY VS. BLOCK SCALE CONDUCTIVITIES

7. DISCUSSION AND CONCLUSIONS

The first phase of the present modelling study successfully produced the following results:

- A Discrete Fracture Network (DFN) conceptual model for fracture geometry and hydrology in the Finnsjön rock block below Zone 2.
- A validated discrete fracture interpretation based upon a limited set of simulated hydrologic tests,
- Preliminary estimates of rock block effective hydraulic conductivity and anisotropy distributions for 25 m and 50 m rock blocks.
- Demonstration of the application of generalized-dimension flow packer test interpretations for a sample of 13 tests.
- Demonstration of two methods for using data on single-fracture aperture variation and surface roughness measurements to formulate a model for transmissivity variation within single fractures.
- Data sets for 25 m, 50 m, and 100 m scales which are computationally tractable.
- Limited demonstration of the pathways analysis approach which indicated that this approach is not efficient for the particular fracture population at Finnsjön.

The methodology for deducing the relationship between T_{fo} and T_f requires validation of a fractal model for transmissivity variation. Data is available for this purpose from the Stripa Project (Abelin *et al.*, 1990).

The major weaknesses of the preliminary DFN model are:

- Assumption of constant transmissivity within fractures.
- Imprecise estimates of fracture transmissivity and size distributions.
- Assumption of stationary statistics for fracture population.

In spite of these weaknesses, the model gives a good match to the limited set of packer test results that were used for validation.

The applicability of the preliminary DFN model results to stochastic continuum models is limited because of the small number of simulations, and because the simulation of separate blocks as independent realizations means that spatial correlation statistics cannot be developed.

7.1 Adequacy of Database for DFN Modelling

The Phase 1 feasibility study provided an opportunity to assess the adequacy of the database for DFN modelling. A general assessment is that the database is adequate for a demonstration of the methodology, but that there are some deficiencies in the database that may limit the applicability of the DFN model predictions for a full-scale safety assessment study.

The major problem that was evident is the limited amount of complete fracture orientation data. Complete fracture orientations are available only at the surface, and some of the older scanline data from at surface do not include fracture dip angles. The most complete data come from a small area (48 m^2 plus about 50 m of scanline), and a comparison between fracture strike directions from the older scanlines and this detailed-scale mapping (Section 2.1.1) suggests that the detailed-scale mapping data may not be entirely representative of the fracture population over the entire site.

On the other hand, some rough similarities between the strike distributions are noted. The Terzaghi-corrected dip angle distributions from the surface and from at depth also show a rough similarity. This indicates that the fractures seen in the detailed-scale mapping may provide a coarse approximation to the actual fracture population, which may be sufficient for sensitivity analyses to investigate the importance of fracture orientation distribution in the model.

Another weakness of the database is the lack of fracture size (*i.e.*, tracelength) data from at depth. Such data can be obtained only from mapping of tunnel walls. The lack of a clear similarity between orientation data at the surface and at depth makes the use of surface size data to characterize the fracture population at depth somewhat dubious.

However, the use of lineament data from a wide range of mapping scales in the analysis, and the tentative identification of a scale-invariant size distribution provides some justification of the size data to depth. Since the maximum horizontal mapping scale exceeds the depth of interest by more than an order of magnitude, certainly many of the larger lineaments seen at the surface must persist at depth. If there is a structural relationship between fractures and lineaments on different scales that results in a scale-invariant size distribution observed where the large-scale lineaments are exposed, then it seems likely that the same structural relationship should hold at moderate depths, and a similar size distribution should be expected at depths that are small relative to the scale of the larger lineaments.

The use of large-scale lineament data in the present study to supplement the small-scale tracelength data is a significant extension to the methodology of DFN data analysis, as it provides a means of characterizing the widely-spaced, large-scale features that cannot be observed in detailed-scale mapping.

A strong point of the database is the large number of FIL packer tests that have been performed. The present study used only a small fraction of the available data, but this was sufficient to produce a DFN model that successfully reproduced the observed range of packer test results. The database is particularly strong within Zone 2, which was not considered in the Phase 1 analysis.

A problem of non-uniqueness was noted in the FIL test analysis in Section 4.5. This may be partly due to the small amount of the available data that were utilized. However, the non-uniqueness arises in part from the large number of interval transmissivities that are close to the measurement limit for the testing equipment and procedures used. As seen in Figure 4-7, the mode of the transmissivity values is close to the measurement limit.This contrasts sharply with the FIL test results obtained for the Äspö Hard Rock Laboratory (Axelsson *et al.*, 1990), where a clear separation was seen between the measurement limit and the mode of the measureable transmissivities. When such a clear separation is present, the conductive fracture frequency f_c can be estimated independently of the single-fracture transmissivity distribution parameters $\mu_{\log T}$ and $\sigma_{\log T}$. In the present case, the process of estimating f_c is inseparable from estimation of $\mu_{\log T}$ and $\sigma_{\log T}$.

An improvement of one order of magnitude in the transmissivity resolution (to give a resolution equivalent to that in the Äspö study) would probably reduce the degree of non-uniqueness considerably. However, the very presence of this problem indicates something about the fracture population, namely, that there is a very high intensity of marginally transmissive fractures. This contrasts with the Äspö site, where fractures tend to be highly transmissive if they are transmissive at all.

7.2 Flow Dimension and Well Test Interpretation

The usefulness of the Generalized-Dimension Flow (GDF) interpretations of transient data in the present study is limited by the short duration of the tests and lack of early-time data. This results in a fairly high uncertainty in the individual values of Transmissivity (T_L), Storativity (S_L), and Dimensionality (D) obtained from analyses of individual tests. However, the results are useful, in a probabilistic sense, for model validation by comparison with simulated packer testing. If the analysis of simulated packer tests is similarly restricted by using simulated data only from within the time interval for which good data are available for the actual tests, then the sources of the uncertainty that have the most strongly systematic effect can be included in the simulations, and comparisons between simulated and actual tests will be valid. This restriction on the analysis of simulated tests was applied in the present study.

The interval transmissivity values estimated from GDF analysis may differ by as much as two orders of magnitude from the Moye's formula interval transmissivities. However, the Moye's formula estimates may be either higher or lower than the GDF estimates, depending on the flow dimension. Rather surprisingly, the best agreement between the two interpretations is obtained for $D \approx 2$, and not for $D \approx 3$. Since Moye's formula is derived based on a spherical flow geometry, this suggests that the formula does not correctly estimate the effective source radius in fractured rock, possibly due to non-porous medium behaviour on the scale of a packer interval.

For the Finnsjön data, Moye's formula seems to provide a reasonable estimate of interval transmissivity in an average sense, since for the sample of 13 tests considered the Moye's estimates are scattered somewhat evenly above and below the GDF estimates. This statement could be quantified in terms of a log-log correlation of Moye's estimates to GDF estimates,

given a larger, randomly-selected set of type-curve analyses. However, for the present set of analyses, a quantitative statement would not be meaningful.

The approximate flow dimensions *D* seen in a suite of FIL tests is a very useful type of information that can be reliably estimated from GDF analysis. One statement that can be made with a high degree of certainty about the sample of 13 tests that were analyzed is that only two of them are cases of near-linear flow, while the other 11 tests have *D* in the range 2 to 3. If this behaviour is observed in the full suite of FIL tests (not just in this non-random sample), it indicates a fracture network that is well-connected.

An important question related to the validity of any particular stochastic continuum or channel network model that may be used is whether the most conductive test intervals tend to be of low flow dimension. If so, this would indicate that the most conductive features have nearly one-dimensional flow within the zone of influence of a packer test, *i.e.*, that single-channel flow is dominant in the most conductive zones, on the scale of a packer test. On the other hand, if the most conductive test intervals have higher *D*, this indicates that the most conductive zones behave less like single channels, and more like a porous medium or a well-connected channel network. This would have a strong influence on mixing lengths for radionuclide transport. It is suggested that any model to be used for transport predictions should have an effective *D* for the principal conduits that matches the *D* of the most conductive packer test intervals. The sample of thirteen tests analyzed herein is insufficient to characterize the rock mass in this respect. Analysis of the full suite of transient tests in Phase 2 of this study should provide an answer to this question.

In spite of its limitations, the GDF methodology probably provides a more accurate interpretation of the constant-head tests than the Moye's formula interpretation. In the best cases, this approach provides an additional type of information, flow dimension, which should be a distinctive characteristic of local fracture network variability. The transmissivity values obtained in such cases are probably significantly more accurate than those obtained from the steady-flow interpretations, especially for the cases of low flow dimension.

In the worst cases, the GFD methodology still yields a rough estimate of the flow dimensionality, and is probably as accurate as the steady-flow interpretation approach, especially for the cases when semilog straight-line behaviour is not achieved due to non-spherical flow geometry or noisy data.

7.3. Significance of Results for Stochastic Continuum Modelling

The distributions of hydraulic conductivity and anisotropy, produced by this feasibility study are insufficient for use in further modelling of the Finnsjön site. However, the forms of the distributions appear to be more or less unimodal and lognormal for all of these quantities.

For the purpose of stochastic continuum (SC) modelling, the distributions of anisotropy can be interpreted as indicative of the range of anisotropy that might need to be dealt with in the model. The range of anisotropy appears to be on the same order as the standard deviation of average, block-scale conductivity, which suggests that the effects of block anisotropy are likely to be only marginally significant.

The fairly small difference observed between 25 m and 50 m scales suggests that, within this range of scales, the behaviour of the rock mass is approaching that of an equivalent porous medium insofar as the average flow properties are concerned. This observation supports the proposed use of SC models for modelling the head and flux distributions for the local-scale model. However, the flux distribution within these blocks has not been characterized, and hence nothing can be said about whether the model behaves as an EPM for other situations, such as transport modelling. The large difference between the simulated distributions for 25 m block scale conductivity and the distributions of hydraulic conductivity measured on the scale of packer tests indicates that significant scale effects occur for block sizes somewhat less than 25 m.

Although the number of simulations is insufficient to fully characterize the distributions, the variability of the block-scale conductivities is surprisingly low. For both 25 m and 50 m cubes, the standard deviation of log K_s is only 0.3 to 0.4 orders of magnitude. This is less than half of the standard deviation of log transmissivity (1.06 orders of magnitude) seen in the 2 m packer intervals used for the OxFILET analysis. Thus the DFN conceptual model seems to predict a strong scale effect with respect to conductivity variability, occurring within the scale range from 2 m to 25 m.

The high degree of simplification in the present DFN model should be remembered in considering these results. In particular, the use of constant transmissivity within single fractures may bias this model toward more well-behaved, equivalent-porous-medium behaviour. If the flow through this model is dominated by a few large fractures (as the limited results of the pathways analysis seem to suggest), then introduction of variable transmissivity within fracture planes may produce a model that predicts much stronger heterogeneity, anisotropy and scale effects.

7.4 Feasibility of Modelling Methodology

The Phase 1 DFN model for the Finnsjön rock block initially caused computational difficulties in finite element mesh generation, due to the very well-connected nature of the fracture population in the model. These difficulties were removed by implementation of the variable transmissivity model for individual fractures, which can be used with a specification of zero variability to prediscretize the larger fractures in the population, and thus reduce the number

of intersections per fracture, which has a dominant influence on the time needed for mesh generation.

Another problem was encountered in the simulation of packer tests, in that early-time behaviour could not be simulated due to a too-coarse mesh around the boreholes. This was circumvented by providing for automatic mesh refinement around boundaries which are small in relation to fracture size. This adaptation worked very well.

After making these two improvements to the mesh generation program, the problems of block scale and packer test simulations became very tractable. Typical mesh generation times for a 50 m cube were about 15 CPU minutes. Cross-block flow simulations on this scale required less than 10 CPU minutes for each flow direction. Packer test simulations, depending on the number of time steps specified, generally required about 15 CPU minutes. Based on these figures, and assuming a usage of about 50 percent of CPU time on the SKB Convex, a modelling rate of at least 10 simultaneous packer-test/block-scale simulations per day can be achieved.

7.5 Recommendations for Phase 2

The following work is recommended for the formulation of a DFN model for Phase 2 of the present project:

- Calculation of statistics for alternative conceptual models, including termination of fractures at intersections and non-stationary fields for fracture intensity (*e.g.*, Nearest-Neighbor and Levy-Lee model statistics)
- Improved derivation of fracture size distribution $f_r(r_c)$, based upon simultaneous treatment of all fracture trace data from cell and lineament maps.
- GDF analysis of additional packer tests to quantify errors due to use of Moye's formula interpretations.
- Derivation of fractal model for transmissivity variation within single fractures based upon generic data from Abelin *et al.*, 1990.
- Derivation of at-borehole *vs.* cross-fracture transmissivity (T_{fo} *vs.* T_f) relationship.
- Estimation of P_{32c} and $f_{Tf}(T_f)$ from all 2 m and 3 m FIL test data using OxFILET and T_{fo} *vs.* T_f relationship.
- Refinement of basis for assumed storativity values or correlations.
- Characterization of uncertainty for all DFN model parameters.
- Interpretation of fracture geometry and hydrologic test results within fracture zones.

Pathways analysis to estimate the occurrence and properties of preferential pathways between a repository and the accessible environment within the Finnsjön rock block is not recommended due to the very well-connected nature of the DFN model.

The following work is recommended to provide an interface between the discrete fracture network and stochastic continuum models:

- Definition of a nested fracture generation scheme, so that spatial correlation among rock blocks due to the larger fractures can be quantified, while avoiding the posing of unnecessarily large mesh-generation problems. This generation scheme must also consider positioning of simulated packer tests within the blocks, to develop the probabilistic relationship between observed well test conductivities and block conductivities.

- Implementation of a postprocessor to calculate averages of velocity and head gradient within averaging volumes, to allow estimation of the full permeability tensor for each block.

The following work is recommended for the interface between discrete fracture network and channel network models:

- Derivation of parameters for the variable-transmissivity model to allow realistic simulation of channeling in large fractures.

- Implementation of a principal-conduit identification algorithm in the postprocessor for the block-scale simulations, by identification of elements within the meshes that carry the highest quantity of flow.

- Estimation of specific surface and porosity fractions as functions of flux magnitude within block-scale simulations. These fractions are calculated by dividing the fracture elements into classes according to flux magnitude, and then calculating the specific surface and porosity for each flux range.

Specific details of these tasks were still being discussed between the discrete fracture network, stochastic continuum and channel network modelling groups at the time of this report.

8. ACKNOWLEDGEMENTS

The modelling work described in this report was supported by SKB, Stockholm. The authors wish to extend their thanks to Dr. Sverker Nilsson of SKB for his assistance in the use of SKB computer facilities, Dr. Sven Tirén and Mr. Jan-Erik Andersson of SGAB for their assistance in providing the data, and Mr. Nils Kjellbert and Mr. Anders Ström for their support in project management and data analysis.

The authors also wish to recognize the contributions of their colleagues in Seattle, in particular Dr. William Dershowitz for his many suggestions regarding the data analysis, Dr. Thomas Doe and Mr. Mark Cunnane for their help with the GDF analysis, and Mr. Carl Einberger for his simulations of flow using replicated fracture geometry.

9. REFERENCES

Abelin, H., L. Birgersson, H. Widén, T. Ågren, L. Moreno, and I. Neretnieks, 1990. "Channeling Experiment," Stripa Project Technical Report 90-13, SKB, Stockholm.

Andersson, J-E., L. Ekman, and A. Winberg, 1988. "Detailed investigations of fracture zones in the Brändan area, Finnsjön study site. Single-hole water injection tests in detailed sections," SKB Progress Report 88-08. Stockholm.

Andersson, J-E., R. Nordqvist, G. Nyberg, J. Smellie, and S. Tiren (1989). "Hydrogeological conditions in the Finnsjön area - Compilation of data and conceptual model." SKB Arbetsrapport 89-24. Stockholm

Axelsson, C-L., E-K. Jonsson, J. Geier, and W. Dershowitz (1990). "SKB Hard Rock Laboratory Discrete Fracture Modelling." SKB Swedish Hard Rock Laboratory Progress Report 25-89-21. Stockholm

Baecher, G.B., N.A., Lanney, and H.H. Einstein, 1977. "Statistical Description of Rock Properties and Sampling," *Proceedings of the 18th U.S. Symposium on Rock Mechanics*, American Institute of Mining Engineers, 5C1-8.

Barker, J. (1988). "A Generalized Radial Flow Model for Hydrologic Tests in Fractured Rock." *Water Resources Research*, Vol. 24, pp. 1796-1804.

Bingham, C., 1964. "Distribution on the Sphere and on the Projective Plane," Ph.D. Dissertation, Yale University, New Haven, Connecticut, USA.

Brandstetter, A. and B.E. Buxton, 1987. "The Role of Geostatistical, Sensitivity, and Uncertainty Analysis in Performance Assessment," *Proceedings of the Conference on Geostatistical, Sensitivity, and Uncertainty Methods for Groundwater Flow and Radionuclide Transport Modeling*, U.S. Department of Energy and Atomic Energy of Canada, Ltd., San Francisco, California, USA, September 15-17.

Brown, S.R., 1986. "Fluid Flow Through Rock Joints: The Effect of Surface Roughness," *Journal of Geophysical Research.*

Brown, S.R. and C.H. Scholz, 1985. "Broad Bandwidth Study of the Topography of Natural Rock Surfaces," *Journal of Geophysical Research*, Vol. 90, pp. 12,575-12,582.

Dershowitz, W.S., 1979. "A Probabilistic Model for the Deformability of Jointed Rock Masses" MSc Thesis, Massachusetts Institute of Technology, Cambridge, Massachusetts.

Dershowitz, W. S., 1985. "Rock Joint Systems," PhD dissertation, Massachusetts Institute of Technology, Cambridge, Massachusetts.

Dershowitz, W.S. and H.H. Einstein, 1988. "Characterizing Rock Joint Geometry with Joint System Models," Rock Mechanics and Rock Engineering, Vol. 21, pp. 21-51.

Dershowitz, W.S., J.E. Geier and G. Lee, 1990. "FracMan Interactive Discrete Fracture Simulator: User Documentation. Version Beta 2.3." Golder Associates Inc., Redmond WA.

Dershowitz, W., A. Herbert, and J. Long, 1989. "Fracture Flow Code Cross-Verification Plan," Stripa Project Technical Report 89-02, SKB, Stockholm.

Doe, T. and J. Remer, 1980. "Analysis of Constant-Head Well Tests in Nonporous Fractured Rock," *Proceedings of the Third Invitational Well-Testing Symposium*, Berkeley, California, USA.

Doe, T.W. and J.D. Osnes, 1985. "Interpretation of Well Test Geometry from Well Tests," *Proc. of the International Symposium on Fundamentals of Rock Joints*, Björkliden, Sweden.

Doe, T.W. and J.E. Geier, "Interpretation of Fracture System Geometry Using Well Test Data," Stripa Project Technical Report 90-xx, SKB, Stockholm.

Efron, B. 1982, "The Jacknife, the Bootstrap, and other Resampling Plans". *SIAM Monograph No. 38*, Society of Industrial and Applied Mathematics. Palisades Software, 1989.

Fisher, R.A., 1953. "Dispersion on a Sphere," *Proceedings of the Royal Society of London*, Series A, Vol. 217, pp. 295-305.

Fournier, A., D. Fussell, and L. Carpenter, 1982. "Computer rendering of stochastic models," *Communications of the Association for Computing Machinery*, Vol. 25, pp. 371-384.

Geier, J., W. Dershowitz, and G. Sharp, 1990. "Prediction of Inflow into the D-Holes at the Stripa Mine," Stripa Project Technical Report 90-06, SKB, Stockholm.

Geier, J. E., K. Lee, and W. S. Dershowitz, 1989. "Field Validation of Conceptual Models for Fracture Geometry", submitted to *Rock Mechanics and Rock Engineering*.

Gilmour, H.M.P., D. Billaux, and J.C.S. Long, 1986. "Models for Calculating Fluid Flow in Randomly Generated Three-Dimensional Networks of Disc-Shaped Fractures; Theory and Design of FMG3D, DISCEL, and DIMES," Report LBL-19515 prepared for U.S. Dept. of Energy, Office for the Crystalline Repository Project by Lawrence Berkeley Laboratory, Berkeley, California, USA.

Hakami, E., 1989. "Water Flow in Single Rock Joints," Stripa Project Technical Report 89-08, SKB, Stockholm.

Herbert, A.W. and B.A. Splawski, 1990. "A Prediction of Flows to be Measured in the Stripa D-Hole Experiment: An Application of the Fracture Network Approach," Stripa Project Technical Report 90-xx, SKB, Stockholm.

Hoek, E., E. Brown, and D. Wylie (1981). "Rock Slopes: Design, Excavation, Stabilization." US Department of Transportation, Federal Highway Administration, Washington.

Iwai, K., 1976. "Fundamental Studies of Fluid Flow Through a Single Fracture," Ph.D. thesis, University of California, Berkeley.

Jaeger and Cook, 1977. *Fundamentals of Rock Mechanics*, 2nd edition, Halsted Press, New York, New York.

Karasaki, K., 1986. "Well Test Analysis in Fractured Media," Ph.D. thesis, University of California, Berkeley.

Kenrick, M.P., P.J. Fennessy, and G. Sharp, 1989. "Hydrological Testing of Channelized Rock Fractures; A Numerical Simulation," report prepared for Battelle Office of Waste Technology Development by Golder Associates Inc., Redmond, Washington, USA.

Long, J.C.S., J.S. Remer, C.R. Wilson, and P.A. Witherspoon, 1982. "Porous Media Equivalents for Networks of Discontinuous Fractures," *Water Resources Research*, Vol. 18, pp. 645-658

Long, J.C.S. and P.A. Witherspoon, 1985. "The Relationship of the Degreee of Fracturing to Permeability," *Water Resources Research*, Vol. 90, pp. 3087-3098.

Mandelbrot, B.B., 1983. *The Fractal Geometry of Nature*, W.H. Freeman, San Francisco. 468 pp.

Mardia, K.V., 1972. *Statistics of Directional Data*, Academic Press, New York.

Miller, I., 1990. "MAFIC Version Beta 1.2 Matrix/Fracture Interaction Code with Solute Transport -- User Documentation," Golder Associates Inc. report prepared for Battelle Memorial Institute, Office of Waste Technology Development, Willowbrook, Illinois, USA.
Golder Associates Inc., 1989. "FracMan Version, Beta 2.1 Interactive Rock Fracture Geometric Model: User Documentation," prepared for Battelle Office of Waste Technology Development, Willowbrook, Illinois.

Moyes, D.G., 1967. "Diamond Drilling for Foundation Exploration," *Civil Engineering Transactions*, pp. 95-100.

Osnes, J.D., A. Winberg, and J. Andersson, 1988. "Analysis of Well Test Data -- Application of Probabilistic Models to Infer Hydraulic Properties of Fractures," Topical Report RSI-0338, RE/SPEC Inc., Rapid City, South Dakota.

Pearson,K., 1895. "Skew Variations in Homogenous Material, Contributions to the Mathematical Theory of Evolution," *Philosophical Transactions of the Royal Society*, Vol. 186.

Sehlstedt, S. and Stråhle, A., 1989. "Geological core mapping and geophysical bore hole logging in the bore holes KFI 05 - KFI 08 at Finnsjön," Swedish Hard Rock Laboratory, SKB PR 25-89-09. Stockholm.

Stråhle, A. and Fridh, B., 1989. "Orientation of selected drillcore sections from the boreholes KFI 05 and KFI 06 Finnsjön, Sweden. - A televiewer investigation in small diameter boreholes," Swedish Hard Rock Laboratory, SKB PR 25-89-08, Stockholm.

SKB, 1989. "R&D-PROGRAMME 89 - Handling and final disposal of nuclear waste. Programme for research development and other measures." SKB, Stockholm.

Tirén, S., 1990. "Detailed Fracture Mapping - Cell mapping and Scanline Maping at Borehole KFI 11, Brändan Area, Finnsjön, Central Sweden," SGAB internal Report 90251.

Terzaghi, R., 1965. "Sources of error in joint surveys," *Geotechnique*, Vol. 15, pp. 287-304.

Tsang, Y.W., 1984. "The Effect of Tortuosity on Fluid Flow Through a Single Fracture," *Water resources Research*, Vol. 20, pp. 1209-1215.

Tsang, Y.W. and C.F. Tsang, 1987. "Channel Model of Flow Through Fractured Media," *Water Resources Research*, Vol. 23, pp. 467-489.

Tsang, Y.W. and P.A. Witherspoon, 1983. "The dependence of fracture mechanical and fluid properties on fracture roughness and sample size," *Journal of Geophysical Research*, Vol. 88 (B3), pp. 2359-2366.

Walsh, J.B., 1981. "Effect of pore pressure and confining pressure on fracture permeability," *International Journal of Rock Mechanics and Min. Sci.*, Vol. 18, pp. 2359-2366.

10. NOTATION

A = area

A_c = conduit cross-sectional area

A_f = area of a fracture

b = power-law exponent

C_e = effective conductance of a pathway

C_p = ratio of fracture frequency to fracture intensity = f/P_{32}

D = flow dimension

D_L = flow dimension for a packer section of length L

f_c = conductive fracture frequency

h = head

h_{w0} = head at wellbore

H = head at a boundary

H_o = value of head at the origin (0,0,0)

H_i = coefficient of head variation with respect to x_i

I_i = Intensity (number) of fracture intersection per unit area mapped.

K = conductivity

K_c = conduit conductivity

K_{ij} = equivalent hydraulic conductivity tensor component

K_s = block-scale average conductivity

L = packer separation

L_e = effective length of a pathway

P_{32} = fracture intensity (area per unit volume)

P_{32c} = conductive fracture intensity

Q = flux at a boundary

Q_i = Flux across the ith boundary

Q_{Dmatch} = Dimensionless flux at match point

Δq_i = flux imbalance at ith node

q_i = Component of flux per unit width in the ith direction

r = distance

r_e = fracture effective radius

r_w = well radius

r_{min} = minimum radius

s = block scale

S = storativity

S_f = fracture storativity

S_L = storativity for a packer section of length L

S_s = Specific storage

t_{Dmatch} = Dimensionless time at match point

t_p = termination probability

$t_{\%}$ = termination percentage at intersections

t_v = termination percentage visible

t_{fi} = intensity (number) of fracture termination at intersection per unit area mapped

t_{ri} = intensity (number) of fracture termination in rock per unit area mapped

T = transmissivity

T_f = cross-fracture transmissivity

T_{fo} = at-borehole transmissivity

T_L = transmissivity for a packer section of length L

T_{min} = minimum radius

$\boldsymbol{u}$ = fluid velocity vector

V_w = volume of water

$\boldsymbol{x}$ = vector location in space

x_i = ith component of location vector $\boldsymbol{x}$

Θ = azimuth of a dip or pole vector

ϵ_g = global mass balance measure

ϵ_ℓ = local mass balance measure

κ = Fisher concentration

κ_{ij} = K_{ij}/K_s = anisotropy ratio

λ = trace length

$\mu_{\log T}$ = mean of log T

ϕ = inclination of a dip or pole vector

$\sigma_{\log T}$ = standard deviation of log T

ξ = vector location with in a fracture plane

APPENDICES

APPENDIX 1: HYDRAULIC CONDUCTIVITY PROFILES

This appendix presents profiles of interpreted hydraulic conductivities versus test section depth for boreholes BFI 01-02, HFI 01, and KFI 01-12 (Figure A1-1). These figures show the heterogeneity that can be observed on a 2 m, 3 m or 20 m scale in the borehole tests.

The figures are plotted as (12 + log K) *vs.* depth. The locations of fracture zones as identified by Andersson *et al.* (1989) are shown on the plot. Outside of these zones, the measured conductivities range from a maximum value of about 10^{-6} m/s to a minimum value below the measurement limit of the equipment (about 10^{-10} to 10^{-9} m/s, depending on the equipment used and the interval length). Intervals for which no test data are available are indicated by a slight negative value on the plot; intervals below the measurement limit are indicated by a zero value.

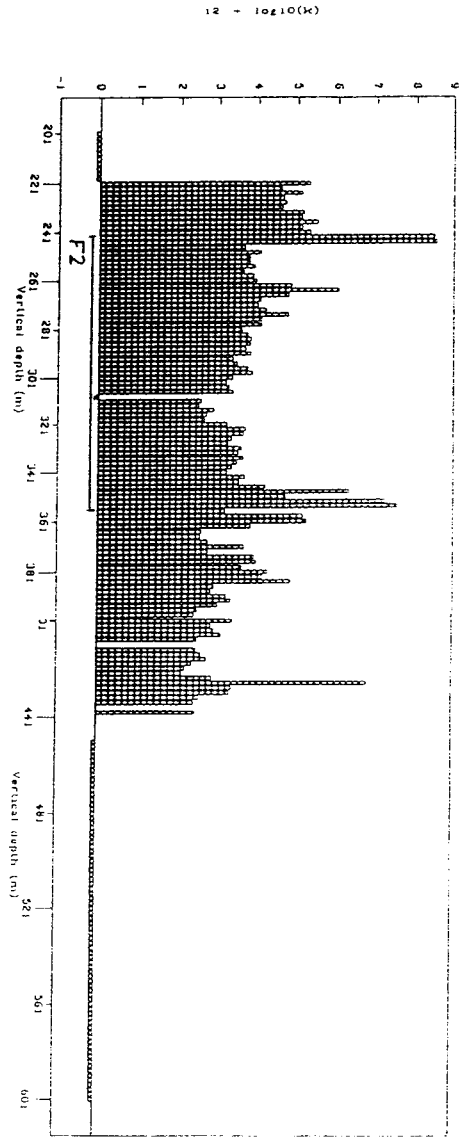

a) BFI 01

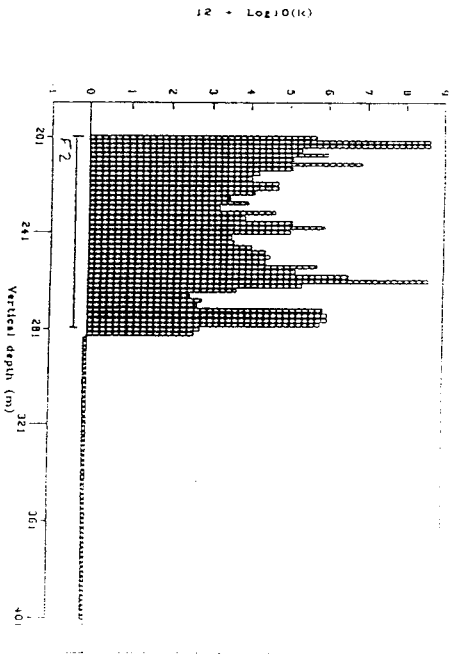

b) BFI 02

FIGURE A1-1
HYDRAULIC CONDUCTIVITY PROFILES FOR BOREHOLES

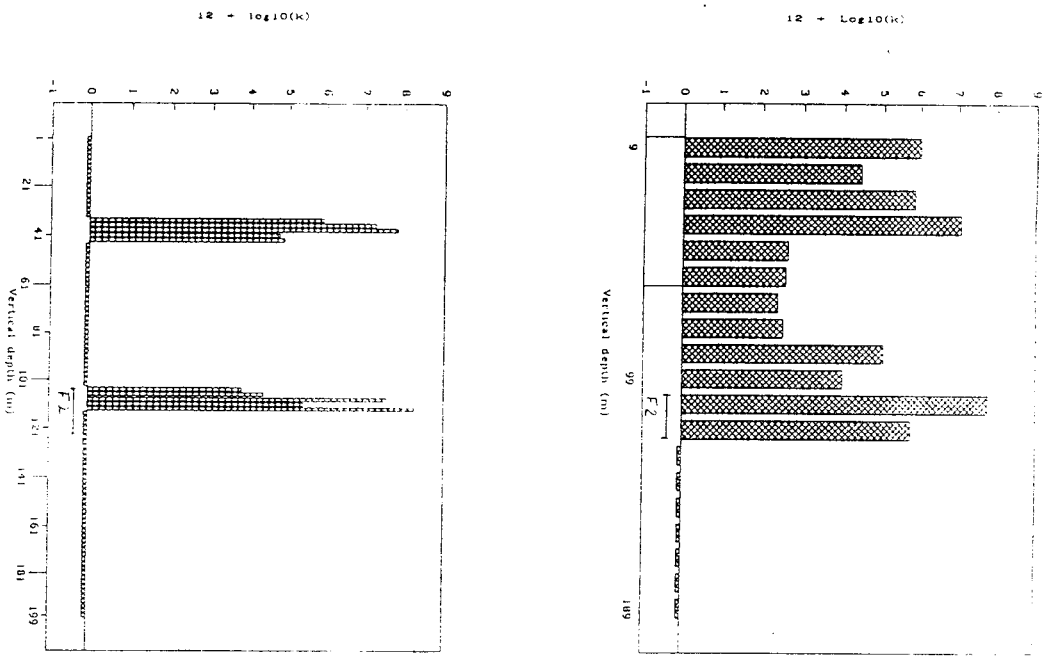

c) HFI 01

FIGURE A1-1, ctd.
HYDRAULIC CONDUCTIVITY PROFILES
FOR BOREHOLES

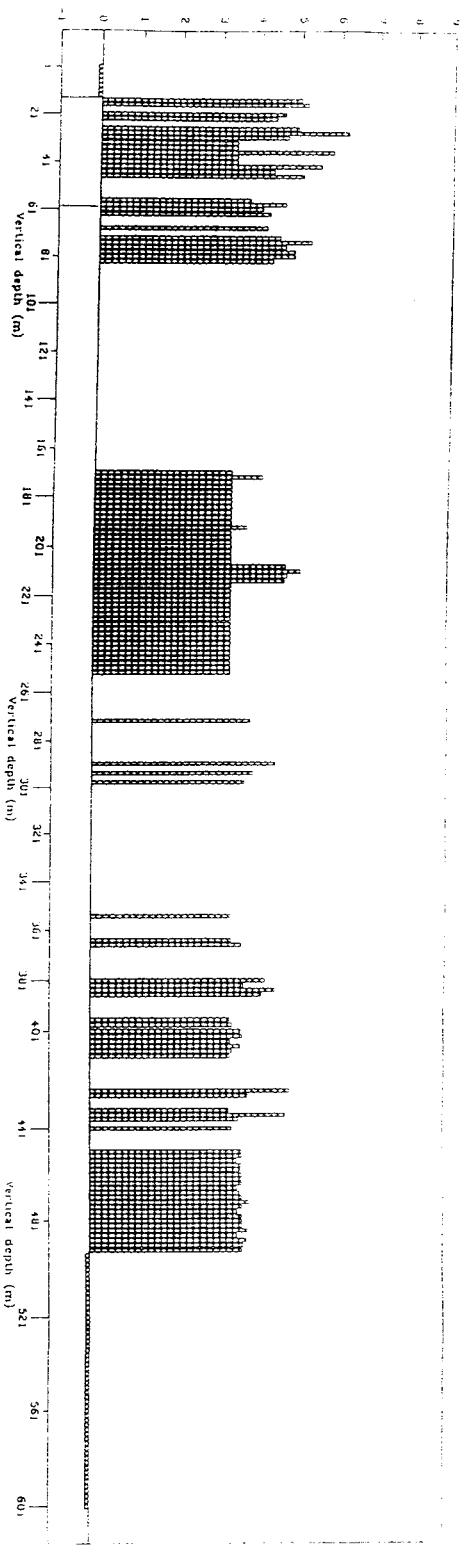

d) KFI 01

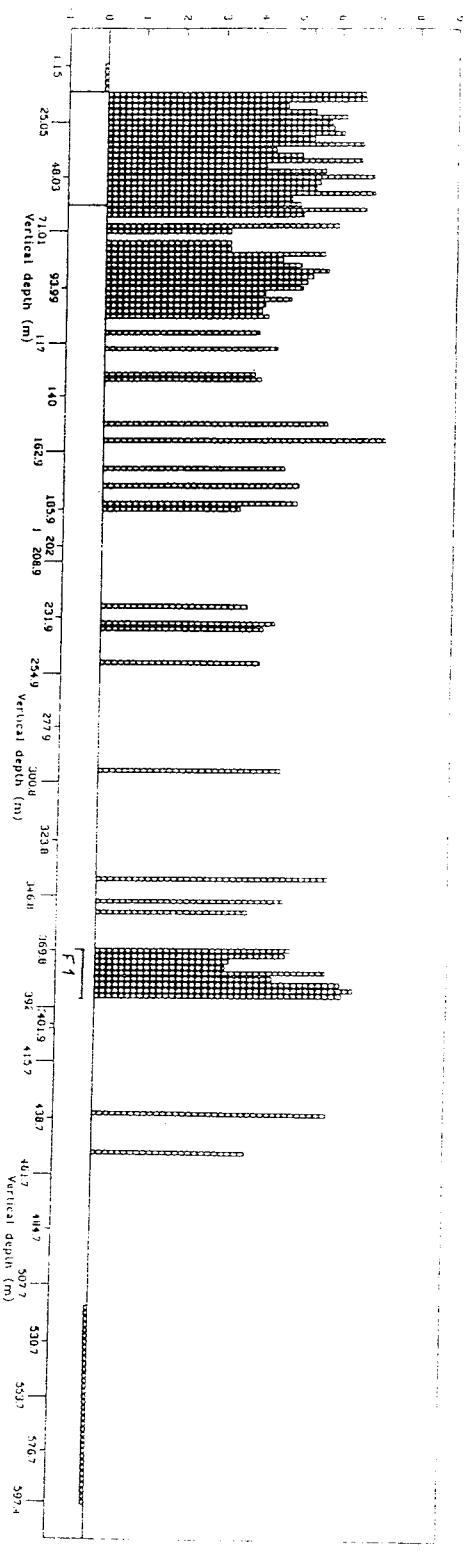

e) KFI 02

FIGURE **A1-1, ctd.**

HYDRAULIC CONDUCTIVITY PROFILES FOR BOREHOLES

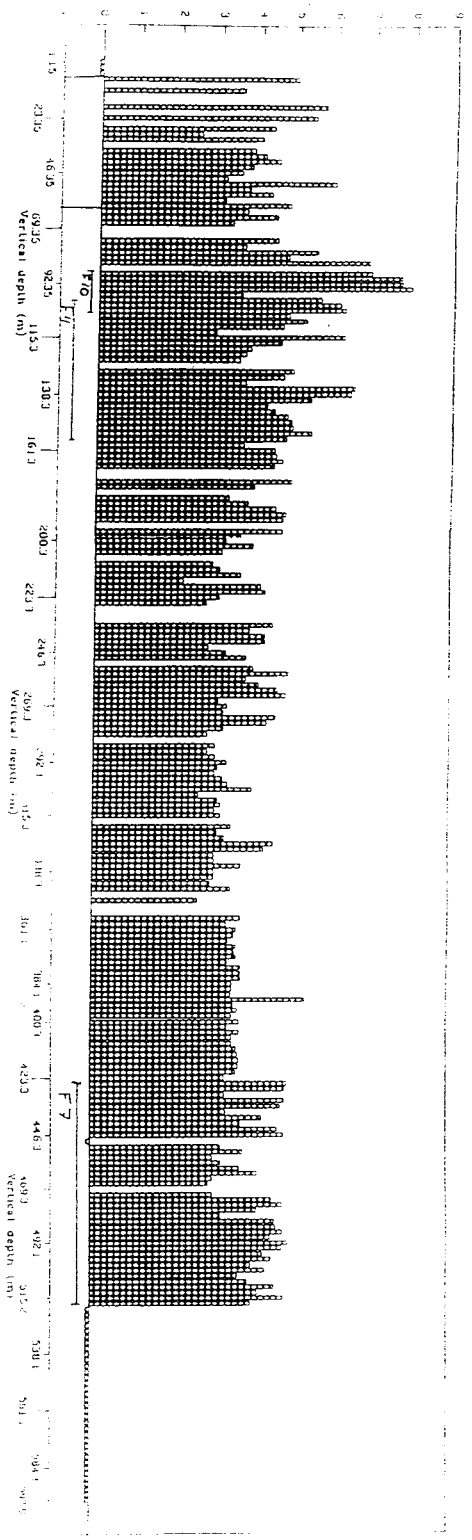

f) KFI 03

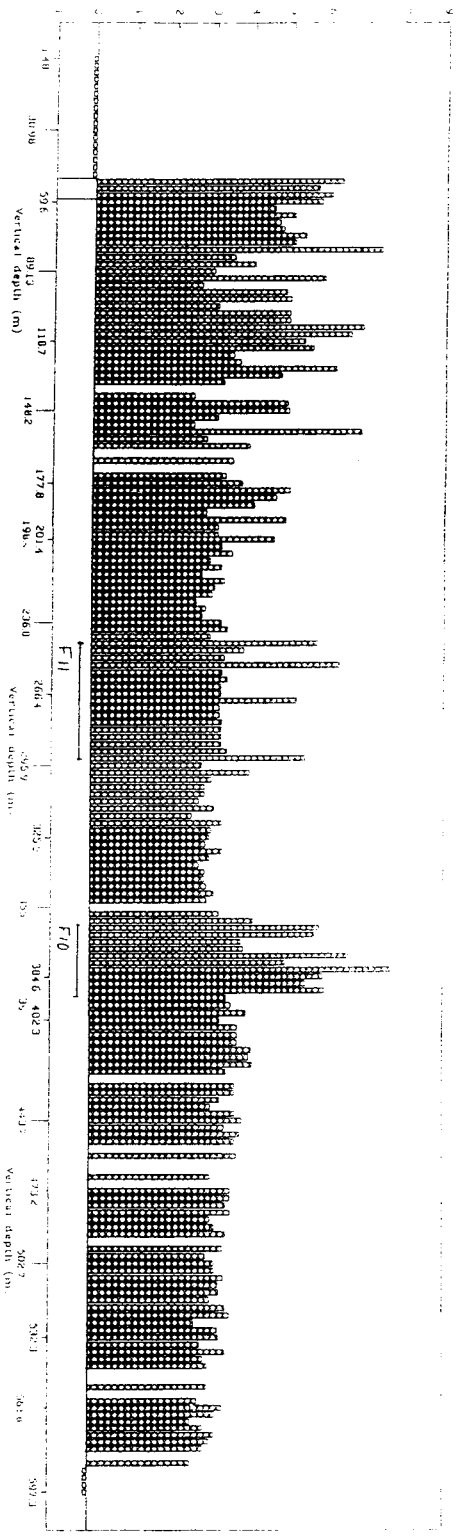

g) KFI 04

FIGURE **A1-1, ctd.**

HYDRAULIC CONDUCTIVITY PROFILES FOR BOREHOLES

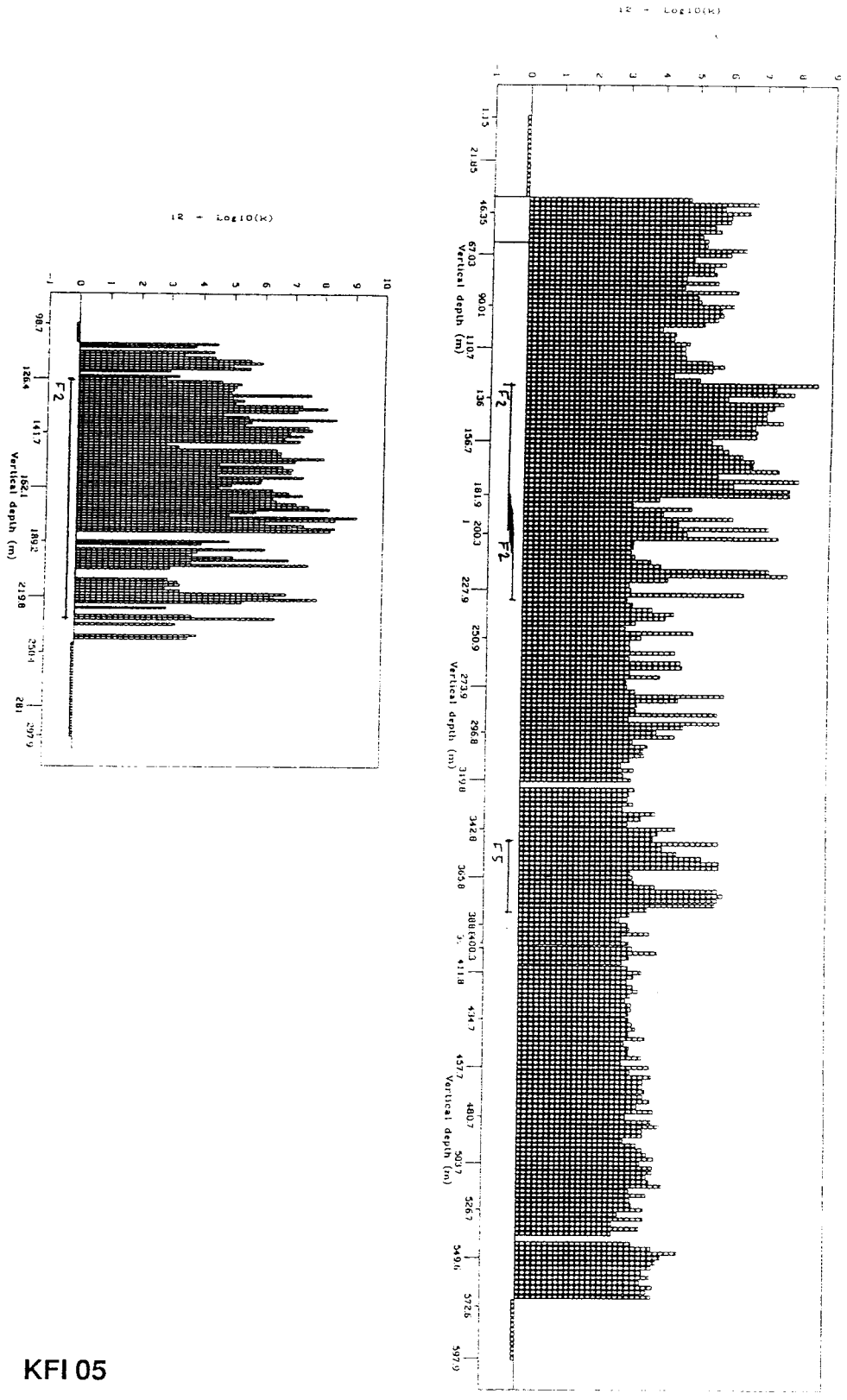

h) KFI 05

FIGURE **A1-1, ctd.**

HYDRAULIC CONDUCTIVITY PROFILES FOR BOREHOLES

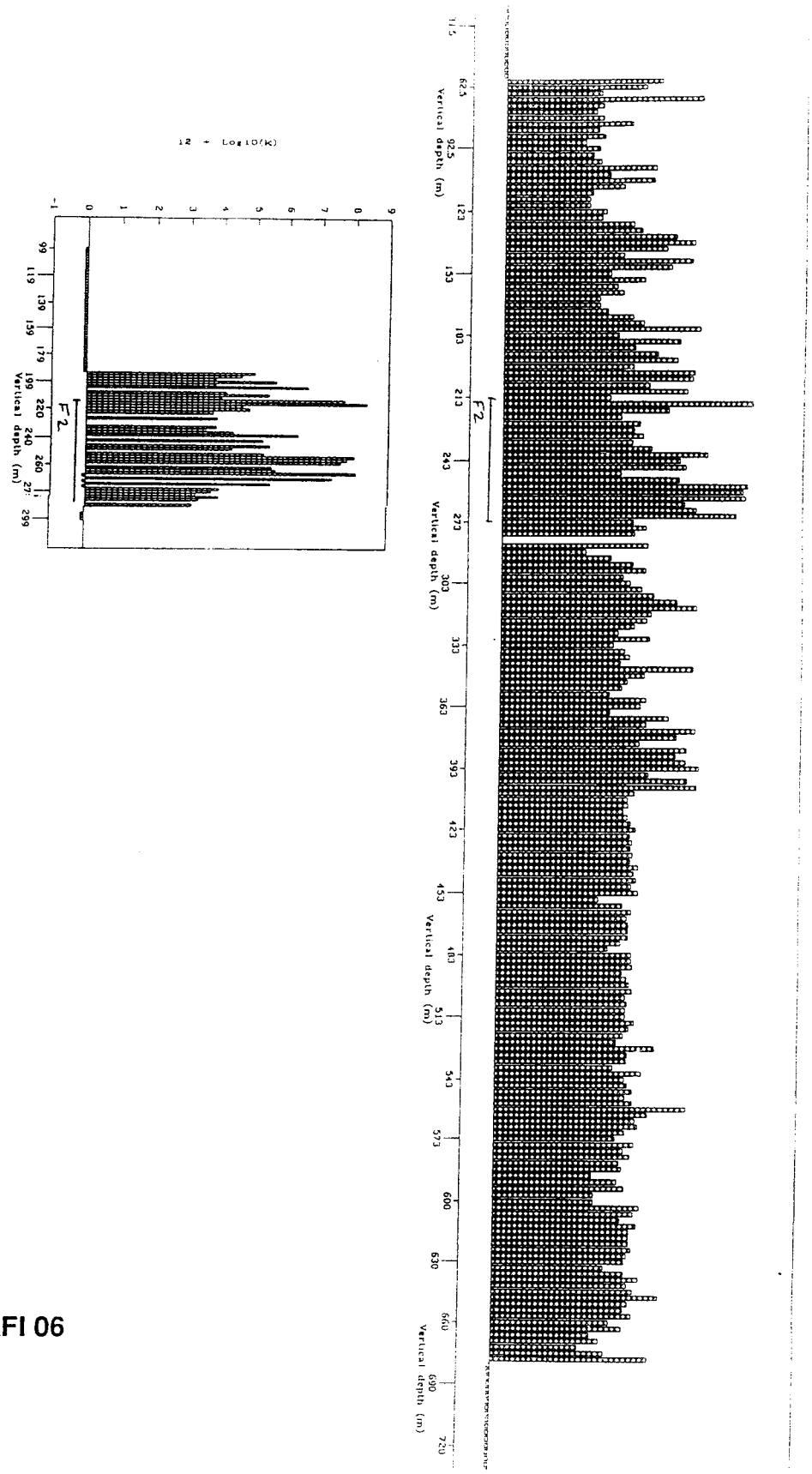

i) KFI 06

FIGURE A1-1, ctd.
HYDRAULIC CONDUCTIVITY PROFILES
FOR BOREHOLES

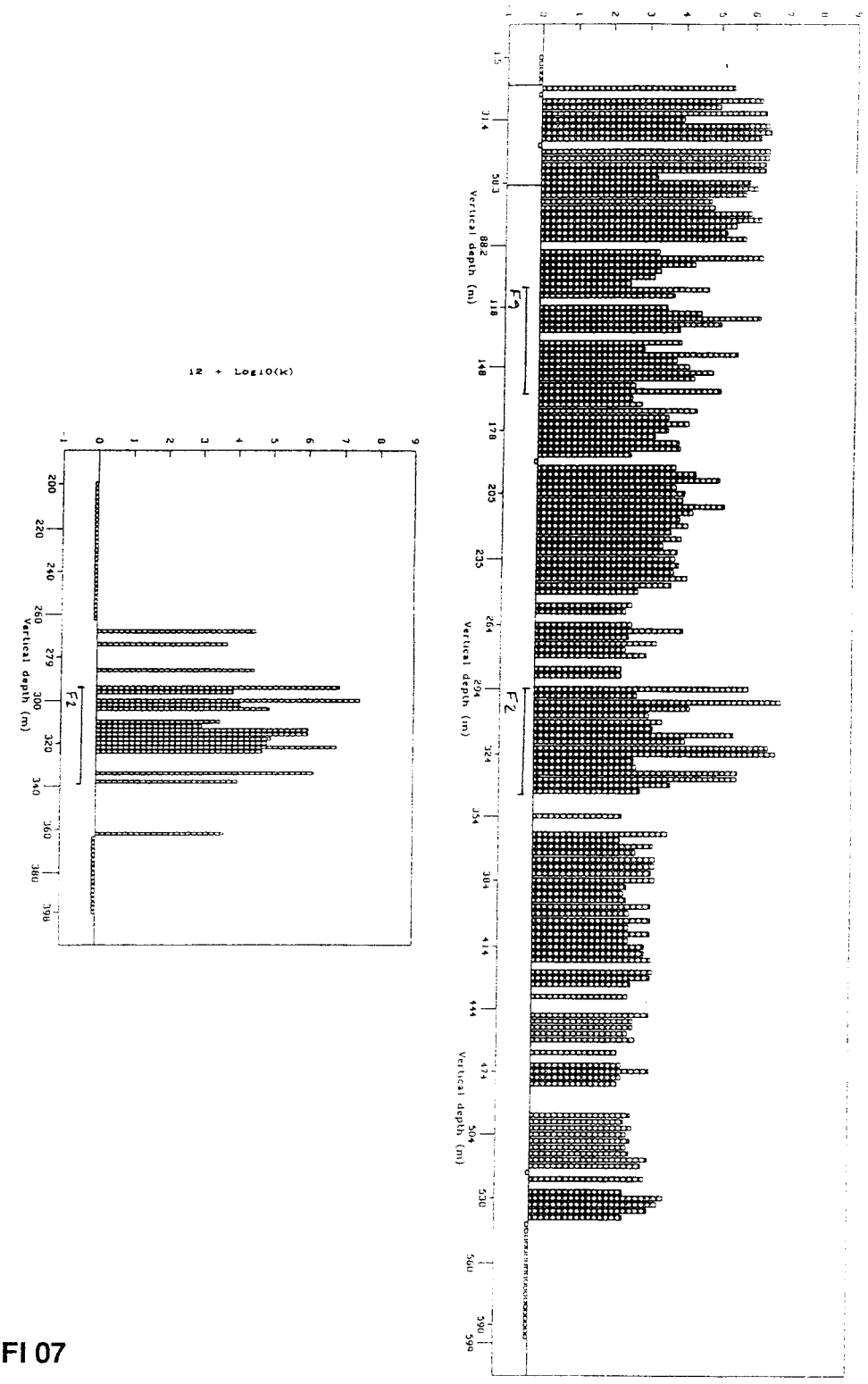

j) KFI 07

FIGURE **A1-1, ctd.**
HYDRAULIC CONDUCTIVITY PROFILES FOR BOREHOLES

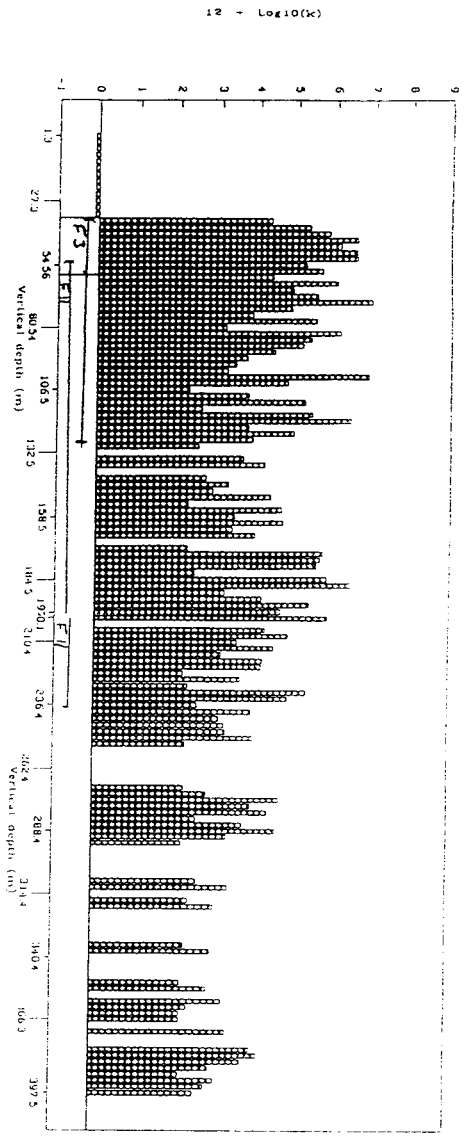

k) KFI 08

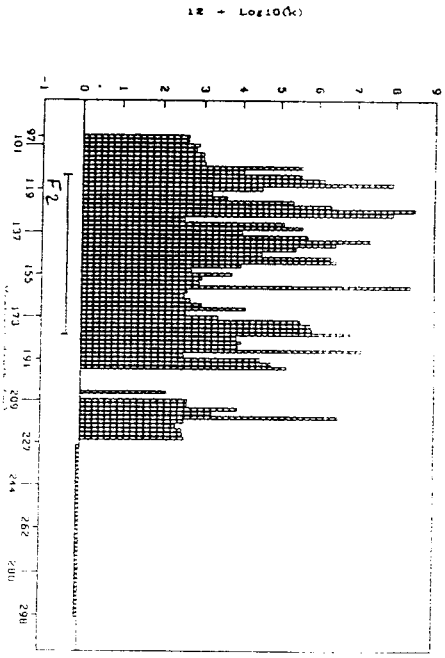

l) KFI 09

FIGURE A1-1, ctd.
HYDRAULIC CONDUCTIVITY PROFILES
FOR BOREHOLES

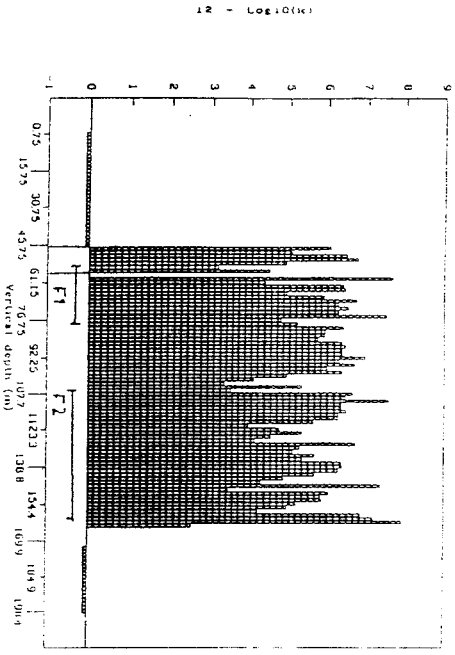

m) KFI 10

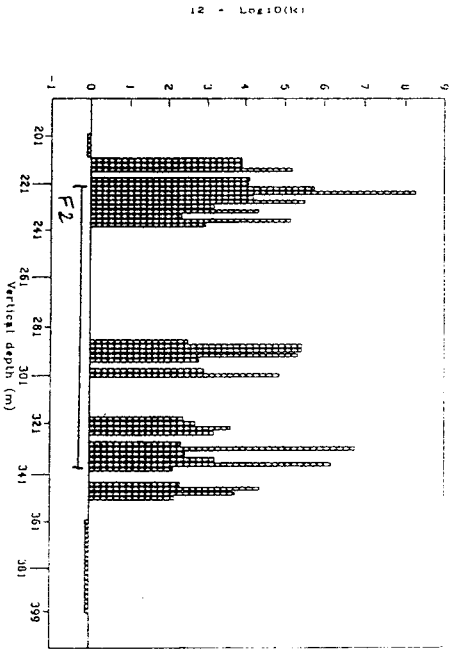

n) KFI 11

FIGURE A1-1, ctd.
HYDRAULIC CONDUCTIVITY PROFILES
FOR BOREHOLES

APPENDIX 2: DESCRIPTION OF COMPUTER PROGRAMS USED IN MODELLING

Discrete-fracture-network modelling was performed using the **FracMan** Discrete Fracture Network Modelling package (Dershowitz *et al.*, 1990) and the finite element program MAFIC (Miller, 1990). The FracMan package was used to evaluate fracture geometric and hydrologic data, to develop conceptual models for conductive fractures, to simulate data collection for validation of the conceptual models, and to generate finite element meshes for flow simulation, and to identify potential pathways for radionuclide migration. The FEM editing program **EdMesh** (Golder Associates Inc., 1990), was used in calibration and final runs to redefine boundary conditions and element properties in the FEMs. **MAFIC** is used to solve the flow and transport equations for the finite element meshes for simulation of the transient response during hydrologic packer testing, and the effective hydrologic properties of rock blocks controlled by discrete fractures.

2:1 Fracman Fracture Geometric Model

FracMan is an interactive, discrete fracture analysis package that runs on MS-DOS computers. **FracMan** consists of five principal modules (Figure A2-1):

- **FracSys**, a data-analysis system for discrete fracture data. FracSys modules include the ISIS Iterative Set Identification System for fracture set classification based upon orientation, infilling, and other fracture characteristics, the FracSize module for analysis of fracture tracelength data, and OxFILET for derivation of conductive fracture intensity and transmissivity distribution parameters from fixed-interval-length (FIL) packer test data.

- **FracWorks**, a fracture modelling system for producing stochastic realizations of geometric conceptual models. FracWorks capabilities include generation and display of fractures in three-dimensional space, simulation of fracture sampling methods used in site-characterization programs, and calculation of connectivity statistics for simulated fracture populations. FracWorks can generate fractures deterministically, stochastically, or by combined deterministic-stochastic processes. In the present analysis, FracWorks was used for generating fractures and calculating connectivity statistics.

- **MeshMaker**, a finite-element preprocessing system that transforms FracWorks fracture realizations into finite-element meshes for MAFIC. MeshMaker allows interactive definition of boundary geometries and boundary conditions. After the boundaries are defined, MeshMaker discretizes the polygonal fractures into triangular elements, and creates MAFIC input files. In the present study, Meshmaker was used to interactively define and display boundary geometries. To produce meshes more rapidly, MeshMonster (a batch-mode version of MeshMaker which runs on UNIX and VAX operating systems), was used to discretize fractures on a Convex mini-supercomputer.

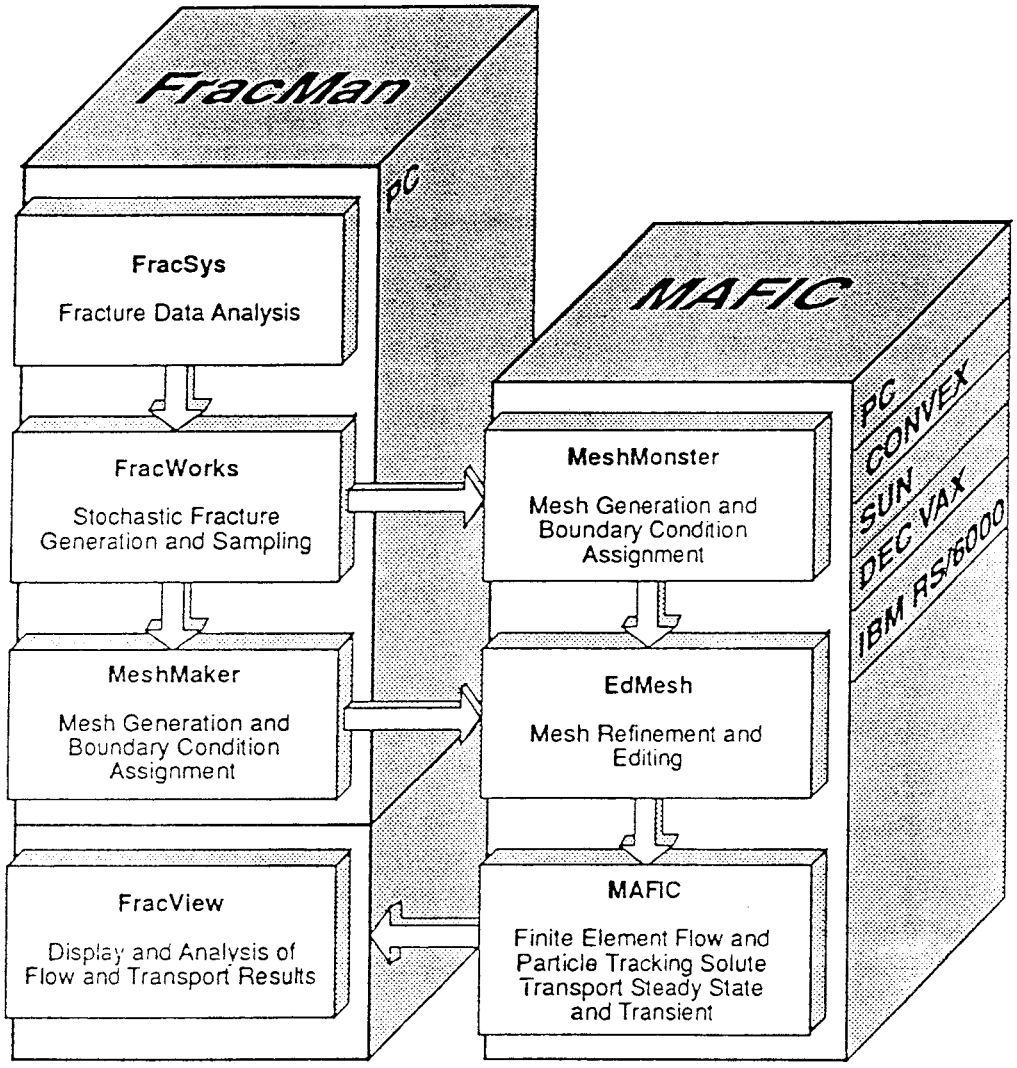

FIGURE **A 2-1**

FRACMAN FRACTURE GEOMETRIC MODEL

- **FracView**, a finite element post-processing system for analysis of MAFIC output. FracView was used in the present study to produce contour plots of heads, and fluxes in cross-sections through the simulated rock masses.

- **FracSimile**, which prints images of screen graphics from the other four modules.

The features of these programs are described in detail by Dershowitz et al., 1990.

2:2 MAFIC Fracture Flow and Solute Transport Simulator

MAFIC is a Galerkin finite-element code for solution of the finite element equations for transient, saturated flow and transport within networks of discrete fractures and rock matrix blocks. The features and theory of MAFIC have been described by Golder Associates, 1990a. Important features of MAFIC include:

- Iterative, incomplete Cholesky conjugate-gradient matrix solver.

- Choice of linear or quadratic basis functions for triangular elements.

- Automated nodal renumbering, variable-bandwidth storage and dynamic memory allocation to minimize matrix computation and array storage requirements.

- Simulation of solute transport by means of a particle tracking algorithm that models both advective transport and longitudinal and transverse dispersion within the fracture planes.

- Rapid solution of steady-state flow equations as a special case of transient flow, by suppressing storage terms in the finite-element formulation.

- A group flux boundary condition that allows specification of the net fluxes into and/or out of an arbitrary number of nodal groups, such that the heads at all nodes within the group are equal.

- Time-varying head and flux boundary conditions for additional nodal groups.

MAFIC has undergone verification for simple test cases for which analytical solutions are available (Golder Associates Inc., 1990), but due to the uncertain nature of large-scale stochastic simulations, this code cannot be verified absolutely. Cross-verification exercises undertaken as part of the Stripa Project compared the calculations of MAFIC for more complex flow problems with two other discrete-fracture flow packages, DISCEL, developed by Lawrence Berkeley Laboratory (Gilmour *et al.*, 1986) and NAPSAC, developed by Harwell Laboratories (Herbert and Splawski, 1990). The results (Dershowitz *et al.*, 1990) showed that MAFIC was substantially in agreement with these other codes for the flow problems considered in the Stripa Cross-Verification project.

In the model for the present study, flow within homogeneous, triangular areas (referred to as **elements**) of each fracture is assumed to be governed by an equation of the form:

$$S_e \frac{\partial h}{\partial t} - T_e \nabla^2 h = q \qquad \text{(A2-1)}$$

where:

S_e	= element storativity	[-]
h	= hydraulic head	[L]
t	= time	[T]
T_e	= element transmissivity	[L^2/T]
q	= source flux density	[L/T]

This in effect means that each element is treated as a homogeneous section of a planar aquifer. Fracture aperture is not directly relevant to this formulation. This approach is convenient for modelling fractures which may have permeable infillings, in which case the mechanical aperture is not indicative of the fracture transmissivity.

T_e and S_e are taken to be descriptive of the average properties of a fracture element. This description is presumably valid for fractures in which the local values of T_e and S_e may vary due to aperture variation or obstruction by infilling, but in which the spatial correlation structure of aperture is more or less isotropic, with a correlation length that is small relative to element size. If the elements are sufficiently small, channeling effects can be simulated within fracture planes by allowing elements transmissivity to vary within each fracture plane.

Flow within a network of fracture elements is modelled using a Galerkin finite element approximation to Equation A2-1,

$$\sum_{m=1}^{N}\left[h_m \int_R \nabla\xi_n \cdot \nabla\xi_m T_{nm}\, dR\right] + \sum_{m=1}^{N}\left[\frac{dh_m}{dt}\int_R S_{nm}\xi_n\xi_m dR\right] - \int_R q_n \xi_n dR \qquad \text{(A2-2)}$$

where:

T_{nm}	= transmissivity of element	[L^2/T]
S	= storativity of element	[-]
q_n	= source flux density at node n	[L/T]
ξ_n	= linear or quadratic basis function for element	[-]
R	= element area	[L^2]
h_n	= hydraulic head at node n	[L]
t	= time	[T]
N	= number of nodes	[-]

The solution of this equation is by means of an incomplete Cholesky decomposition, conjugate-gradient matrix solver as described in the MAFIC user documentation (Miller, 1990).

The **hydraulic aperture** used to calculate velocities from head gradients was calculated from transmissivity according to the cubic law:

$$T_e = \frac{b_e^3}{12\mu_w \rho_w g} \qquad \text{(A2-3)}$$

where:

b_e	= hydraulic aperture	[L]
μ_w	= absolute viscosity of fluid	[MT/L^2]
ρ_w	= fluid density	[M/L^3]
g	= gravitational acceleration	[L/T^2]

This hydraulic aperture may also be used in calculations of porosity, but the distinction between hydraulic aperture and mechanical aperture should be taken into consideration.

2:3 EdMesh Mesh Editing Utility

The **EdMesh** finite element mesh editor was developed as a tool for performing complex, multistep flow and transport simulations in conjunction with the **FracMan** and MAFIC codes. EdMesh allows the following mesh editing functions to be performed automatically:

- Changing boundary conditions and boundary condition types for selected nodal groups in a mesh;
- Probabilistic or deterministic scaling of transmissivities, storativities, and apertures of fracture elements for selected regions within a mesh;
- Defining correlations among storativity, transmissivity, and aperture for fracture elements;
- Changing MAFIC solution mode from steady-state to transient or vice-versa, or from flow-only to flow-and-transport mode;

In the present study, EdMesh was used to automate modification of boundary conditions to simulate flow in response to gradients in different directions, and in response to transient head changes applied in simulated well test intervals. EdMesh was also used to implement correlations between fracture storativity and transmissivity.

APPENDIX 3: GENERALIZED-DIMENSION FLOW INTERPRETATION OF PACKER TESTS

3:1 Definitions for Generalized-Dimension Flow

The theory of generalized-dimension flow (GDF) developed by Barker (1988) is based upon the concept of a conduit of constant conductivity, which varies in area with distance from the source as a power of the distance r:

$$A_c = \alpha_D r^{D-1} \tag{A3-1}$$

where α_D is defined by:

$$\alpha_D = \frac{2\pi^{\frac{D}{2}}}{\Gamma\left(\frac{D}{2}\right)} \tag{A3-2}$$

and $\Gamma(z)$ is the gamma function of argument z. The exponent D in Equation A3-1 is interpreted as the *dimension* of the conduit. For integral values of D (D = 1, 2, or 3), the flow geometry is referred to as being of integral-dimension (linear, radial, or spherical, respectively). For non-integral values of D, the flow geometry is referred to as fractional-dimension.

The generalized fluid flow equation for such a conduit is given by Barker as:

$$\frac{K}{r^{D-1}} \frac{\partial}{\partial r}\left(r^{D-1} \frac{\partial h}{\partial r}\right) = S_s \frac{\partial h}{\partial t} \tag{A3-3}$$

where:

K_c	= conduit conductivity	[L/T]
r	= distance from the source	[L]
h	= hydraulic head	[L]
S_s	= specific storage	[T^{-1}]

An alternative interpretation of GDF has been suggested by Doe and Geier (1990) in terms of the product of conduit conductivity and cross-sectional area. In this interpretation, the flow dimension is defined in terms of the power by which conductivity and cross-sectional area increase (or decrease) as a power of the distance from the source:

$$\left[K_c(r) A_c(r)\right] \propto r^{D-1} \tag{A3-4}$$

where

A_c	= cross-sectional area of conduit	[L^2]
D	= the flow dimension	[-]
r	= distance from the packer interval	[L]

For the extreme case of a linear conduit (*i.e.*, a conduit of constant aperture), a partial differential equation of form identical to that of Equation A3-3 arises if the conductivity of the conduit increases in proportion to the distance r raised to the power D-1, and if K is taken to be the conductivity at the source.

3:2 Solution for Constant-Head Tests

Barker (1988) gives a Laplace transform solution for a generalized well test, and gives specific solutions for common tests including constant-head, constant-rate, and slug tests. By defining a dimensionless time and flowrate as:

$$t_D = \frac{K_c t}{S_s r_w^2} \tag{A3-5}$$

and:

$$Q_D = \frac{Q}{h_{w0} K_c L^{3-D} \alpha_D r_w^{D-2}} \tag{A3-6}$$

respectively, where:

Q	= the flowrate from the well	[L^3/T]
h_{w0}	= the constant head applied at the well	[L]
L	= the length of the test interval	[L]
r_w	= the radius of the well	[L]

the Laplace transform solution for Equation A3-6 can be expressed as:

$$\bar{Q}_D = \frac{K_{\nu-1}(\sqrt{s})}{\sqrt{s}\, K_\nu(\sqrt{s})} \tag{A3-7}$$

where:

s	= the Laplace transform variable
ν	= 1 - $D/2$
$K_\nu(z)$	= the modified Bessel function of the second kind, of order ν

and where the bar denotes the Laplace transform of dimensionless flow. The expression in Equation A3-7 was evaluated by numerical inversion using the algorithm of Stehfest (1970).

3:3 Type Curve Matching Approach for Constant-Head Test Interpretation

Type curves of dimensionless flowrate versus dimensionless time for arbitrary flow dimension were obtained by numerical inversion of Equation A3-7, using the program FRACDIMH (Doe and Geier, 1990).

Figure A3-1 shows log-log type curves for integral dimensions from 0 to 4, and half dimensions 1.5 and 2.5. The type curve for linear flow (dimension $D = 1$) plots as a negative, half-slope line. The curve for spherical flow (dimension $D = 3$) asymptotically approaches a steady flow with a dimensionless value of unity. For small values of t_D all of the curves converge to a negative half-slope line, reflecting the influence of finite well diameter.

Type-curve matching is carried out by overlaying a log-log plot of well test data (flowrate versus time) with a plot of dimensionless type curves. Values of S_s, K, and D are estimated from the coordinates of a match point in each of the two plots, using the definitions of t_D and Q_D in Equations A3-5 and A3-6.

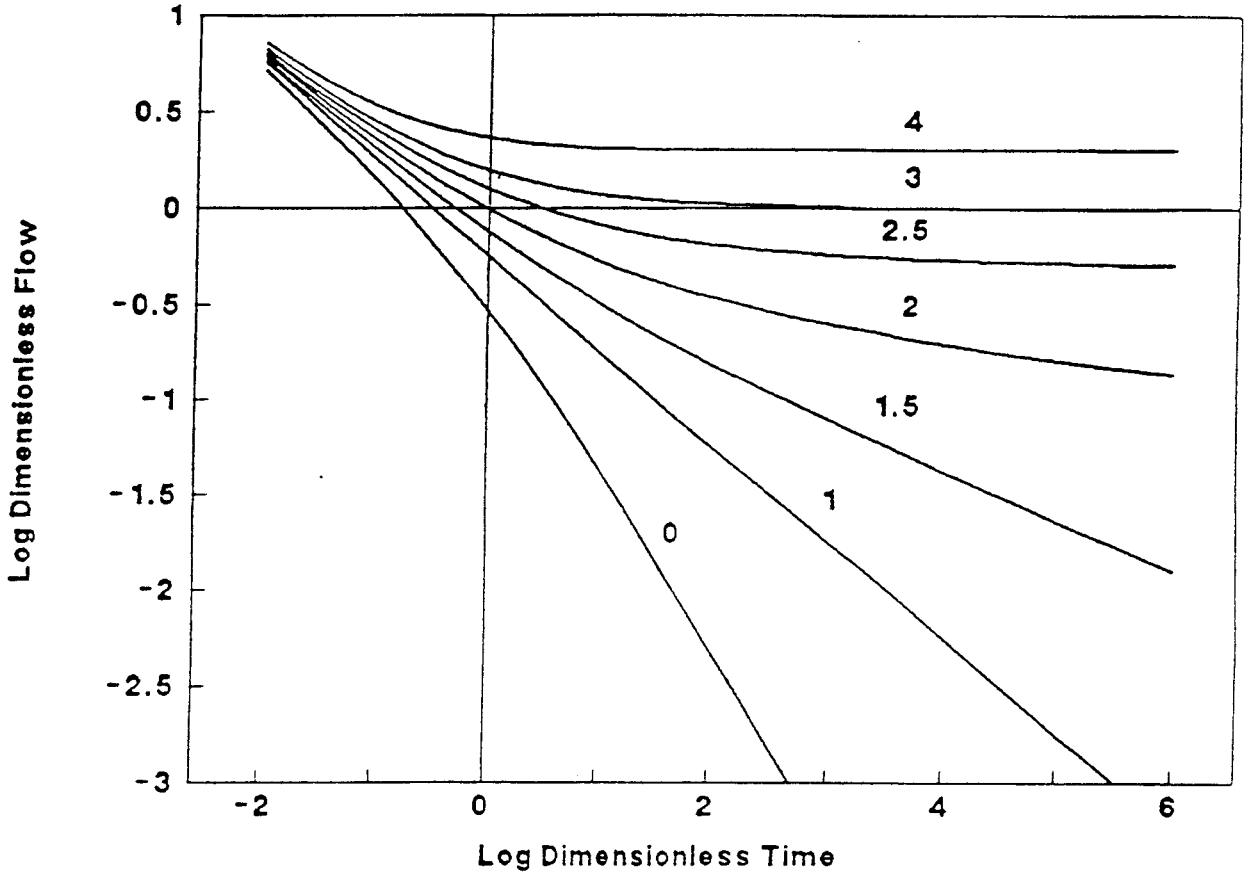

FIGURE **A3-1**

CONSTANT-PRESSURE TYPE CURVES FOR GENERALIZED FLOW DIMENSION ANALYSIS

APPENDIX 4: SOURCE DATA AND DERIVATION OF BOOTSTRAP DATASET FOR ORIENTATION

Fracture orientations for the simulations were generated by smoothed bootstrap sampling. Data from cell maps, scanlines, and core were combined to produce the data for bootstrap sampling. The original data for orientation were taken from the following files, which were furnished by Sveriges Geologiska AB (SGAB):

CELLMAP.DOS	Strike, dip, tracelength, and miscellaneous fracture characteristics from cell mapping in the cleaned trench near KFI 11.
PROF50.DOS	Strike, dip, and miscellaneous fracture characteristics from a scanline survey in the same trench.
KFI06.TXT	Fracture locations, infillings, and angles with the core axis for the vertical borehole KFI 06.
KFI11.TXT	Fracture locations, infillings, and angles with the core axis for the vertical borehole KFI 11.

The cell map and scanline fracture orientation data were extracted in the form of fracture pole directions, with Terzaghi correction factors. Terzaghi correction factors and fracture dip angles were calculated for all coated fractures in the core data. These extracted data are listed in following files:

CELLORS.PRN	Fracture pole directions and Terzaghi correction factors for cell map fractures.
SCANORS.PRN	Fracture pole directions and Terzaghi correction factors for scanline fractures.
KFI06ORS.PRN	Fracture dip angles and Terzaghi correction factors for borehole KFI 06.
KFI11ORS.PRN	Fracture dip angles and Terzaghi correction factors for borehole KFI 11.

The final dataset for bootstrap simulation was compiled as described in Section 4.1, by using fracture dip angles from the core to augment the more poorly sampled classes of orientation data in the surface data. This was done using a short FORTRAN code. The source code, executable code, and the orientation file produced are in the files:

ALLORS.ORS	Bootstrap simulation dataset.
MAKEORS.FOR	FORTRAN source code to produce ALLORS.ORS.
MAKEORS.EXE	Executable code for MS-DOS computers.

The files referred to in this appendix have been supplied to SKB in accordance with quality assurance guidelines.

APPENDIX 5: SOURCE DATA FOR FRACTURE SIZE ANALYSIS

The following files furnished by SGAB were used as the source data for fracture size analysis:

CELLMAP.DOS	Fracture trace length and other data (see Appendix 3).
REG1	Regional-scale lineament mapping data (first order).
REG2	Regional-scale lineament mapping data (second order).
SEMI1	Semiregional-scale lineament mapping data (first order).
SEMI2	Semiregional-scale lineament mapping data (second order).
SEMI3	Semiregional-scale lineament mapping data (third order).
SEMI4	Semiregional-scale lineament mapping data (fourth order).
LOKAL1	Local-scale lineament mapping data (first order).
LOKAL2	Local-scale lineament mapping data (second order).
LOKAL3	Local-scale lineament mapping data (third order).
LOKAL4	Local-scale lineament mapping data (fourth order).

The lineament files give starting and end coordinates, length, and azimuth for each lineament mapped. The classification of the lineaments has been described by Ahlbom and Tirén (1989). The length data were extracted from each of these files and combined in the following input files:

CELLMAP.PRN	Trace lengths from cell maps.
LOKAL.PRN	Local-scale lineament lengths (all orders)
SEMIREG.PRN	Semiregional-scale lineament lengths (all orders)
REGION.PRN	Regional-scale lineament lengths (both orders)

The above files were used for preliminary tracelength analysis. For the FracSize analysis, the cell map and local-scale lineament data were converted into binary files for FracSize input:

CELLMAP.FSZ	Cell map trace lengths.
LOKAL.FSZ	Local-scale lineament lengths.

The files referred to in this appendix have been supplied to SKB in accordance with quality assurance guidelines.

APPENDIX 6: GENERALIZED/DIMENSION FLOW TYPE CURVE MATCHES

This appendix describes GDF interpretation of packer test data for the Phase 1 feasibility study. A limited sample of transient FIL test data was selected from the results of the testing program in the boreholes BFI 01-02. Thirteen separate tests were included in this sample.

The selection of tests data was not random; tests with relatively good data (low "noise" level) were preferentially selected. A few of the test records were selected because they looked interesting; that is, they showed markedly non-radial behaviour that was apparent from visual inspection. The selection of relatively good data probably means that the sample is biased toward more conductive zones, since a high noise level suggests that the flowrate during the test was near the lower limit of the flowmeter range.

6:1 Analysis Procedure

Test data were provided by SGAB in the form of data-logger output files. The tests were analysed according to the generalized theory of constant-pressure well test analysis as outlined in Appendix 3. The steps in the analysis procedure were as follows:

- Identification of the beginning and ending points of the constant-pressure injection test period.
- Plotting the data as log flowrate versus log of time (from the beginning of the injection period).
- Matching the log-log plots to fractional-dimension type curves to determine D.
- Calculation of K, S_s, T, and S from the type curve match points.

The complete test sequence included data from packer inflation, shut-in, injection, and recovery periods. The starting and ending points of the injection period were recorded by the data logger, but due to a lag between triggering of the injection and the onset of the pressure rise within the test zone, it was necessary to estimate the starting point based upon the pressure rise recorded by a transducer in the zone (J-E Andersson, personal communication, 1990).

6:2 Type-Curve Matches

Figure A6-1 shows the type curve matches obtained by plotting the test data on a log-log scale and matching to fractional dimension type curves for all thirteen tests that were analysed. Conductivity and storativity values were calculated from the match points using Equations A3-5 and A3-6, to produce the values given in Table A6.1. These equations contain three unknowns: the desired properties K and S_s, plus the conducting thickness of the test zone, L. For conventional, radial-flow analysis in porous media, the last quantity is defined by the packer spacing. In fractured rock, the conducting thickness of the test zone is unknown (but certainly much smaller), and an effective L must be assumed.

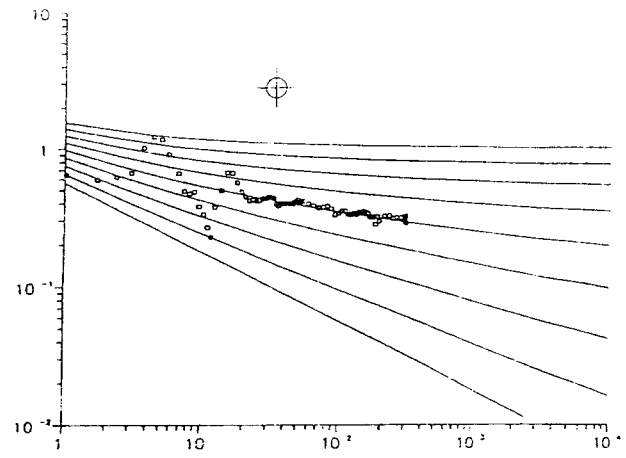

a) BFI 01 356-358 m

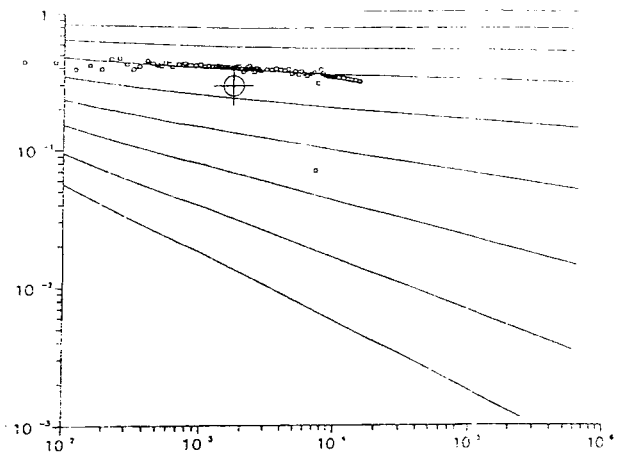

b) BFI 01 358-360 m

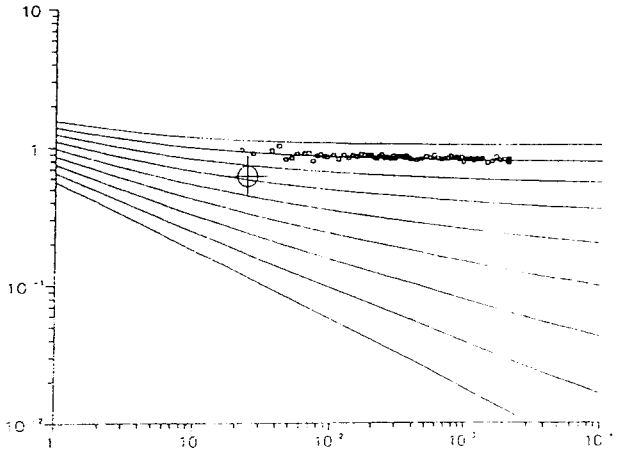

c) BFI 01 360-362 m

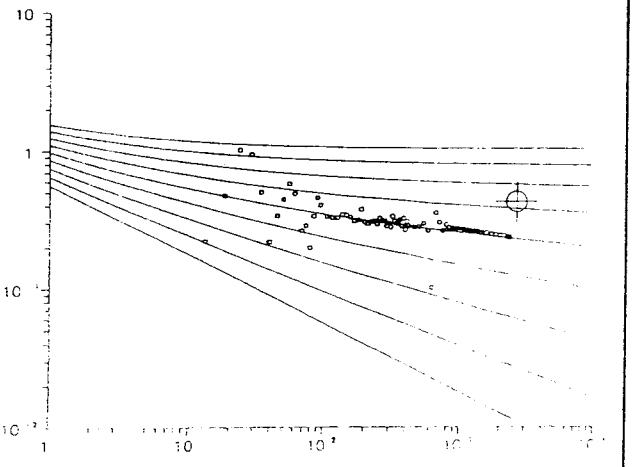

d) BFI 01 362-364 m

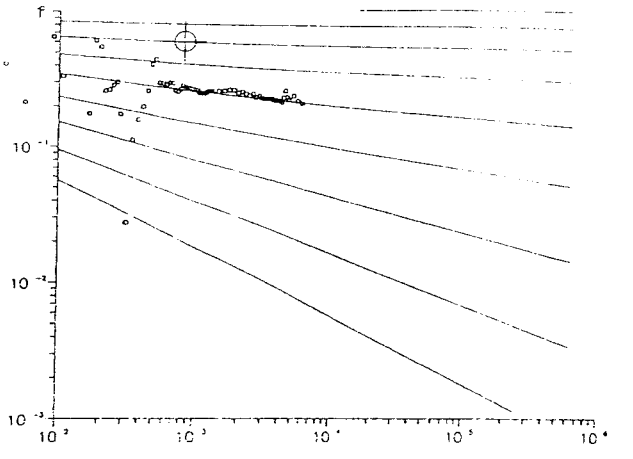

e) BFI 01 370-372 m

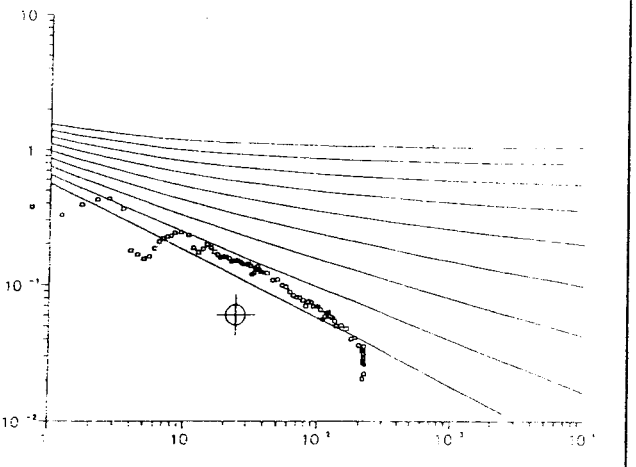

f) BFI 01 372-374 m

FIGURE **A6-1**
GENERALIZED-DIMENSION FLOW TYPE CURVE MATCHES

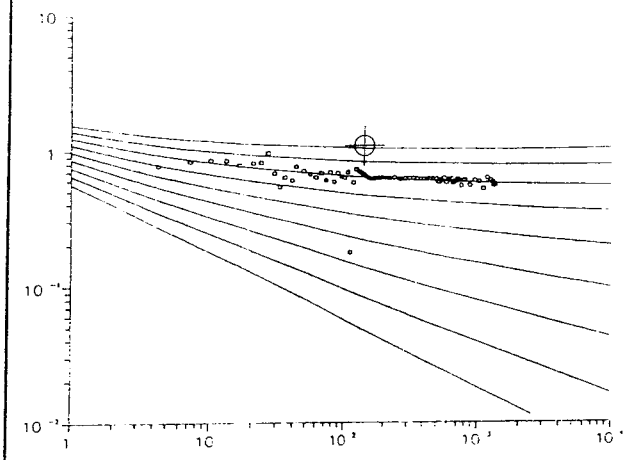

g) BFI 01 374-376 m

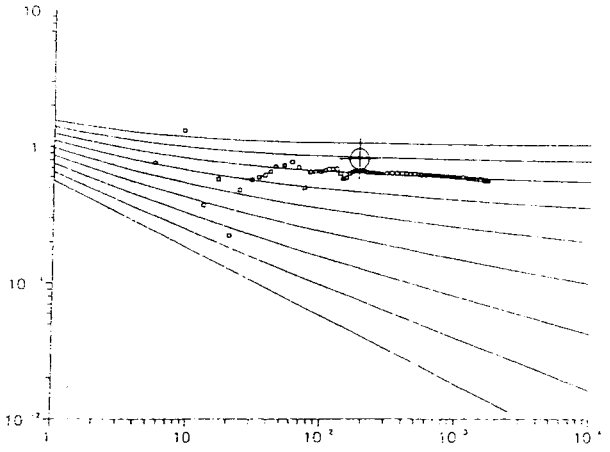

h) BFI 01 376-378 m

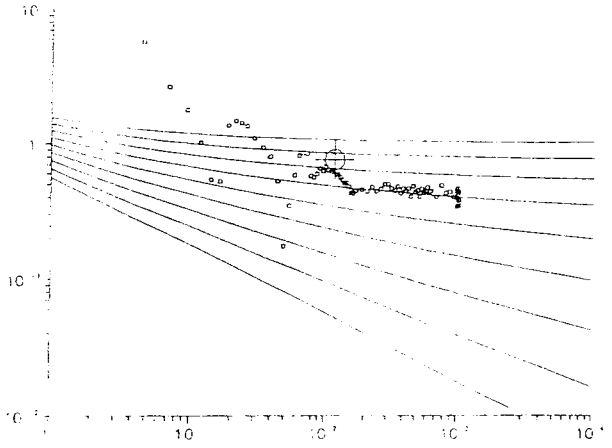

i) BFI 01 386-388 m

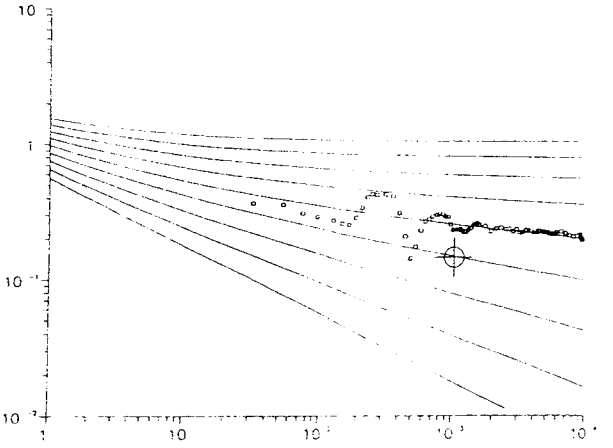

j) BFI 01 392-394

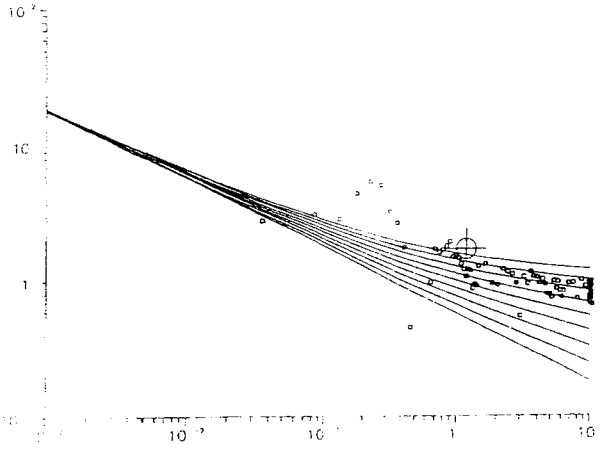

k) BFI 01 424-426 m

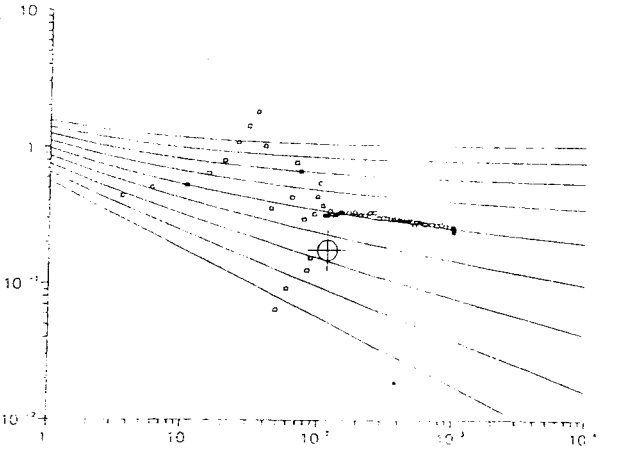

l) BFI 01 430-432

FIGURE A6-1, ctd.
GENERALIZED-DIMENSION FLOW
TYPE CURVE MATCHES

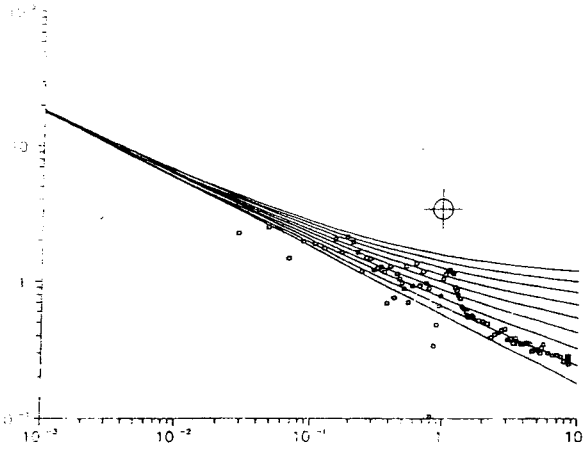

m) BFI 02 280-282

FIGURE **A6-1, ctd.**
GENERALIZED-DIMENSION FLOW TYPE CURVE MATCHES

Table A6.1 Fractional-Dimension Interpretations of Selected FIL Tests from Boreholes BFI 01 and BFI 02.

Borehole	Interval (m)	Flow Dimension	Log Conductivity (m/s)	Log Specific Storage (m^{-1})	Log Transmissivity (m/s^2)
BFI 01	360-362	2.75	-5.49	-3.03	-7.13
	370-372	2.00	-5.58	-3.66	-7.88
	356-358	2.00	-6.26	-2.95	-8.56
	358-360	2.25	-4.57	-2.97	-6.66
	362-364	2.00	-6.01	-4.59	-8.31
	372-374	1.13	-4.40	-0.95	-7.47
	374-376	2.50	-6.46	-3.76	-8.32
	376-378	2.50	-6.51	-3.94	-8.38
	386-388	2.25	-6.99	-4.21	-9.07
	392-394	2.00	-5.96	-4.14	-8.26
	424-426	2.50	-7.64	-2.88	-9.51
	430-432	2.00	-6.05	-3.27	-8.35
BFI 02	280-282	1.25	-5.33	-0.47	-8.29

For interpreting well tests in terms of equivalent-porous-medium hydraulic conductivities K_e the need to assume a value of L is problematic, since an incorrect value could lead to a gross misestimation of K_e. This means that comparisons of K_e values from different intervals, or direct application of the values to Stochastic Continuum or Channel Network models may not be meaningful. This error can be reduced by using a reasonably small value of L rather than the packer separation. In Table A6.1 a value of L = 5 mm was assumed, which is probably somewhat larger than the effective conducting thickness for most of the test zones.

Alternatively, the conductivities can be expressed in terms of a generalized transmissivity defined by T. Doe (personal communication, 1990) as:

$$T = \frac{KL^{3-D}}{r_w^{2-D}} \qquad \text{(A6-1)}$$

which effectively removes the unknown L from Equation A3-6, giving:

$$Q_D = \frac{Q}{h_{w0} T \alpha_D} \qquad \text{(A6-2)}$$

In the case of radial flow this is the usual definition of transmissivity. For non-radial flow the use of this generalized transmissivity must be qualified by stating the dimensionality of the flow.

The issue of effective conductive thickness is less problematic for the purposes of the present study, in which the interpreted transmissivities are used to define and validate a DFN model. Particularly in the validation and/or calibration of DFN models, if interpretations of field results are compared with interpretations of simulated tests, the values of K_r are comparable provided that the two sets of tests are interpreted in a consistent manner.

A second problem in the method is that the effective radius r_w of the test section is not necessarily known. Although the borehole radius is quite well known due to the high quality of the rock, the effective radius is uncertain. The fractional-dimension interpretation approach described in Appendix 3 is based upon an idealized model in which the product of conductivity times conduit area varies in proportion to some power of distance from the center of the source. If the variation of the KA product is less regular than this (*e.g.*, if there are strong skin effects), then what the method actually measures are the properties of the idealized conduit that gives the best match to the data, which may have a significantly different effective source radius. This uncertainty in r_w means that, for cases of high-dimension ($D \geq 2.5$) flow, the K values are uncertain, and, in all cases, storage values as calculated are suspect.

6:3 Comments on Type-Curve Matches

As the packer test interpretations given above are intended as a demonstration of a rather novel methodology, some remarks should be made regarding the individual type-curve matches.

In general, it must be said that the test data are rather ambiguous, due to the short time span of useable data. Ideally the method should be used for tests covering at least two or preferably three orders of magnitude. However, for most of the tests the early-time data are not reliable under 100 seconds or so, and the duration of the tests is only about 1000 s. Thus for most of the tests only about one order of magnitude of data is available for type-curve matching.

The basic difficulty is that these tests were planned and carried out with steady-flow interpretations in mind, so that, although transient data were recorded to check if steady flow was achieved, insufficient time and money were allocated to obtain data for transient analysis. Hence the present analysis is limited by the fact that the testing program was not designed for transient analysis.

For future tests, the usefulness for type-curve matching could be improved by:

1) Using test equipment designed to capture data at an earlier time, *cf* the data obtained in similar rock during the course of the Stripa Site Characterization and Validation Project (Holmes *et al.*, 1989), or
2) Running the tests for 2 hours instead of 15 minutes to get an extra order of magnitude in the late-time data.

The following comments pertain to the reliability of the type-curve matches for each test in the sample:

BFI01 360-362: This is a good test of apparently high dimension, with possibly near-spherical flow geometry.

BFI01 370-372: This test contains only one order of magnitude of useable data. A match is made using D = 2.0, but matches to other type curves are possible.

BFI01 356-358: This test contains only slightly more useable data than Test BF101370-372. Again, a match is made using D = 2.0, but other matches are possible.

BFI01 358-360: The early-to-mid time data allow a match to a type curve with D = 2.25. The late-time steepening of the log-log plot may indicate a closed-boundary effect (*i.e*, a restriction in the conduit). A variation in background head due to a disturbance in the hole is also a possible explanation, though perhaps less likely.

BFI01 362-364: Early-time oscillation in the data make a precise fit difficult, but the general trend of the data support a fit to the D = 2.0 curve.

BFI01 372-374: Although the data for this test are noisy, the half-slope behaviour gives an excellent indication of near-linear (D = 1) flow. The late-time decline in the flowrate may be a closed-boundary effect (due to a restriction in the conduit), but a more likely explanation may be that the flowmeter has been underranged.

BFI01 374-376: Two reasonable orders of magnitude on the time scale provides a fairly decent match to a type curve with D = 2.5.

BFI01 376-378: This test provides a slightly less certain match than Test BF101374-376, due to the somewhat poorer quality of the early-time data. The match is made to a type curve with D = 2.5, but dimensions of 2.0 to 2.25 could also provide matches at higher values of dimensionless time.

BFI01 386-388: Only one good order of magnitude means that this data could be fit to any curve between dimensions 2 and 3. A multirate correction (*cf* Doe and Geier, 1990) could improve the usability of this type curve for transient analysis. A conditional match is made for $D = 2.25$.

BFI01 392-394: This test has some unusual behaviour in the middle of the test, possibly reflecting a disturbance in the hole. The late-time data allow a somewhat uncertain fit with $D = 2.0$.

BFI01 424-426: This test contains only one order of magnitude of still somewhat noisy, but usable data. A fit is made to $D = 2.5$, but matches with other curves from $D = 2.0$ to 3.0 are possible.

BFI01 430-432: This test also contains little useable data. The late time data fits $D = 2.0$, but other matches are possible.

BFI02 280-282: This data is noisy, but clearly of a low flow dimension as evidenced by the steep slope. The slope is slightly less than -1/2, so a match is made to $D = 1.25$.

These interpretations illustrate the fact that, for higher-dimension flow, the precise dimensionality of the flow is difficult to distinguish without early-time data. However, lower-dimension (nearly linear) is distinctive because of its steep slope on a log-log plot.

The only statement that can be made with a high degree of certainty about this sampling of 13 tests is that only two of them are cases of near-linear flow, while the other 11 tests have flow dimensions that are most probably in the range 2 to 3. If this behaviour is observed in the full suite of FIL tests (not just in this non-random sample), it indicates a fracture network that is well-connected.

APPENDIX 7: DERIVATION OF AT-BOREHOLE VS. CROSS-FRACTURE TRANSMISSIVITY RELATIONSHIP

This methodology is based upon numerical experiments performed by Kenrick *et al.*, 1988, who performed numerical simulations of transient packer tests and steady-state, cross-fracture flow for various patterns of transmissivity variation within a single hexagonal fracture. For the packer test simulations, constant-head boundary conditions were applied around the outer boundary of the fracture, and a fixed increase in head was applied at a simulated well through the center of the fracture (Figure A7-1a). The resulting transient flow response was analyzed using the method of Jacob and Lohman (1952).

To measure cross-fracture transmissivity, Kenrick *et al.* applied head gradients in each of three directions across the fracture (Figure A7-1b) and measured the steady flow between opposite sides. In each of these simulations, a fixed head difference was applied between one pair of opposing sides, and no-flow boundary conditions were imposed on the other four sides. The results gave a comparison of cross-fracture and at-borehole transmissivity for each of the transmissivity patterns thus simulated.

The work of Kenrick *et al.* provides the inspiration for the methodology applied herein, but their work cannot be used directly because it is mainly based upon idealized fracture aperture patterns, and not observed fracture transmissivity or aperture patterns.

7:1 Replication of Aperture Maps

Detailed contour maps of fractures in granitic rock were produced by the Stripa Project (Hakemi, 1989). One of these maps (Figure A7-2) was chosen for simulation of at-borehole and cross-fracture transmissivity measurements to demonstrate this approach in the present study. Aperture values were taken from this map by use of a digitizer. The digitized apertures were converted to transmissivity according to the cubic law (Equation A2-3), and a uniform mesh was generated from the digitized points using the program Surfer (Golden Graphics, Inc.). Three locations were chosen within the mesh for packer test simulations, as indicated on the map in Figure A7-2.

The transmissivities that were calculated according to the cubic law were on the order of 3.1×10^{-6} to 1.4×10^{-3}. This seemed very high in relation to *in situ* transmissivities. The transmissivities were accordingly scaled by a factor of 10^{-5} to produce a range of transmissivities more comparable to the fractures at Finnsjön.

Uniform storativity of $S = 10^{-5}$ was assumed. Cross-fracture transmissivity was measured by simulating steady flow in two orthogonal directions across the grid, aligned with the boundaries. The measured transmissivities were:

Left to Right flow: $T_f = 1.1\times10^{-9}$ m²/s
Top to Bottom flow: $T_f = 1.2\times10^{-9}$ m²/s

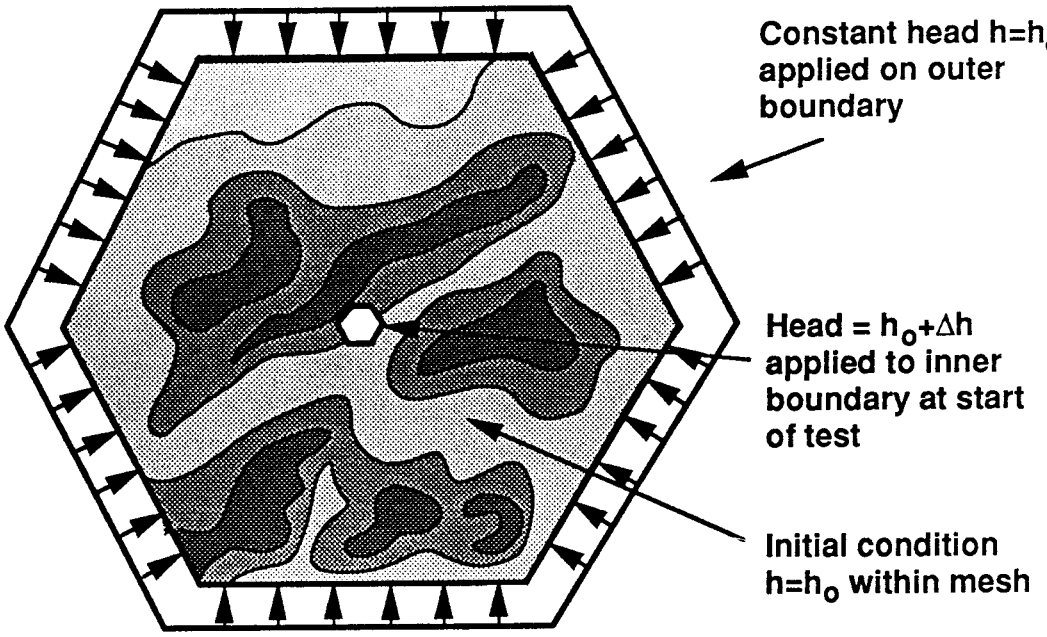

a) At-Borehole Measurements of Transmissivity

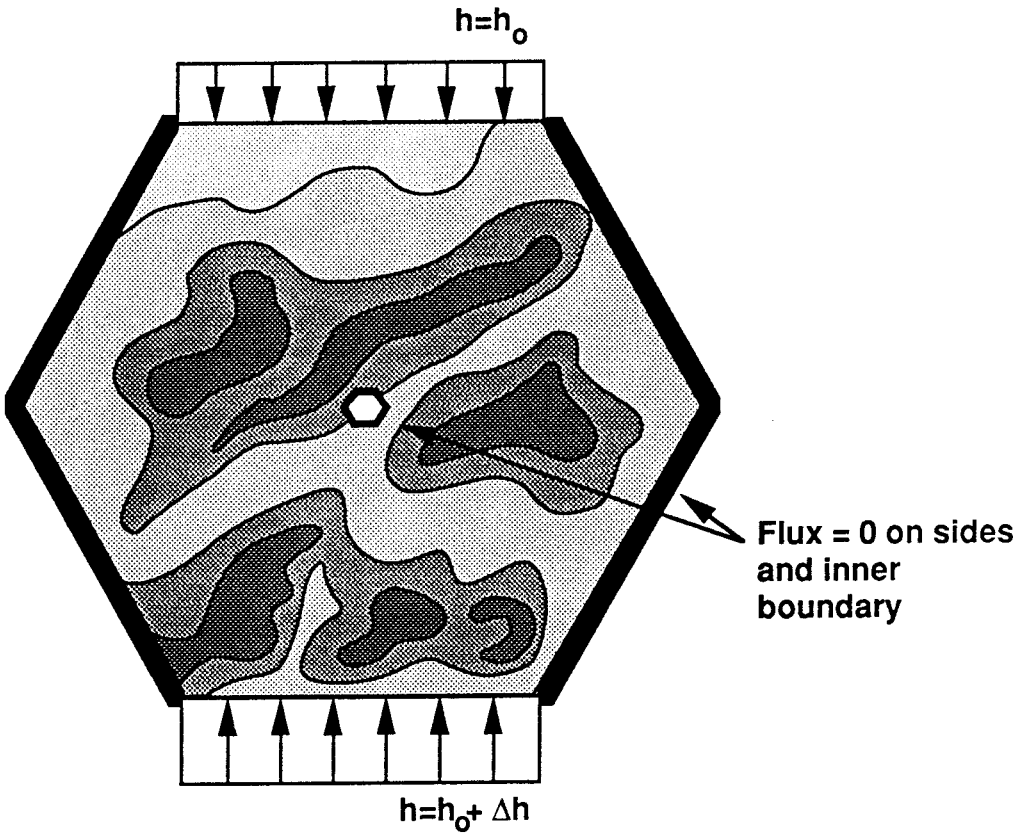

b) Cross-Fracture Measurement of transmissivity

FIGURE A7-1
BOUNDARY CONDITIONS FOR AT-BOREHOLE AND CROSS FRACTURE FLOW

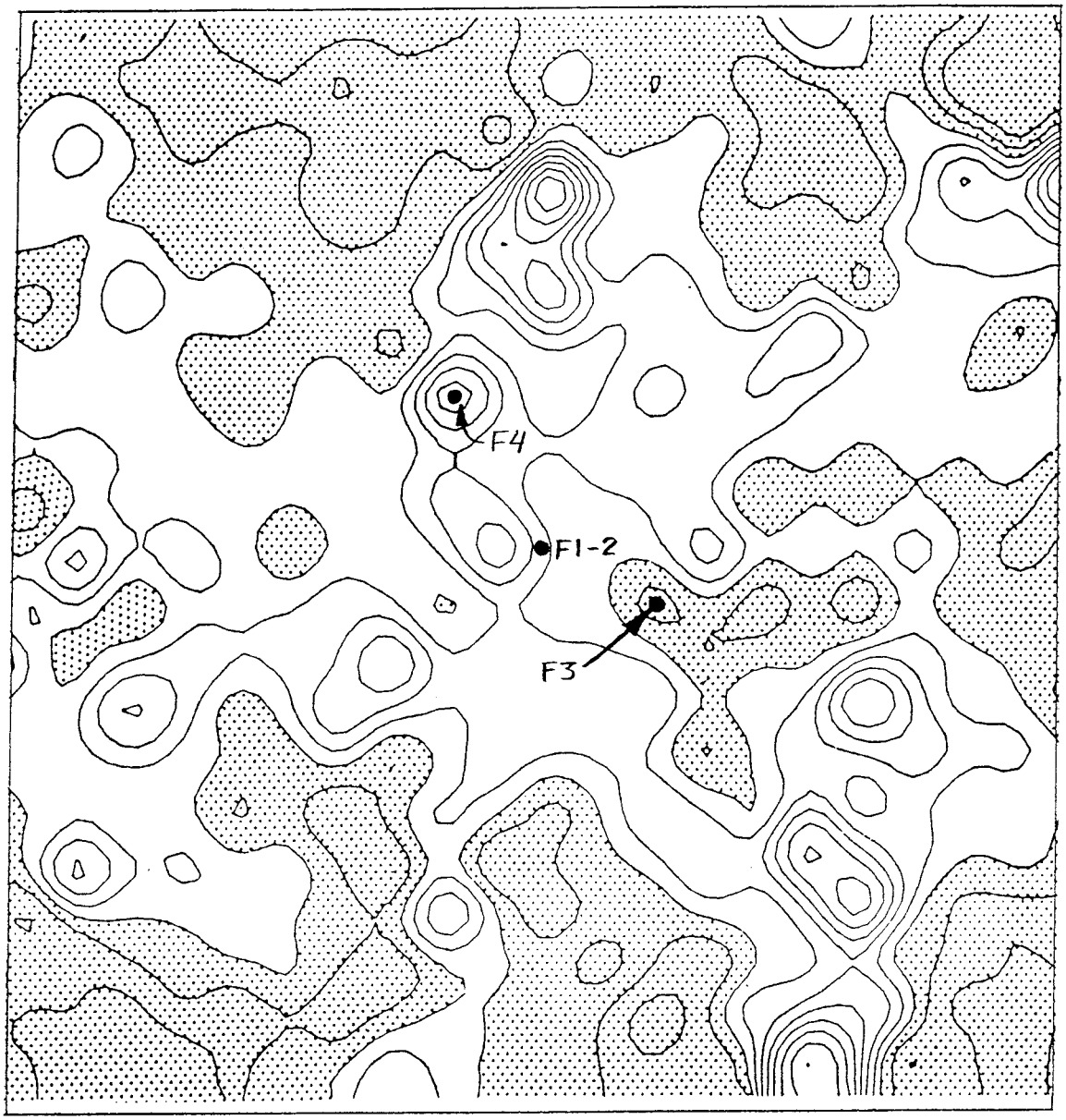

(from Hakami 1989)

FIGURE **A7-2**

CONTOUR MAP OF FRACTURE APERTURE

Constant-head tests were simulated following the methodology of Kenrick *et al.* Due to the very small scale of the mesh (The map in Figure A7-2 is actual scale), very small time steps (0.1 to 200 seconds) and scaled-down boreholes (r_w = 3.28 mm) were used.

Three different locations within the grid were selected for well test simulations:

F1-2 The center of the grid, within a channel.
F3 A point within an island of low aperture, on the edge of a channel.
F4 A point in a very conductive part of a channel.

The transmissivities determined from Jacob & Lohman analysis were:

F1-2: $T_{fo} = 7.2\times10^{-9}$ m²/s
F3: $T_{fo} = 5.8\times10^{-9}$ m²/s
F4: $T_{fo} = 7.7\times10^{-9}$ m²/s

That the measured T_{fo} were all higher than the cross-fracture transmissivities is probably an artifact of the fact that all of the simulated boreholes were located within or close to the edge of the main flow channels. The particular fractures chosen for simulation had no large "islands" of low aperture in the central region (Simulations were restricted to the central region to avoid boundary effects).

Many more replications of fracture geometry would be necessary to adequately define the relationship of at-borehole to cross-fracture transmissivity. The digitization process makes this task rather laborious. The main value of the exercise is to provide a check on the reasonability of the method described in the following section, which is based upon simulations of fracture aperture variation as characterized by fractal methods.

Aside from the large amount of effort required to model replicated aperture maps, two problems that are apparent from this preliminary application of the method. Firstly, the extent of the aperture maps is very small compared to fractures on the scale of interest (> 1 m in radius). Equivalent, 2-D data is not available for larger fracture extents. Secondly, the high aperture values do not appear to be realistic if extended to the scale of larger fractures (although they may be correct over small areas). Statistical characterization of the T_{fo} vs. T_f relationship is difficult to justify without further knowledge of scale effects for fracture aperture variation.

7:2 Simulated Fracture Transmissivity from Fractal Characterization

Numerous researchers have modelled flow within single fractures of variable aperture based upon some type of spatial correlation structure (*e.g.*, Iwai, 1976; Tsang 1984; Brown, 1986; Kenrick *et al.*, 1988, Abelin *et al.*, 1990). Several of these models tend to produce "channeled" patterns of aperture within fractures, notably simulation from a covariance function and simulation from a fractal model of topography. Of these two methods, the fractal model (Brown, 1986) is perhaps the easier to implement, based upon the recursive subdivision algorithm of Fournier *et al.* (1982).

Brown and Scholz (1985) demonstrated that linear profiles of rock have power spectra of the form:

$$G(k) \approx k^s \tag{A7-1}$$

where:

k = $2\pi/\lambda$ = the wave number corresponding to a frequency λ
s = an empirical constant

Brown (1986) noted that s can be related to the fractal dimension D_r of a surface in the fractal topography model of Mandelbrot (1983), with $s = -(7 - 2D_r)$. Values of s measured by Brown and Scholz ranged from 2 to 3 for natural fractures, corresponding to a fractal dimension in the range $2 < D \leq 2.5$. Brown's model for fracture aperture was based upon producing two independent simulations of fractal surfaces, and bringing them together to form the two faces of a fracture. Figure A7-3 shows examples of surface topography and aperture variation simulated by Brown according to this process. The flat areas in the latter plot are contact areas. This specific approach is of theoretical interest, but in the present context it is overly complex, since it requires bookkeeping for two separate fracture surfaces. Furthermore, the model is inapplicable to nearly-mated fractures (those with very little displacement between faces, so that the faces are correlated) or to fractures with infilling.

A more general and direct approach is to model the transmissivity value as a function having fractal topography. This does not necessarily follow directly from the fracture profile measurements of Brown and Scholz (1985); it is not obvious that the cube of the distance between two fractal surfaces at fixed mean separation is a fractal process (although this hypothesis can be tested empirically by simulation after the manner of Brown, 1986).

However, fractal measures for variability of single-fracture transmissivity can be derived from the multipede packer data recently presented by Abelin *et al.* (1990). These data were not available at the outset of the Phase 1 study, but can be utilized in the subsequent stages of the SKB 91 safety assessment study. Fractal models have been demonstrated to be very flexible for describing physical processes of a similar nature, and can be made more flexible by the appropriate transforms of the data, *e.g.* a logarithmic transformation of local T values. For the present phase, a demonstration is given of a fractal model for variable transmissivity, using an assumed fractal dimension for log transmissivity of 2.25. This model was implemented in the FracMan program MeshMonster as a general feature for simulating variable-transmissivity fracture networks.

To demonstrate the use of this model for deriving at-borehole vs. cross-fracture transmissivity relationships, a single, hexagonal fracture ($r_e \approx 10$ m) was rediscretized using different random number generator seeds in ten runs of the model. For each realization of the fractal model, cross-fracture flow was measured in three directions according to the procedure of Kenrick *et al.* (1988). Constant-head well tests were simulated in a hexagonal "borehole" with an effective radius of about 5 cm in the center of the fracture. The transient response was analyzed by matching log flux vs. log time plots against the fractional dimension type curves given in Appendix 3. Figure A7-4 shows log-log plots of the transient response.

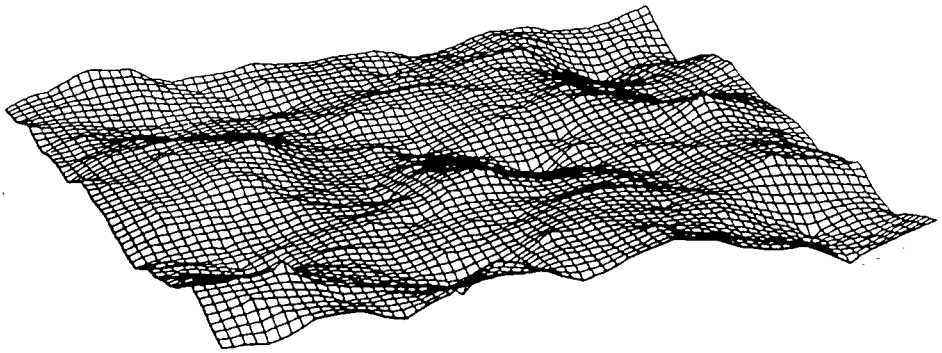

a) Topography

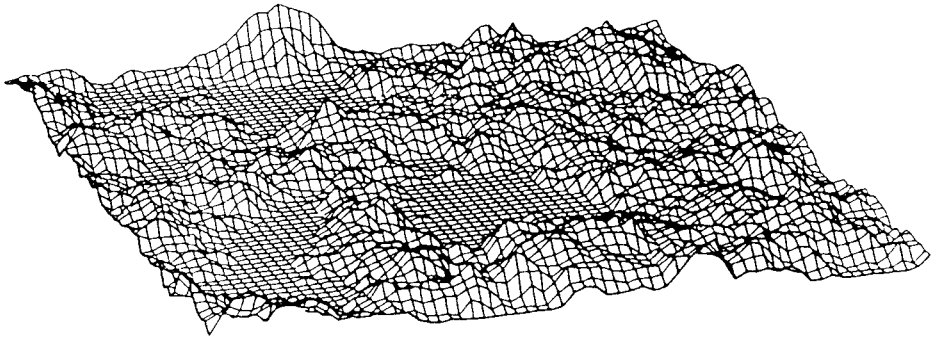

b) Aperture

(from Brown, 1987.)

FIGURE A7-3
FRACTAL MODEL OF FRACTURE SURFACE TOPOGRAPHY AND APERTURE

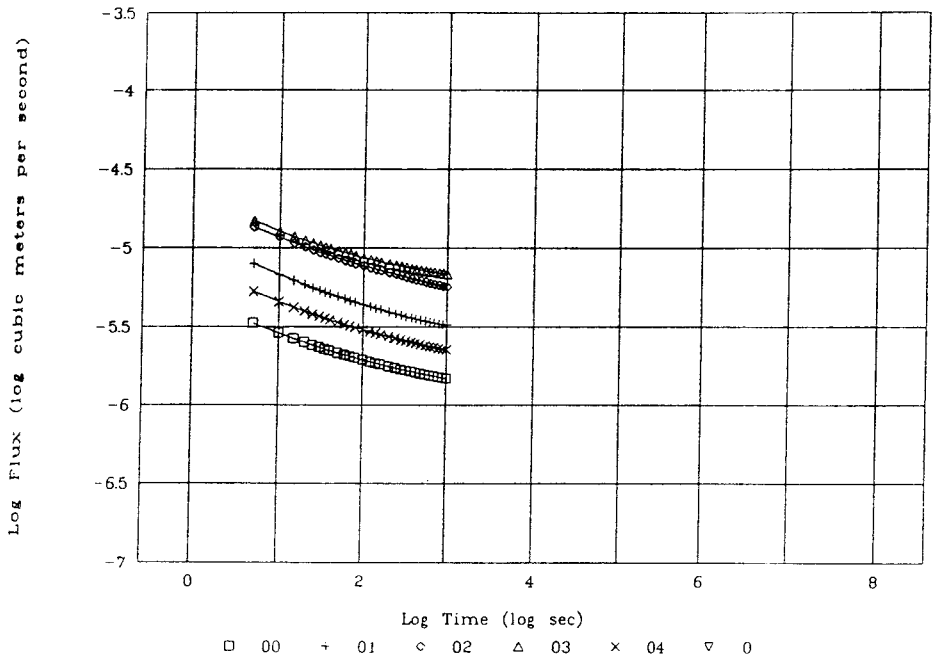

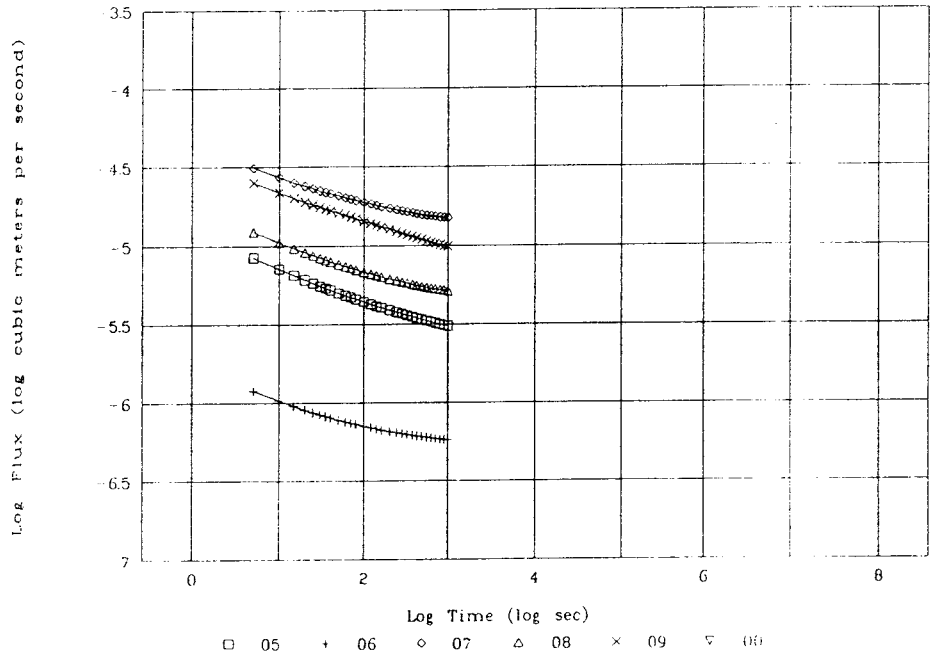

FIGURE **A7-4**
SIMULATED PACKER TESTS IN SINGLE FRACTURES

The interpreted at-borehole transmissivities are plotted versus cross-fracture transmissivity in Figure A7-5. This plot shows that, for this fractal model, the probabilities of the ratio T_{fo}/T_f being greater or less than one are roughly equal, but the degree to which T_{fo} overestimates T_f tends to be less than the degree to which T_{fo} underestimates T_f, in the respective cases.

This methodology for deducing the relationship between T_{fo} and T_f depends upon identification and validation of a valid fractal model for transmissivity variation. However, data is available for this purpose from the Stripa Project (Abelin *et al.*, 1990). Alternative simulation methods using simulations of covariance functions are also possible, and have received validation by Abelin *et al.* However, the fractal model is preferred due to its demonstrated validity for related phenomena, and its relative ease of implementation, as demonstrated here.

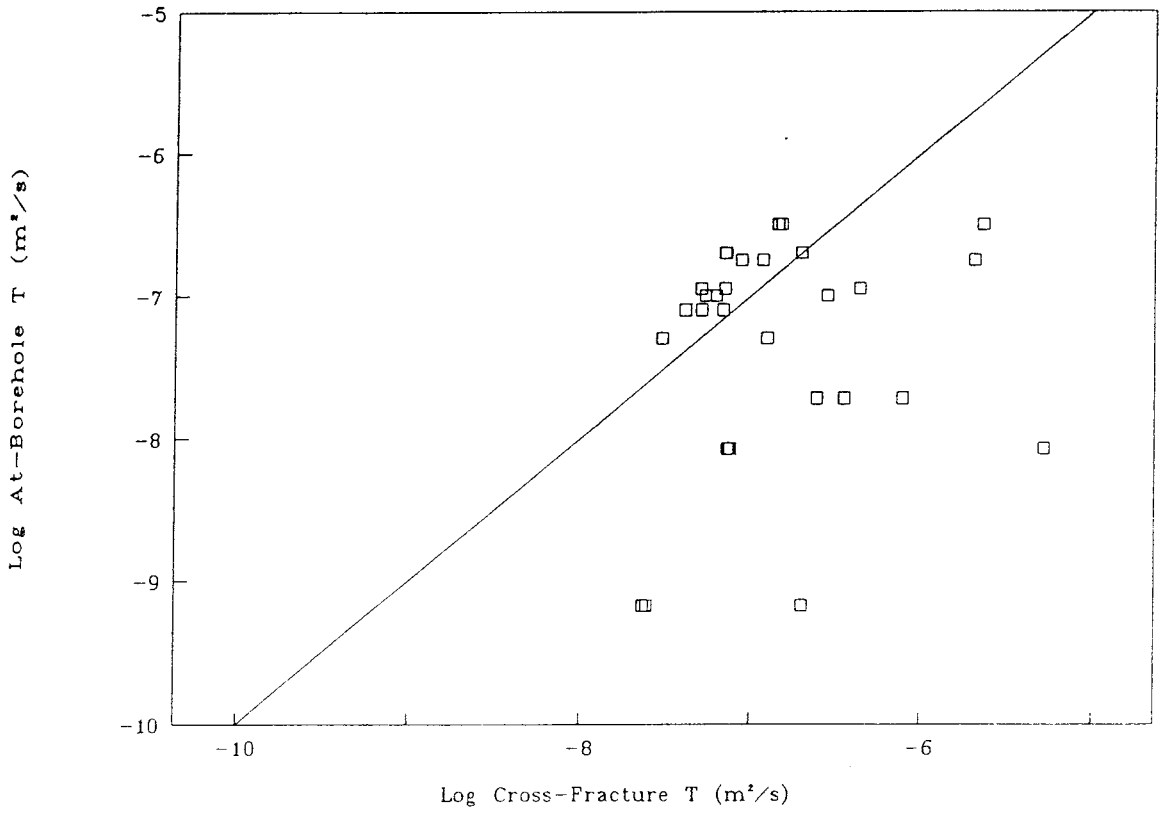

FIGURE **A7-5**

CROSS-FRACTURE VS. AT-BOREHOLE TRANSMISSIVITY FROM SIMULATIONS

APPENDIX 8: TRANSMISSIVITY DATA USED IN OxFILET ANALYSIS

The following files furnished by SGAB were used as the source data for fracture transmissivity analysis:

KMIN.LIS	Listing of conductivity measurement thresholds for each borehole and each packer testing program.
SHSINJCD.LIS	Measured conductivity values for all boreholes (first database).
SHTINJCD.LIS	Measured conductivity values for all boreholes (second database).

The data for 2 m intervals below Zone 2, fracture zones excluded, were extracted from the above files by sorting the data with respect to (1) borehole number, (2) fracture zone membership or non-membership, and (3) packer interval length, and applying a common measurement limit. This was done in a LOTUS 1-2-3 spreadsheet:

FIL2MGOD.WK1	Spreadsheet for sorting hydraulic conductivity data and applying common measurement threshold.

The conductivity values for the borehole intervals used in the analysis were printed to a file:

2MGOOD20.FIL	FIL conductivities for OxFILET analysis.

The files referred to in this appendix have been supplied to SKB in accordance with quality assurance guidelines.

APPENDIX 9: FracMan MACRO FOR GENERATING 50 M DATASETS

The following is the text of the FracMan macro file that was used to generate datasets for 50m blocks. This file completely defines the fracture datasets.

```
<FWn>
{
10
 EXIT
6
 Re-init
1
(any 5-digit #):
1
 UTILS
1
 Change View
3
<<<title>>>  VIEWING REGION
< 4.T>
< 4.N>
< 4.S>
< 10  3  0>  Center (x,y,z)
          0,0,0
< 10  2  0>  Direction(tr,pl)
          345,30
< 11  1  0>  Scale
          0.01
<-12  0  0>       GO!
 GENERATE
2
 Fracture Set
1
<<<title>>>  FRACTURE OPTIONS
< 4.T>
<1111.L>
<1412.P>
< 8.N>
< 8.S>
<-11  0  0>  Model: Enhanced Baecher
<-11  0  0>  Intens: Area/Vol
<-11  0  0>  Region: BOX
<-11  0  0>  Orientations: Pole
< 10  3  0>  Region Min (x,y,z)
          -28,-28,-28
< 10  3  0>  Region Max (x,y,z)
          28,28,28
<  1  1  0>  # of Sides
          6
<-12  0  0>       GO!
<<<title>>>  GENERATE FRACTURES
<16.T>
<1111111111111111.L>
<2614831111101311.P>
<16.N>
<16.S>
< 10  2  0>  Pole (tr,pl)
          0,0
<-11  0  0>  Bootstrap
< 10  1  0>  Concentration
          10.
< 10  1  0>  Size Exponent
          1.89
<-11  0  0>  Power Law
< 10  1  0>  Minimum value
          0.5
< 10  2  0>  Dir of Elong(tr,pl)
          0,0
<-11  0  0>  [constant]
<-10  0  0>
< 10  1  0>  Aspect Ratio
          1
<-11  0  0>  [constant]
<-10  0  0>
< 10  1  0>  Termination %
          0
< 10  1  0>  Frac Area/Vol
          0.487
<-11  0  0>  [constant]
<-12  0  0>       GO!
bootstrap
allors.ors
<<<title>>>  FRACTURE PROPERTIES
<19.T>
<11111111111111111.L>
<11151111111111111.P>
<19.N>
<19.S>
< 10  1  0>  Transmissivity
          5.99e-007
<-11  0  0>  Uncorrelated
<-10  0  0>
<-11  0  0>  TLogNormal
< 10  1  0>  Standard deviation
          0.0715
<-10  0  0>
< 10  1  0>  Storativity
          1e-008
<-11  0  0>  Uncorrelated
<-10  0  0>
<-11  0  0>  [constant]
<-10  0  0>
<-10  0  0>
< 10  1  0>  Frac Thickness
          0.0001
<-11  0  0>  Uncorrelated
<-10  0  0>
<-11  0  0>  [constant]
<-10  0  0>
<-10  0  0>
<-12  0  0>       GO!
<<<title>>>  Transmissivity
< 0.T>
```

```
< 3.N>
< 3.S>
< 10  1  0>  Lower Bound
           1.00e-09
< 10  1  0>  Upper Bound
           0.001
<-12  0  0>          GO!
 FILES
5
 Export File
4
File Option
2
3D data
d2abt##.bab
DELETE FRACTURES
0
}
HALT
999
```

List of SKB reports

Annual Reports

1977-78
TR 121
KBS Technical Reports 1 – 120
Summaries
Stockholm, May 1979

1979
TR 79-28
The KBS Annual Report 1979
KBS Technical Reports 79-01 – 79-27
Summaries
Stockholm, March 1980

1980
TR 80-26
The KBS Annual Report 1980
KBS Technical Reports 80-01 – 80-25
Summaries
Stockholm, March 1981

1981
TR 81-17
The KBS Annual Report 1981
KBS Technical Reports 81-01 – 81-16
Summaries
Stockholm, April 1982

1982
TR 82-28
The KBS Annual Report 1982
KBS Technical Reports 82-01 – 82-27
Summaries
Stockholm, July 1983

1983
TR 83-77
The KBS Annual Report 1983
KBS Technical Reports 83-01 – 83-76
Summaries
Stockholm, June 1984

1984
TR 85-01
Annual Research and Development Report 1984
Including Summaries of Technical Reports Issued during 1984. (Technical Reports 84-01 – 84-19)
Stockholm, June 1985

1985
TR 85-20
Annual Research and Development Report 1985
Including Summaries of Technical Reports Issued during 1985. (Technical Reports 85-01 – 85-19)
Stockholm, May 1986

1986
TR 86-31
SKB Annual Report 1986
Including Summaries of Technical Reports Issued during 1986
Stockholm, May 1987

1987
TR 87-33
SKB Annual Report 1987
Including Summaries of Technical Reports Issued during 1987
Stockholm, May 1988

1988
TR 88-32
SKB Annual Report 1988
Including Summaries of Technical Reports Issued during 1988
Stockholm, May 1989

1989
TR 89-40
SKB Annual Report 1989
Including Summaries of Technical Reports Issued during 1989
Stockholm, May 1990

Technical Reports
List of SKB Technical Reports 1991

TR 91-01
Description of geological data in SKB's database GEOTAB
Version 2
Stefan Sehlstedt, Tomas Stark
SGAB, Luleå
January 1991

TR 91-02
Description of geophysical data in SKB database GEOTAB
Version 2
Stefan Sehlstedt
SGAB, Luleå
January 1991

TR 91-03
1. The application of PIE techniques to the study of the corrosion of spent oxide fuel in deep-rock ground waters
2. Spent fuel degradation
R S Forsyth
Studsvik Nuclear
January 1991

TR 91-04
Plutonium solubilities
I Puigdomènech[1], J Bruno[2]
[1]Enviromental Services, Studsvik Nuclear, Nyköping, Sweden
[2]MBT Tecnologia Ambiental, CENT, Cerdanyola, Spain
February 1991

TR 91-05
Description of tracer data in the SKB database GEOTAB
SGAB, Luleå
April, 1991

TR 91-06
Description of background data in the SKB database GEOTAB Version 2
Ebbe Eriksson, Stefan Sehlstedt
SGAB, Luleå
March 1991

TR 91-07
Plutonium solubilities
Margareta Gerlach[1], Bengt Gentzschein[2]
[1]SGAB, Luleå
[2]SGAB, Uppsala
April 1991

TR 91-08
Overview of geologic and geohydrologic conditions at the Finnsjön site and its surroundings
Kaj Ahlbom[1], Sven Tirén[2]
[1]Conterra AB
[2]Sveriges Geologiska AB
January 1991

TR 91-09
Long term sampling and measuring program. Joint report for 1987, 1988 and 1989. Within the project: Fallout studies in the Gideå and Finnsjö areas after the Chernobyl accident in 1986
Thomas Ittner
SGAB, Uppsala
December 1990

TR 91-10
Sealing of rock joints by induced calcite precipitation. A case study from Bergeforsen hydro power plant
Eva Hakami[1], Anders Ekstav[2], Ulf Qvarfort[2]
[1]Vattenfall HydroPower AB
[2]Golder Geosystem AB
January 1991

TR 91-11
Impact from the disturbed zone on nuclide migration – a radioactive waste repository study
Akke Bengtsson[1], Bertil Grundfelt[1], Anders Markström[1], Anders Rasmuson[2]
[1]KEMAKTA Konsult AB
[2]Chalmers Institute of Technology
January 1991

TR 91-12
Numerical groundwater flow calculations at the Finnsjön site
Björn Lindbom, Anders Boghammar, Hans Lindberg, Jan Bjelkås
KEMAKTA Consultants Co, Stockholm
February 1991